© Arezoo Khodayari, 2013

STUDIES TOWARDS ASSESSING THE EFFECTS OF AVIATION ON CLIMATE

BY

AREZOO KHODAYARI

DISSERTATION

Submitted in partial fulfillment of the requirements
for the degree of Doctor of Philosophy in Environmental Engineering in Civil Engineering
in the Graduate College of the
University of Illinois at Urbana-Champaign, 2013

Urbana, Illinois

Doctoral Committee:

Professor Donald J. Wuebbles, Chair and Director of Research
Associate Professor Tami C. Bond
Assistant Professor Nicole Riemer
Dr. Sotiria Koloutsou-Vakakis
Dr. Seth C. Olsen

ABSTRACT

Emissions from aviation are an important component in the overall concerns about the effects of human activities on climate. Aviation emissions modify the chemical and physical properties of the upper troposphere and lower stratosphere (UTLS) in various ways. Aircraft emit gases and particles that can either directly or indirectly affect climate and air quality, including: carbon dioxide (CO_2); nitrogen oxides (NOx) that can increase ozone (O_3) production and increase the destruction of methane (CH_4); water vapor that under certain atmospheric conditions can lead to contrail formation; and soot and other particles that along with contrails can affect the amount and characteristics of cirrus clouds. Soot and sulfate particles can also change the cloudiness by acting as cloud condensation nuclei. Due to the high growth in air traffic that is projected to continue, it is important to understand the effects of aviation on air quality and climate. Based on then existing analyses of the emissions and their effects, the aviation contribution in changing the radiative forcing on the climate system was about 5% of the total human-related emissions (relative to 1750) in 2005 (Lee et al., 2009). This contribution is a result of various effects, especially the direct effects of CO_2, NOx-induced effects, aerosol direct and indirect effects, and increased cloudiness from contrail formation and aerosols acting as cloud condensation nuclei. One of the main challenges of the aviation scientific community has been to increase the level of scientific understanding of these effects, especially with respect to those most uncertain (i.e. NOx effects, contrail-cirrus and aerosol effects). Another challenge has been to develop a simple climate model (SCM) that has the level of sophistication necessary to accurately assess aviation induced climate effects while being easy to use by policy makers for use in policy considerations.

The main objectives in this study were: (1) to evaluate the capabilities and limitations of simple climate models for evaluating aviation policy options and tradeoffs, and (2) to increase the scientific understanding of aviation NOx-induced effects on climate. With regard to the first goal, enhancing the evaluation of SCMs, the carbon cycle and energy balance treatments in several widely used simplified climate models were evaluated. The findings from this study resulted in modifications to the carbon cycle and energy balance model components of the APMT model that is used extensively by FAA in aviation policy analyses. With regard to the

second goal, 3 lines of research were pursued to increase the scientific understanding of aviation NOx-induced effects on climate. First, aviation NOx-induced effects were quantified using three-dimensional (3-D) climate-chemistry models and further, an intercomparison of NOx-induced effects in 3-D climate-chemistry models was performed. The NOx-induced forcings obtained in 3-D simulations were further used to update the parameterization of these effects in SCMs. Second, two additional NOx-induced effects (i.e., reduction in long-term O_3 concentrations and lower stratospheric water vapor (SWV)) that have not been fully accounted for in previous studies were quantified based on parameterizing the results obtained in the 3-D simulations. Results indicate that the inclusion of long-term O_3 and SWV RFs decreases the net aviation-induced RFs by about 21 to 31% for different range of scenarios studied. Finally, the representation of aviation NOx-induced effects in SCMs were evaluated and improved. The parameterization was improved based on the results of the 3-D simulations and by including the lifetime of the perturbed species and their emissions history into RF calculations. This resulted in 10 to 36% higher aviation NOx-induced net forcing than the net forcings that were reported in the literature, previously. Third, a set of experiments were performed to directly calculate the aviation NOx-induced changes in CH_4 that were otherwise calculated through a simple parameterization, and also to determine the CH_4 feedback factor on its own lifetime. Moreover, the accuracy of the parameterization that is used for the calculation of NOx-induced changes in CH_4 was evaluated. Results indicate that parameterizing the change in CH_4 concentration based on the change in its lifetime overestimates the change in CH_4 by 8.2% while decreases the computational requirements by nearly a factor of 8.

To my parents and my brother, Omid
whose love and support have sustained me throughout.

ACKNOWLEDGMENTS

It is a pleasure to thank the many people who made this dissertation possible. I owe my deepest gratitude and heart-felt appreciation to my advisor, Professor Donald Wuebbles, who was a great source of inspiration and motivation, and whose genuine support and guidance enabled me to do my very best and to develop a deep and unique understanding of my research.

I am indebted to Dr. Seth Olsen for genuinely sharing his knowledge with me and providing excellent guidance and support throughout my research. I am also grateful to Dr. Kenneth Patten and the other members of Dr. Wuebbles's research group at the University of Illinois Atmospheric Science Department for their support and encouragement.

I would like to thank my co-advisor, Professor Tami Bond for hosting me in her research group and all the members of Dr. Bond's research group at the University of Illinois Civil and Environmental Engineering Department for their friendship, support and encouragement. I am also thankful to my PhD committee members, Dr. Donald Wuebbles, Dr. Tami Bond, Dr. Nicole Riemer, Dr. Seth Olsen and Dr. Sotiria Koloutsou-Vakakis.

I am grateful for the financial support from the Federal Aviation Administration, Aviation Climate Change Research Initiative (ACCRI) under Contract #: 10-C-NE-UI amendment 001, The Partnership for AiR Transportation Noise and Emissions Reduction (PARTNER) and by the U.S. Department of Transportation, the Illinois Department of Transportation and the Transportation Research and Analysis Computing Center.

I would like to thank the National Center for Atmospheric Research (NCAR) for the support with computing time and for hosting me as a visiting scholar for a semester. I would like to thank NCAR scientists Dr. Jean-Francois Lamarque, Dr. Simone Tilmes and Dr. Andrew Gettelman and especially Dr. Francis Vitt for all their support.

Finally, I wish to thank my parents and my brother for their never-ending love and support which gave me the power and encouragement to successfully complete my PhD degree as well as all my other endeavors in life.

TABLE OF CONTENTS

CHAPTER 1: INTRODUCTION……..1

CHAPTER 2: INTERCOMPARISON OF THE CAPABILITIES OF SIMPLIFIED CLIMATE MODELS TO PROJECT THE EFFECTS OF AVIATION CO_2 ON CLIMATE……...…..…...…20

CHAPTER 3: AVIATION 2006 NOx-INDUCED EFFECTS ON ATMOSPHERIC OZONE AND OH IN COMMUNITY EARTH SYSTEM MODEL (CESM)...…49

CHAPTER 4: EVALUATION OF AVIATION NOx-INDUCED RADIATIVE FORCINGS FOR 2005 AND 2050…….79

CHAPTER 5: AVIATION NOx-INDUCED CH_4 EFFECT: FIXED MIXING RATIO BOUNDARY CONDITIONS VERSUS FLUX BOUNDARY CONDITION …….……...101

CHAPTER 6: METRICS FOR AVIATION EFFECTS ON CLIMATE BASED ON ACCRI CONTRIBUTIONS ……..114

APPENDIX A: ……...……..125

CHAPTER 1: INTRODUCTION

Aviation and the Environment

Aviation environmental impacts have been a concern since the beginning of commercial air travel. Various studies project that commercial aviation growth will outpace the improvements in efficiency that can be reached through improvements in engine design and improved fuels (McCarthy, 2010), and hence results in vast environmental effects (IPCC, 1999; Lee et al., 2009; Lee et al., 2010). The main environmental concerns from the aviation industry are noise, climate change, and effects on air and water quality.

Noise is perceived by the public as a direct result of aircraft operations near airports (Waitz et al., 2004). Aircraft noise has direct behavioral and physiological impacts on people's health. Although significant progress has been made to reduce aircraft noise, the public objection has grown due to the increase in air traffic. 60% of all airports world-wide consider aircraft noise to be a major concern (Sietzen, 2002). In response to the public concern related to aviation noise, airports have adopted operational restrictions to reduce aircraft noise and some prohibit aircraft take-offs and/or landings during the night or at other specific times.

An aircraft jet engine, as shown in Figure 1.1, along with other combustion-based engines, produces emissions, some of which can result in local air-quality-related health effects and some that can affect climate. Emissions from aircraft include carbon dioxide (CO_2), nitrogen oxides (NOx), water vapor (H_2O), carbon monoxide (CO), sulfur oxides (SOx), unburned hydrocarbons or volatile organic compounds (VOCs), soot and other particulates, and other trace compounds. The emissions of NOx, CO, VOCs, SOx and particulates are a place of concern for air quality near airports and are associated with adverse health effects. These pollutants are recognized as "criteria pollutants" by the U.S. EPA and have to follow the standards set by the US EPA under the Clean Air Act.

Many airports are located near water since the most available land for airport construction have often been located near water, and hence, airport operations have the potential

to adversely affect the nearby water quality. The runoff containing the fluid and fuel construction materials generated during airport construction, the airport storm water discharge, and the contaminations from aircraft fueling, maintenance and deicing activities can biologically, chemically, and physically affect the water quality (Aviation environmental and energy policy statement, 2012).

Fourteen years ago, the Intergovernmental Panel on Climate Change (IPCC) published a landmark report on the climate effects of aviation (IPCC, 1999) that gave a comprehensive assessment of aviation climate effects based on what was known at that time. Aviation emissions affect climate by altering the composition of the background atmosphere; this ultimately results in the imbalance of incoming and outgoing radiation at the top of the tropopause. This imbalance of forcing is called "radiative forcing (RF)". The resulting changes in climate affect temperature, precipitation, and extreme weather events, with resulting effects on sea level and other impacts on human and natural systems. Aviation-induced climate effects are the most serious long-term environmental effect of aviation activity, but large uncertainties remain in understanding these effects.

Different environmental impacts of aviation are being addressed by various environmental laws and regulations. A careful quantification of these environmental impacts is required to make such environmental laws and regulations fair and equitable. This work focuses on advancing the understanding of aviation-induced climate effects.

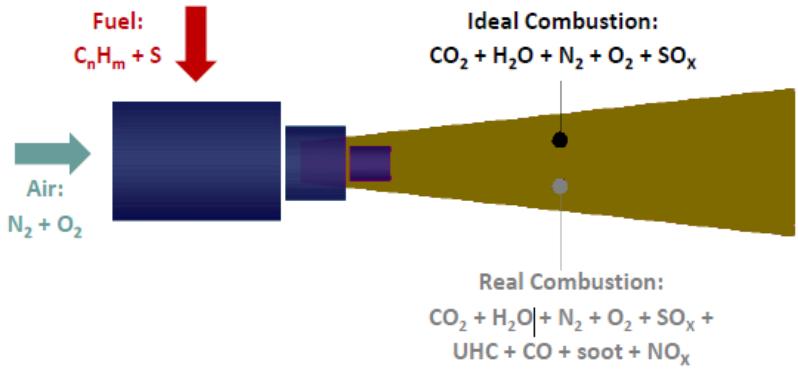


Figure 1.1. Aircraft produced emissions (Norman et al., 2003).

Aviation Emissions and their Climate Effects

Emissions from aviation are an important component in the overall concerns about the effects of human activities on climate. As a result, policy responses to reduce these emissions have been proposed, especially in Europe. However the effects of these emissions on climate are still poorly understood (IPCC, 1999; Wuebbles et al., 2007; Lee et al., 2009). Worldwide emissions of chemically and radiatively important gases (GHGs) and particles from aviation are among the fastest growing sources of human-related forcings on climate (McCarthy, 2010). Figure 1.2 shows the historical trends in aviation fuel usage and traffic to demonstrate that aviation has grown strongly despite economic downturns and other disruptive events that affect the global economy (Lee et al, 2009). As shown in Figure 1.2, aviation fuel usage has grown at a higher rate relative to other industries, as indicated by the higher CO_2 emissions fraction. Due to such a high growth in aviation emissions, the relative effect of aviation on atmospheric composition and on climate is likely to increase. This indicates the importance of better quantifying aviation-induced effects on climate.

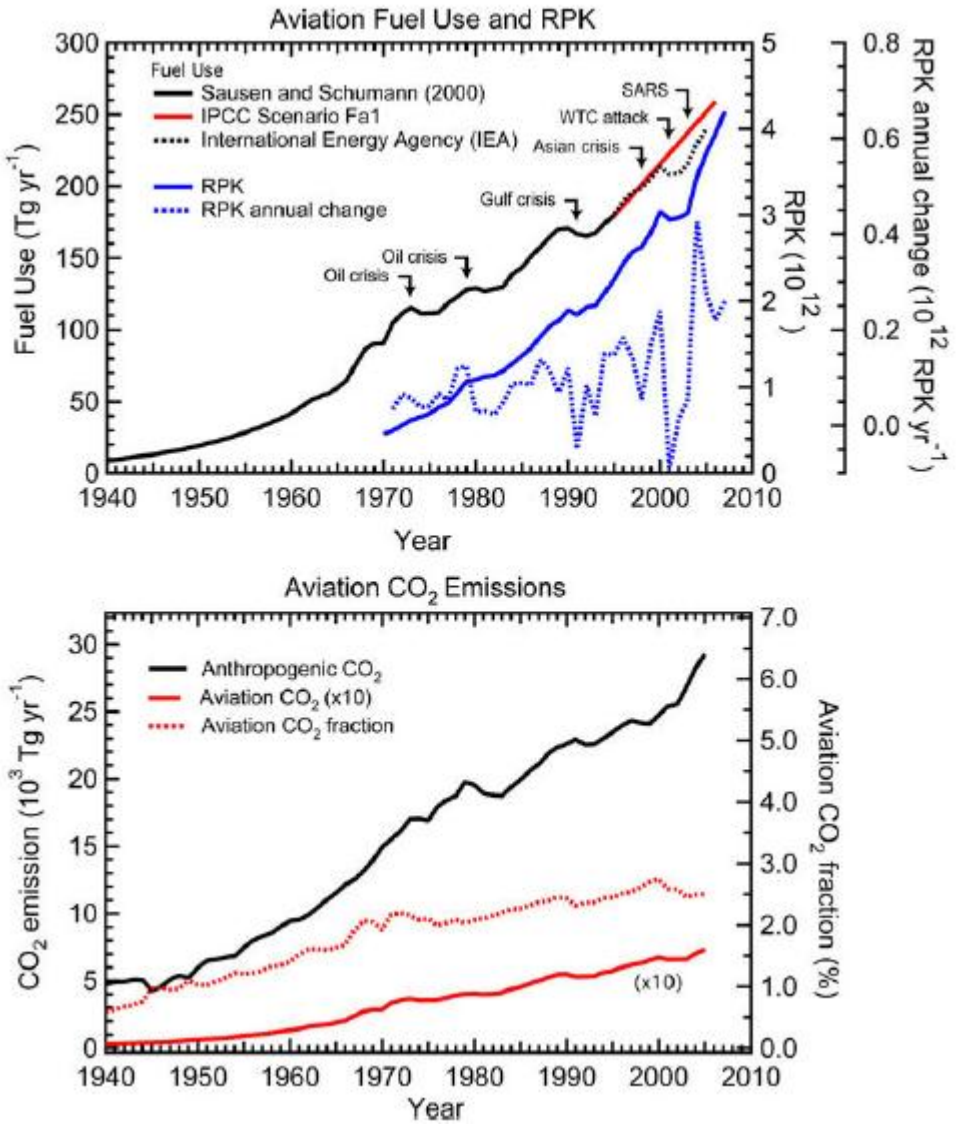


Figure 1.2. (Top) Historical and predicted aviation fuel use, (Bottom) Growth in aviation and anthropogenic CO_2 emissions (from Lee et al., 2009).

Aviation contributes to climate change in various ways. It directly emits carbon dioxide (CO_2) that is associated with positive RF on the Earth's climate system. Aircraft also emit nitrogen oxides (NOx) that can affect climate in three different ways, resulting in an overall positive RF. In general, in the troposphere, NOx emissions in the presence of hydrocarbons can drive complex nonlinear photochemistry that can either increase or decrease ozone (O_3) depending on the background atmosphere (Jacob, 1999). At commercial aircraft cruise altitudes

in the upper troposphere and lower stratosphere (UTLS), background NOx is low and aviation NOx emissions increase O_3 (Lee et al., 2009). Aviation NOx emissions in the UTLS are about four times more efficient in producing O_3 than ground sources (Hodnebrog et al., 2011). The tropospheric O_3 produced by aviation NOx emissions undergoes photolysis and produces excited oxygen atoms that then react with water vapor to produce OH. In the UTLS, OH is the dominate sink for methane (CH_4) and reduces the concentration of CH_4. Both ozone and methane are radiatively important gases that can affect climate. The reduction in CH_4 results in additional chemistry effects on the concentration of O_3. Aircraft also release water vapor into the atmosphere, which under certain atmospheric conditions can lead to contrail formation and resulting effects on cirrus clouds that are associated with positive forcings. Aircraft SOx and soot emissions result in sulfate and carbon-based particles that are associated with negative and positive radiative forcing, respectively. These particles can further change the cloudiness by acting as cloud condensation nuclei. All these emissions modify the chemical properties of the upper troposphere and modify the cloud microphysics with resulting effects on the Earth's climate.

What makes aviation emissions unique relative to other human-related emissions is that they are released primarily in the upper troposphere and lower stratosphere (UTLS). The spatial distributions and temporal variations of radiatively active chemical species in the UTLS, exactly where emissions occur from subsonic aircraft at cruise altitudes, can especially affect the Earth's climate system. For example, a number of studies have shown that surface temperature is strongly affected by the radiative influence of near-tropopause ozone (Lacis et al., 1990; Forster and Shine, 1997; Hegglin et al., 2008).

Figure 1.3 shows Lee et al. (2009) reported values for 2005 aviation forcing based on then existing atmospheric climate-chemistry modeling studies. Lee et al. reported that aviation contributed approximately 3.5% of the total anthropogenic radiative forcing (RF) on climate for the year 2005 (relative to 1750), excluding the highly uncertain aviation-induced effects on cirrus clouds. CO_2 emissions have the largest contribution to aviation forcings and accounts for roughly half of this total RF (aviation accounts for 2% of total human-related emissions of CO_2). The

dominant components of non-CO_2 forcings are NOx forcings and cloud forcings that are associated with a medium-low and low level of scientific understanding, respectively.

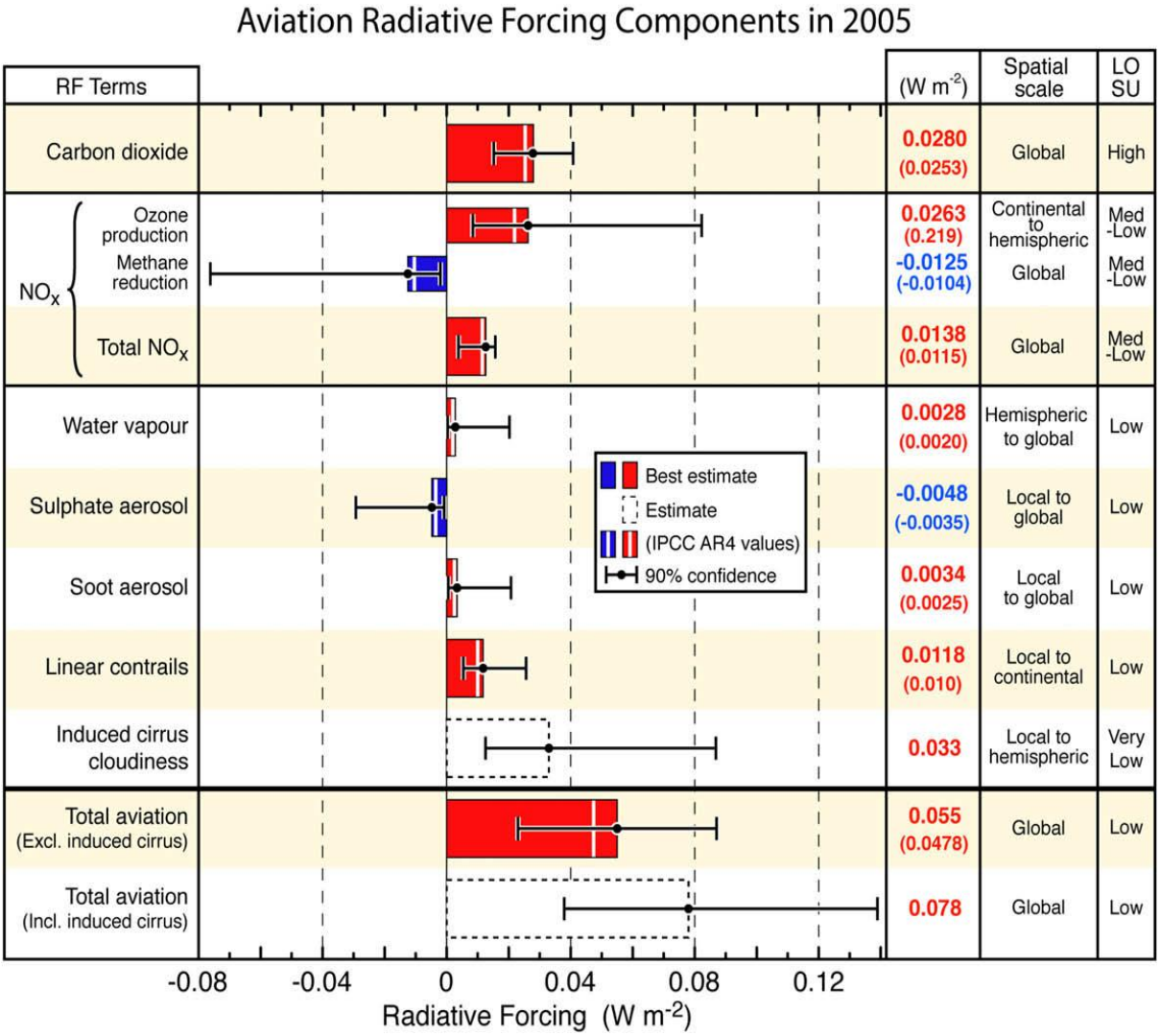


Figure 1.3. Aviation radiative forcing in 2005 (from Lee et al., 2009).

Modeling the Effects of Aviation Emissions on Climate

Climate models have different levels of complexity based on the number of spatial dimensions represented in the model, the extent to which different physical and chemical processes are explicitly represented and the level at which parameterizations are involved. Hence, these models require different simulation qualities. A wide spectrum of models has been

used to qualify the effects of natural and human-related emissions on the climate system. These models are designed for various applications and the purposes to which they are applied are different. The IPCC has used models with different levels of complexity, ranging from simple to complex, for projecting climate change in different cases. Their work acknowledges the need for such a wide spectrum of models (IPCC, 2007). Both complex and simple models have an important role in enhancing our understanding of future climate change.

In complex models the effect of any perturbation on the climate system is calculated by accounting for all the key physical and chemical processes operating in the Earth system in relation to atmosphere, ocean, terrestrial, biosphere, glaciers, ice sheets and land surface. These processes are typically represented in mathematical terms following the fundamental physical laws such as the conservation of mass, momentum, and energy. Such a mathematical formulation that includes adequate representation of Earth system physical and chemical processes is usually implemented in a computer program and called a "Global Climate Model" or GCM (more complete versions including the biological processes are also called "Earth System Models" (ESMs)). Complex models are expensive to run, and are necessary when regional effects, climate variability, seasonal patterns and changes in extreme events are needed to be studied.

On the other hand, in simple models most of the Earth system processes are highly parameterized and as such these models are inexpensive to run, and are useful when only global scale changes are to be explored. Additionally, simple models are useful when there is need for a large number of simulations to inform climate change policy options and tradeoffs (Houghton et. al., 1997).

Global Climate Models

Global Climate Models (GCMs) are models with complex mathematical representations of well-established physical and chemical principals. The representation of complex mathematical equations results in complex computer programs that have high computational demand for simulating the Earth system. These models are designed for decade to century time scale, or longer, simulations. There is a hierarchy of different GCMs based on their level of

complexity. The most complex GCMs are atmosphere-ocean general circulation models (AOGCMs), ESMs (more complete versions of AOGCMs that include biological processes) and climate-chemistry models (CCMs, same as AOGCMs with additional chemistry). These models aim to simulate the Earth system as close to the physical world as possible and with high credibility (McGuffie and Henderson, 2005). These models represent the physical and chemical quantities of interest by a three-dimensional (3-D, longitude-latitude-height) grid with typical horizontal resolution of a couple of hundred kilometers (newer models are now being run at 100 km or less), and have temporal scales down to a couple of hundred seconds. For many of the processes in the Earth system (e.g., clouds, land surface) the horizontal resolution is generally larger than the scale at which these processes happen in reality. However, running these models at finer resolutions is computationally expensive. Therefore, such models present the effect of these sub-grid scale processes through parameterizations (Houghton et. al., 1997). They have the capability to simulate the Earth system both in a fully interactive mode, the key components of Earth system (i.e. atmosphere, ocean, and land and sea ice) are coupled, and in an uncoupled mode. The credibility of these models predictions is evaluated against observations of past climate. IPCC (2007) used 23 AOGCMs for climate impact analysis in the Fourth Assessment Report. Based on IPCC (2007) evaluations, these models are able to provide credible analyses of past changes in climate and predictions of future climate change, especially at continental and higher scales. Such credibility is a result of explicit presentation of well-established physical and chemical principals. However, running these models can take weeks to months, depending on the available computational resources, and as such, are not always well-suited for applications that require long-term or a large number of simulations (Lim et al., 2006).

Earth System Models of Intermediate Complexity (EMICs) are the next hierarchy of GCMs in complexity. They usually have simpler atmosphere and/or ocean and have lower spatial resolution compared to AOGCMs. They are typically used to study large-scale processes and feedbacks in the climate system (IPCC, 2007). Other hierarchies of GCMs with intermediate complexity are chemical transport models (CTMs). These models focus on individual components of climate system and use parameterization to represent the interaction with other components of climate system, and are typically run with offline meteorology data. The focus of CTMs is atmospheric dynamic. These models are capable of both 2-D and 3-D simulations.

These models are still computationally expensive and hence, are not well-suited for applications that require long term or large number of simulations. Table 1.1 lists a number of widely used GCMs found in literature.

Table 1.1. A number of widely used GCMs.

Model	**Spatial Resolution**	**Hierarchy**
CESM (http://www.cesm.ucar.edu/)	3-D	ESMs
HadCM3 (Gordon et al., 2000; Pope et al., 2000)	3-D	AOGCMs
Atmospheric component of CESM (CAM) (http://www.cesm.ucar.edu/)	3-D	ESMs
GEOS-Chem www.acmg.seas.harvard.edu/geos/doc/man	3-D	CTMs
OsloCTM2 (Gauss et al., 2003; Søvde et al., 2008)	3-D	CTMs
GATOR-GCMOM (Jacobson et al., 2011)	3-D	CCMs
GEOS-CCM (Oman et al., 2011)	3-D	CCMs
NASA ModelE2 (Schmidt et al., 2006)	3-D	CCMs
BERN2.5CC (Plattner et al., 2001; Joos et al., 2001)	3-D	EMICs
MIT-IGSM (Sokolov et al., 2005)	2-D	EMICs
UVIC (Weaver et al., 2001)	2-D	EMICs

Simple Climate Models

Simple climate models (SCMs) have a simplified representation of the climate system (Warren et al., 2009). They include approximations for the dominant and most important

processes in the climate system and as such, are relatively easy to follow and inexpensive to run. The common simplified approaches to represent the climate system in SCMs include systems-dynamics models, reservoir models and impulse-response functions (Mahashabde, 2009). Systems-dynamics models simulate the climate system by modeling stock and flow between different components of the climate system, taking feedbacks into consideration (Fiddaman et al., 2009). Reservoir models are similar to systems-dynamics models; in this case, different components of the climate system are characterized by boxes representing the atmosphere and different layers of the ocean (Nordhaus and Boyer, 2000; Anthoff and Tol, 2008). An impulse response function (Green's function) is an analytical expression that represents the response of climate system to a small perturbation (unit-delta function forcing) and is a sum of exponentially decaying functions that correspond to different modes of climate response (Hasselmann, 1993). SCMs usually represent the physical and chemical quantities of interest in a global, zonally-averaged or hemispherical spatial scale and have an annual temporal resolution.

SCMs are mostly used to do cost-benefit analysis and to understand the relationship between climate effects and socio-economic impacts (Jain et al., 1994; Goodess et al., 2003). SCMs that evaluate both physical effects and socio-economic impacts are called integrated assessment models (IAMs). Due to SCMs flexibility and low computational costs, they are also appropriate for applications that require a large number of simulations and for uncertainty analysis. SCMs are usually calibrated to replicate the response of complex GCMs; they can also be calibrated to global scale observations (Houghton et. al., 1997). It should be noted that, it is important for SCMs to adequately imitate the key features of their parent GCMs. IPCC used a SCM, Model for the Assessment of Greenhouse-gas Induced Climate Change (MAGICC) calibrated to 19 different AOGCMs for climate change projections of different emission scenarios in the Fourth Assessment Report. Table 1.2 lists a number of widely used SCMs found in literature.

Table 1.2. A number of widely used SCMs.

Model	Sector	Spatial Resolution	Approach
MAGICC (Meinshausen et al., 2008)	All sources	Global, hemispherical land/ocean	Systems-dynamics model
ISAM (Jain et al., 1994)	All sources	Global	Systems-dynamics model
C-ROADS (Fiddaman, 2009)	All sources	Global	Systems-dynamics model
FUND (Anthoff, 2008)	All sources	Global, regional	Reservoir model
DICE (Nordhaus, 2008)	All sources	Global	Reservoir model
CICERO-2 Fuglesvedt and Berntsen, 1999; Skeie et al. 2009)	All sources	Global, hemispherical	Reservoir model
CICERO-1 (Berntsen, 2008)	Transportation	Global	Impulse response
APMT (Marais, 2008)	Aviation	Global	Impulse response
AirClim (Grewe, 2008)	Aviation	Global, zonally-averaged	Impulse response
LinClim (Lim et al., 2007)	Aviation	Global	Impulse response
Schwartz, 2009	Aviation	Global	Impulse response

Research Objectives and their Significance

Given the potential effects of aviation emissions on climate and the strong growth of aviation in past decades (and likely continued growth), it is important to quantify and analyze the current and future effect of aviation emissions on climate (Wuebbles et al., 2010; IPCC, 1999; Lee et al., 2009). This project is broken into two parts: (1) evaluation of simple climate models, and (2) new studies using a state-of-the-art CCM.

Intercomparison and Evaluation of SCMs Carbon Cycles and Energy Balance Sub-Models

Although three-dimensional CCMs are being used to evaluate the climate effect of different perturbations, including aviation, the complexity and computational expense of these models make them difficult to be used as policy tools for applications that requires a large number of simulations. SCMs that simplify the complex understanding of Earth system processes, while preserving their scientific accuracy, can be important tools for policy considerations. Such SCMs need to be scientifically well structured to properly address the dominant processes affecting the Earth's climate system in relationship to particular emissions. At their best, SCMs can approximate the accuracy of the much more complex models while being much less computationally expensive and offering the simplicity and transparency needed to evaluate multiple policy options and tradeoffs. There are different SCMs that are either being used or could be used for policy analyses. However, there is no published assessment of their performance for use in aviation-related effects on climate. This study (Chapter 2) is the first effort towards evaluating and enhancing the understanding of the capabilities of SCMs to project aviation effects on climate. In this study, two core components of six existing SCMs, the carbon cycles and energy balance sub-models, are evaluated. Moreover, recommendations for an appropriate carbon cycle and energy balance sub-model that can be used in SCMs to explore aviation effects on climate are provided. Chapter 2 provides a detailed description of this study.

Evaluation of Aviation NOx-Induced Effects in Earth System Models

Although aviation NOx emissions are 3% (Dameris et al., 1998) of the total human-related NOx emissions, they are important due to their effects on upper tropospheric chemistry. NOx emissions from aviation can change the background concentration of atmospheric NOx and change the atmospheric O_3, CH_4 and OH concentrations. Previous studies show that model evaluations of the O_3 produced by aviation NOx substantially, by over 100%, due to different model representations of various parameters, including the ratios of NO: NO_2 and OH:HO_2, background NOx levels, location and time of emissions, the amount of sunlight, and atmospheric mixing (Holmes et al., 2011). A recent study by Olsen et al. (2012) shows that there is a large difference between the evaluations of aviation NOx-induced climate effects in CCMs. Moreover,

there is a large uncertainty in the net RF associated with aviation NOx emissions, largely because it is the sum of a positive RF associated with an short-term increase in tropospheric and lower stratospheric O_3 concentration and three negative RFs associated with a reduction in CH_4 concentrations, a longer-term reduction in O_3 concentration and a reduction in stratospheric water vapor. IPCC (2007) evaluated the state of scientific understanding of NOx-induced effects in climate models as medium–low. Therefore, a 3-D climate-chemistry model with state-of-art knowledge of the resolved physical, chemical and biochemical processes in the Earth's climate system is necessary in evaluating the aviation NOx effects. In this research (Chapter3) the most up-to-date atmospheric component of NCAR 3-D Community Earth System Model (CESM) model, CAM5, with its detailed representation of atmospheric microphysics, is used for the first time to quantify the aviation NOx effects on climate. Results were further compared with the results obtained from the previous version of CESM, CAM4, to determine the impact of the changes in the model on the aviation NOx-induced effects. The results from this study can be further used to update the representation of aviation NOx effects in SCMs. Chapters 4 and 5 will explain the details associated with this research activity.

In Chapter 4, two additional NOx-induced effects (i.e. reduction in long-term O_3 concentrations and lower stratospheric water vapor (SWV)) that have not been fully accounted for in previous studies were parameterized based on the results obtained in the 3-D simulations. Moreover, the representation of aviation NOx-induced effects in SCMs was improved by including the lifetime of the perturbed species and their emissions history into RF calculations. The effect of the lifetime of the perturbed species and their emissions history were not previously accounted for in calculating the aviation NOx-induced RFs reported in Lee et al. (2009).

Finally, in Chapter 5, three different sets of experiments were performed to evaluate the accuracy of the simple parameterization that has been widely used to calculated the changes in CH_4 concentrations based on the changes in its lifetime, and also to evaluate the CH_4 feedback factor on its own lifetime (previously, calculated to be 1.4). The accuracy of the aforementioned parameterization and feedback factor has never been evaluated for the case of aviation emissions.

Dissertation Structure and Overall Research Methodology

In the first part of this dissertation, Chapter 2, the capabilities of 6 existing SCMs in projecting aviation effects on climate are evaluated. This task was accomplished by evaluating SCMs two core components, their treatment of the carbon cycle and their representation of the Earth's (approximate) energy balance. The Aviation Environmental Portfolio Management Tool (APMT) Impacts climate model, two models used at the Center for International Climate and Environmental Research-Oslo (CICERO-1 and CICERO-2), the Integrated Science Assessment Model (ISAM) model as described in Jain et al. (1994), the simple Linear Climate response model (LinClim) and the Model for the Assessment of Greenhouse-gas Induced Climate Change version 6 (MAGICC6) are evaluated. Different case studies were performed to illustrate the behavior of the carbon cycle and energy balance sub-models in these models.

In the next part of the dissertation, Chapter 3, CAM5, the latest in a series of CESM's atmospheric component and its predecessor CAM4 were used to quantify aviation NOx-induced climate effects. To evaluate the performance of CAM4 and CAM5, different benchmark diagnostic tests were carried out. In these diagnostic tests the performance of atmospheric and chemistry modules were evaluated by comparing CAM4 and CAM5 modeled fields against available observational data. The aviation NOx-induced changes in the chemistry of the background atmosphere induced by Aviation Environmental Design Tool (AEDT) (Roof et al., 2007; Wilkerson et al., 2010; Olsen et al, 2012) NOx emissions from the year 2006 were calculated based on the results of both CAM4 and CAM4 simulation. Simulations were performed in offline mode driven with 2005 meteorology from the GEOS DAS v5.1. To avoid high computational cost, the concentrations of long-lived gases such as CO_2, CFCs and CH_4 were prescribed as a lower boundary condition in the simulations. The University of Illinois Radiative Transfer Model (UIUC RTM) was used offline to calculate the radiative forcing associated with aviation NOx-induced changes in short-term O_3.

In Chapter 4, a parameterization of aviation NOx-induced forcings based on the results of CCM simulations is implemented in a SCM setting. To accomplish this task, a set

of steady-state simulations in a 3-D CCM, CAM4, the atmospheric component of NCAR CESM model, version 4, was performed to obtain aviation NOx-induced specific forcings (forcing per amount of NOx emissions). The aviation NOx emissions from the year 2006 were obtained from the AEDT emission inventory. Simulations were performed in offline mode driven with 2005 meteorology from the GEOS DAS v5.1. To avoid high computational cost, the concentrations of long-lived gases were prescribed as a lower boundary condition. The calculated specific forcings were used as the basis for the parameterization of aviation NOx-induced effects, taking into account the lifetime of the NOx-induced perturbations and the history of emissions.

In Chapter 5, the same simulations that were performed as in Chapter 3 were done but using CH_4 fluxes as input instead of using fixed CH_4 at the surface into the CAM4 simulations. The CH_4 fluxes that were inputted to the model were calculated from the steady-state loss of CH_4 in the simulations with fixed CH_4. The results were compared with the results obtained with fixed CH_4 at the surface to evaluate the effect of CH_4 feedback on its own lifetime and the accuracy of the parameterization used to calculate the changes in CH_4 concentration based on the changes in its lifetime.

In Chapter 6, the current evaluation of aviation induced effects obtained from a collaborative effort of 9 different FAA-Aviation Climate Change Research Initiative (ACCRI) research groups including this work, are presented and discussed. Also, the research that could be built upon the work that has been done in this research is discussed. Chapter 2 appeared in its entirety in the Journal of Atmospheric Environment and the results in the following chapters have been submitted for journal publication.

BIBLIOGRAPHY

Anthoff D. and R. S. J. Tol (2008), The Climate Framework for Uncertainty, Negotiation, and Distribution (FUND), Technical Description, Version 3.3. Available at http://www.mi.uni-hamburg.de/fileadmin/fnu-files/staff/tol/FundTechnical Description.pdf.

Aviation environmental and energy policy statement (2012), Department of Transportation, Federal Aviation Administration.

Berntsen, T., J. S. Fuglestvedt (2008), Global temperature responses to current emissions from the transport sectors, *Proceedings of the National Academy of Sciences*, USA 105, 19154–19159.

Dameri, M., V. Grewe, I. Kohler, R. Sausen, C. Bruhl, J. U. Grooss and B. Steil (1998), Impact of aircraft NOx emissions on tropospheric and stratospheric ozone. Part II: 3-D model results, *Atmospheric Environment*, 32, 3185–3199.

Dallara, E. S. (2011), Aircraft design for reduced climate impact, PhD dissertation.

Fuglesvedt, J. S., and T. Berntsen (1999), A simple model for scenario studies of changes in climate, Version 1.0, CICERO, Oslo, Norway, pp. 59.

Fiddaman, T., L. S. Siegel, E. Sawin, A. P. Jones, and J. Sterman (2009), C-ROADS Simulator Reference Guide.

Grewe, V. and A. Stenke (2008), AirClim: an efficient tool for climate evaluation of aircraft technology, *Atmospheric Chemistry and Physics*, 8:4621–4639.

Gauss, M., I. S. A., Isaksen, S. Wong, and W. C. Wang (2003), Impact of H_2O emissions from cryoplanes and kerosene aircraft on the atmosphere, *Journal of Geophysical Research*, 108, 4304, doi:10.1029/2002jd002623.

Gordon, C., C. Cooper, C. A. Senior, H. Banks, J. M. Gregory, T. C. Johns, J. F. B. Mitchell, and R. A. Wood (2000), The simulation of SST, sea ice extents and ocean heat transports in a version of the Hadley Centre coupled model without flux adjustments, *Climate Dynamics*, vol 16, p147-168. (doi:10.1007/s003820050010).

Goodess, CM, Hanson C, Hulme M, Osborn TJ (2003) Representing climate and extreme weather events in integrated assessment models: a review of existing methods and options for development. Integrated Assessment, 4:145–171.

Holmes, C. D., Q. Tang, and M. J. Prather (2011), Uncertainties in climate assessment for the case of aviation NO, *Proceedings of the National Academy of Sciences*, U.S.A., 108, 10 997–11 002, doi:10.1073/pnas.1101458108.

Houghton, J. T., L. G. Meira Filho, D. J. Griggs, K. Maskell (1997), An Introduction to Simple Climate Models used in the IPCC Second Assessment Report, IPCC Technical Paper 2.

Hasselmann, K., R. Sausen, E. Maier-Reimer, and R. Voss (1993), On the cold start problem in transient simulations with coupled atmosphere-ocean models, *Climate Dynamics*, 9:53–61.

Hegglin, M. I., et al. (2008), Validation of ACE-FTS satellite data in the upper troposphere/lower stratosphere (UTLS) using non-coincident measurements, *Atmospheric Chemistry and Physics*, 8, 1483-1499.

Hodnebrog, Ø., T. K. Berntsen, O. Dessens, M. Gauss, V., Grewe, I. S. A. Isaksen, B. Koffi, G.,Myhre, D. Olivié, M. J. Prather, J. A. Pyle, F. Stordal, S. Szopa, Q. Tang, P. Velthoven, J. E. Williams, and K. Ødemark (2011), Future impact of non-land based traffic emissions on atmospheric ozone and OH – an optimistic scenario and a possible mitigation strategy, *Atmospheric Chemistry and Physics*, 11, 11 293–11 317, doi:10.5194/acpd-11-11293-2011, www.atmos-chem-phys.net/11/11293/2011.

IPCC, (1999), Aviation and the global atmosphere 1999, In: E Penner, J., Lister, D.H., Griggs, D.J., Dokken, D.J., McFarland, M. (Eds.), Intergovernmental Panel on Climate Change. Cambridge University Press, Cambridge, UK.

IPCC, (2001), Climate change 2001: the scientific basis. In: Houghton, J.T., Ding, Y., Griggs, D.J., Noguer, M., van der Linden, P.J., Dai, X., Maskell, K., Johnson, C.A. (Eds.), Contribution of Working Group I to the Third Assessment Report of the Intergovernmental Panel on Climate Change. Cambridge University Press, UK.

IPCC, (2007), Climate change 2007, The physical science basis. In: Solomon, S., Qin, D., Manning, M., Marquis, M., Averyt, K., Tignor, M.M.B., Miller, H.L., Chen, Z. (Eds.), Contribution of Working Group I to the Fourth Assessment Report of the Intergovernmental Panel on Climate Change. Cambridge University Press, UK.

Jain, A. K., H. S. Kheshgi, and D. J. Wuebbles (1994), Integrated science model for assessment of climate change, UCRL-JC-116526, Lawrence Livermore Nat. Lab., Livermore, Calif.

Joos, F., I. C. Prentice, S. Sitch, R. Meyer, G. Hooss, G.-K. Plattner, S. Gerber, K. Hasselmann (2001), Global warming feedbacks on terrestrial carbon uptake under the Intergovernmental Panel on Climate Change (IPCC) emission scenarios, *Global Biogeochemical Cycles*, 15/4, 891-907.

Lacis, A. A., et al. (1990), Radiative forcing of global climate changes in the vertical distribution of ozone, *Geophysical Research Letter*, 95(D7), 9971-9981.

Lee, D. S., et al. (2010), Transport impacts on atmosphere and climate: Aviation, *Atmospheric Environment*, 44:4678–4734.

Lee, D. S., D. W. Fahey, P. M. Forster, P. J. Newton, R. C. N. Wit, L.L., Lim, B. Owen, R. Sausen (2009), Aviation and global climate change in the 21st century, *Atmospheric Environment*, doi:10.1016/j.atmosenv.04.024.

Lim, L., D. S. Lee, R. Sausen, M. Ponater (2007), Quantifying the effects of aviation on radiative forcing and temperature with a climate response model, Proceedings of an International Conference on Transport, Atmosphere and Climate (TAC). Office for Official Publications of the European Communities, Luxembourg, ISBN 92-79-04583-0, pp. 202–207.

McCarthy J. (2010), Aviation and climate change, in G. Blumenthal (ed.), Aviation and climate change (USA: Nova Science Publishers, Inc.).

Marais K., S. P. Lukachko, M. Jun, A. Mahashabde, and I. A. Waitz (2008), Assessing the impact of aviation on climate, *Meteorologische Zeitschrift*, 17:157–172, 2008.

Mahashabde, A. (2009), assessing environmental benefits and economic costs of aviation environmental policy measures, PhD dissertation.

Meinshausen, M., S. C. B. Raper and T. M. L. Wigley (2008), Emulating IPCC AR4 atmosphere-ocean and carbon cycle models for projecting global-mean, hemispheric and land/ocean temperatures: MAGICC 6.0, *Atmospheric Chemistry and Physics Discuss*, 8, 6153–6272.

McGuffie, K. and A. Henderson-Sellers (2005), A Climate Modelling Primer, 3rd Ed. John Wiley & Sons Ltd., NJ.

Norman, P.D., D.H. Lister, M. Lecht, P. Madden, K. Park, O. Penanhoat, C. Plaisance, and K. Renger (2003), Development of the technical basis for a new emissions parameter covering the whole aircraft operation: NEPAIR, final technical report. Technical Report Contract Number G4RD-CT-2000-00182, European Community.

Nordhaus, W. D. and J. Boyer (2000), Warming the world : economic models of global Warming, MIT Press, Cambridge, Mass..

Nordhaus. W. D. (2008), A Question of Balance: Weighing the Options on Global Warming Policies, Yale University Press, New Haven.

Olsen, S. C., G. P. Brasseur, D. J. Wuebbles, S. R. H. Barrett, H. Dang, S. D. Eastham, M. Z. Jacobson, A. Khodayari, H. Selkirk, A. Sokolov, N. Unger (2012), Comparison of model estimates of the effects of aviation emissions on atmospheric ozone and methane, Submitted, *Geophysical Research Letters*.

Oman, L. D., J. R. Ziemke, A. R. Douglass, D. W. Waugh, C. Lang, J. M. Rodriguez, and J. E. Nielsen (2011), The response of tropical tropospheric ozone to ENSO, *Geophysical Research Letter*, 38, L13706, doi:10.1029/2011GL047865.

Pope, V. D., M. L. Gallani, P. R. Rowntree and R. A. Stratton (2000), The impact of new physical parametrizations in the Hadley Centre climate model - HadAM3, *Climate Dynamics*, vol 16, 123-146. (doi:10.1007/s003820050009).

Plattner, G.-K., F. Joos, T. F. Stocker, O. Marchal (2001), Feedback mechanisms and sensitivities of ocean carbon uptake under global warming, Tellus B, 53/5, 564-592.

Sietzen, Jr. F., (2002) New Blueprint for NASA Aeronautics, Aerospace America, p.25.

Sokolov, A.P., et al. (2005), The MIT Integrated Global System Model (IGSM) Version 2: Model description and baseline evaluation. Report 124, MIT Joint Program for the Science and Policy of Global Change, Cambridge, USA.

Søvde, O. A., Gauss, M., Smyshlyaev, S. P., and I. S. A. Isaksen (2008), Evaluation of the chemical transport model Oslo CTM2 with focus on arctic winter ozone depletion, *Geophysical Research*, 113, D09304, doi:10.1029/2007jd009240.

Schmidt, G. A., et al. (2006), Present-day atmospheric simulations using GISS ModelE: Comparison to in situ, satellite, and reanalysis data, *Journal of Climate*, 19(2), 153-192.

Schwartz, E. and I. M. Kroo (2009), Aircraft design: Trading cost and climate impact, *American Institute of Aeronautics and Astronautics*, 2009-1261.

Waitz, I., J. Townsend, J. Cutcher-Gershenfeld, E. Greitzer, and J. Kerrebrock (2004), Aviation and the Environment: A National Vision Statement, Framework for Goals and Recommended Actions.

Weaver, A. J. et al. (2001), The UVic earth system climate model: Model description, climatology and applications to past, present and future climate, *Atmosphere–Ocean*, 39, 361–428.

Wuebbles, D., M. Gupta, and M. Ko (2007), Evaluating the impacts of aviation on climate change, Eos, Trans, *American Geophysical Union*, 88, 157–168.

Wuebbles D., P. Forster, H. Rogers, and R. Herman (2010), Issues and uncertainties affecting metrics for aviation impacts on climate, *Bulletin* of the *American* Meteorological *Society*, 91, 491–496.

CHAPTER 2: INTERCOMPARISON OF THE CAPABILITIES OF SIMPLIFIED CLIMATE MODELS TO PROJECT THE EFFECTS OF AVIATION CO_2 ON CLIMATE[1]

Abstract

This study evaluates the capabilities of the carbon cycle and energy balance treatments in several existing simplified climate models that are either being used or could be used for evaluating the effects of aviation on climate. Since these models are used in policy-related analyses, it is important that the capabilities of such models represent the state of understanding of the science. We compare the Aviation Environmental Portfolio Management Tool (APMT) Impacts climate model, two models used at the Center for International Climate and Environmental Research-Oslo (CICERO-1 and CICERO-2), the Integrated Science Assessment Model (ISAM) model as described in Jain et al. (1994), the simple Linear Climate response model (LinClim) and the Model for the Assessment of Greenhouse-gas Induced Climate Change version 6 (MAGICC6). In this paper we do select case studies to illustrate the behavior of carbon cycle and energy balance model in these models. The results are not intended to show the absolute and likely range of the expected climate response in these models. Our intercomparison points to specific features in model representations of the carbon cycle and the energy balance model that need to be carefully considered in studies of aviation effects on climate. These results suggest that carbon cycle models that use linear impulse-response-functions (IRF) in combination with separate equations describing air-sea and air-biosphere exchange of CO_2 can account for the dominant nonlinearities in the climate system that would otherwise not have been captured with an IRF alone, and hence, produce a close representation of more complex carbon cycle models. Moreover, results suggest that an energy balance model with a 2-box ocean sub-model, and IRF that is tuned to reproduce the dominant mode of a new generation of coupled Earth system models produce a close representation of the globally-averaged temperature response of more complex energy balance models.

[1]This chapter appeared in its entirety in the Journal of Atmospheric Environment as Khodayari, A., D. Wuebbles, S. Olsen, J. Fuglestvedt, T. Berntsen, M. Lund, I. Waitz, P. Wolfe, P. Forster, M. Meinshausen, D. S. Lee and L. L. Lim, (2013),"Intercomparison and Evaluation of the Capabilities of Simplified Climate Models to Project the Effects of Aviation on Climate", Atmospheric Environment, 75, 321-328.

Introduction

Worldwide emissions of greenhouse gases (GHGs) and particles from aviation are among the fastest growing sources of human-related forcings on climate (McCarthy, 2010). Aviation contributes to changes in climate forcing directly through emissions of gases like carbon dioxide (CO_2), water vapor, and emissions of particles and particle precursors (e.g., affecting soot and sulfates), indirectly through effects on ozone (O_3) and methane (CH_4) through emissions of nitrogen oxides (NOx), and through increased cloudiness from contrail formation and the particle emissions.

Lee et al. (2009) estimates that aviation contributed approximately 3.5% (range 1.3% to 10%) of the total anthropogenic radiative forcing (RF) on climate for the year 2005 (relative to 1750), excluding the highly uncertain aviation-induced effects on cirrus clouds. CO_2 forcing account for 50% (range 15% to 200%) of this RF and as such, is a major component of aviation forcing. Coupled Earth system models (ESMs) are being used to project the climate effects from natural and human-related emissions including aviation emissions. However, ESMs, while scientifically comprehensive, are computationally expensive, and therefore not ideal for the large number of simulations necessary to address questions of interest to policymakers related to the effects of aviation on climate. As such, development of Simplified Climate Models (SCMs) that can emulate the global averaged results of the more comprehensive climate models on decade to century time scales is important to evaluating policy options and tradeoffs. This would also imply the need for intercomparison studies to assess the behavior of such SCMs and the quality of their projections. Such intercomparisons reported a wide range of model responses to the same emission scenario due to different parameterization of the climate response (e.g., van Vuuren et al. 2009; Warren et al., 2010). In SCMs, the climate response is either parameterized by adjusting a single impulse-response-function (IRF) to the results of more sophisticated parent models, or by adjusting IRFs to dominant physical processes in the system and coupling them to form a non-linear convoluted system model (hereafter called “process specific IRFs”), or by explicitly solving for the dominant processes in the climate system. IRFs are modeled based on linear response theory and are used to reproduce the characteristics of the system response of the sophisticated parent models by assuming a linear response of the system to a perturbation from

its equilibrium state. The linear response in this context means, once the IRF's fit coefficients are obtained by adjusting to sophisticated parent models under an arbitrary perturbation, they are fixed regardless of how the background concentration of atmospheric species or other atmospheric states are changing. Previous studies suggest that while IRFs can be used as a surrogate for their parent models within a linear domain, such IRFs degrade in their skill if they are used beyond the linear domain and outside of the original calibration space (Joos et al., 1996 and 2001; Hooss et al., 2001; van Vuuren et al. 2009; Marten, 2011). These studies suggest extending the applicability of these IRFs to the nonlinear domain by explicitly treating the dominant nonlinearities in the climate system. Overall, these studies as well as other studies such as Thompson and Randerson (1999) and Li et al. (2009) while acknowledging the challenge, suggest the use of such IRFs is justified due to their simplicity. However, they expect that updating IRFs fit parameters based on more recent generations of ESMs and incorporating dominant nonlinearities in the climate system will improve the skill of such models. Nevertheless, these studies suggest that care must be taken when describing a nonlinear system with a single IRF. Most SCMs that are being used specifically for aviation studies use a single IRF to describe the carbon cycle (for determining changes in atmospheric CO_2 concentration from a given emissions scenario) as they assume CO_2 forcing from aviation is small enough that the system responds linearly. In this paper we discuss the applicability of such assumptions for calculating the change in CO_2 concentration induced by aviation emissions.

The level of parameterization of key interactions is different among different SCMs (IPCC, 2007). The level of parameterization is a design decision balancing run time, flexibility, and transparency of physical processes versus model complexity and comprehensiveness. In many SCMs, including the ones used in this study, the parameterization methodology is based on using IRFs that have different fit parameters so that the model can represent the range of results from the literature. In light of the importance of SCMs for policy evaluation, the capabilities for representing the carbon cycle and the energy balance model (used to calculate the temperature change resulting from a change in radiative forcing) are intercompared in this study. Six models were selected for the analysis in this study: the Aviation Environmental Portfolio Management Tool (APMT) model supported by the Federal Aviation Administration (FAA) Partnership for AiR Transportation Noise and Emissions Reduction (PARTNER program (Marais et al., 2008)),

two models used at Center for International Climate and Environmental Research-Oslo (CICERO-1 2-box model (Berntsen and Fuglestvedt, 2008) and CICERO-2 upwelling-diffusion energy model (Fuglesvedt and Berntsen, 1999)), the Integrated Science Assessment Model (ISAM) model (Jain et al., 1994; Jain and Yang, 2005), the simple Linear Climate response (LinClim) model (Lim et al., 2006; Lee et al, 2009), and the Model for the Assessment of Greenhouse-gas Induced Climate Change version 6 (MAGICC6) (Meinshausen et al., 2011). The selected SCMs have different methods for representing the carbon cycle and the Earth's energy balance. The complexity of the representations ranges from relatively simple (APMT, LinClim) to more complex (MAGICC6). Some of these SCMs were specifically designed to evaluate aviation impacts (APMT and LinClim); some were designed for the transportation sectors in general, including aviation (CICERO-1), while others were not and do not directly include aviation (ISAM), or explicitly include aviation (CICERO-2 and MAGICC6). While the distinction of emission location is not important for CO_2 since it is long-lived and well mixed in the atmosphere it is important for other aviation emissions, e.g., NOx, and its effects.

A series of three experiments were conducted to compare and evaluate the capabilities of the SCMs' carbon cycle sub-models. The first evaluates the capability of the SCMs to reproduce background CO_2 concentrations by examining the SCM's carbon cycle response to bounding IPCC Fourth Assessment Report (AR4) CO_2 emissions scenarios (IPCC, 2007). The second evaluates the relative importance of different background emission scenarios on the calculation of aviation-induced CO_2 concentration by examining the SCM's carbon cycle response to a constant year-2000 aviation emission scenario under the different IPCC AR4 emission scenarios. The final evaluates the capability of SCMs to project the aviation-induced changes in atmospheric CO_2 by examining the SCM's carbon cycle response to chosen background and aviation emission scenarios. A second series of three experiments were conducted to compare and evaluate the capabilities of the SCMs energy balance models. The first examines the energy balance model responses of the SCMs to bounding IPCC AR4 total RF scenarios. The second evaluates the capability of SCMs to project the aviation-induced changes in temperature by examining the SCM's energy balance model response to chosen background and aviation RF scenarios. In the following discussion, the general structure of each SCM and its core components, the results of the study and the key conclusions are discussed.

The Models Compared

All of the SCMs included in this study, except MAGICC6 and CICERO-2, calculate global-averaged quantities. MAGICC6 and CICERO-2 both have hemispheric resolution, MAGICC6 calculates the hemispheric land/ocean and globally averaged quantities and CICERO-2 calculates the hemispheric and globally averaged quantities.

APMT

APMT was developed to assess both physical climate effects and socio-economic environmental impacts of aviation activity under different aviation scenarios and to capture the uncertainty associated with aviation effects on climate based on a probabilistic approach using Monte-Carlo methods (Mahashabde et al., 2011; Marais et al., 2008). Typically, APMT runs probabilistically for a policy scenario paired with a baseline scenario. This approach can be used to more accurately represent the uncertainties in outputs by formally accounting for the reduced influence of modeling uncertainties that are common to both the policy and baseline scenarios. In this study, deterministic analyses were used for evaluation of APMT compared with other SCMs as the purpose is to evaluate the underlying physical structure and capabilities of the models. Therefore, while this analysis provides a good indication of the uncertainties and biases in the underlying sub-models, it does not provide an indication of the uncertainties or biases in the overall APMT-Impacts climate model when it is run probabilistically to represent a range of results from the literature (the task for which it was designed).

APMT calculates the CO_2 concentration resulting from an emission perturbation by using a linear-response-function (LRF) (Marais et al., 2008). LRF is "defined as the CO_2 signal observed in the atmosphere for a δ-function atmospheric input at time t=0 (or equivalently a unit step-function change in the initial atmospheric CO_2 concentration)" (Maier-Reimer and Hasselmann, 1987). LRF is derived from an exponential curve fit to the change in atmospheric CO_2 concentration as a function of time for a certain CO_2 emission pulse. The CO_2 concentrations used for this fit result from simulations with a three-dimensional coupled model of the Earth's system. By default, APMT uses the Bern atmospheric LRF (Joos et al., 1996) that

was derived by calibration against the Bern carbon cycle model under a baseline scenario that is an instantaneous release of 1 ppm CO_2 into the background atmosphere with 378 ppm CO_2 (IPCC, 2007). APMT also has the option of using other atmospheric LRFs, including Hasselmann et al. (1993), Hasselmann et al. (1997) and Hooss et al. (2001). These atmospheric LRFs have a same form as the default Bern LRF with different coefficients. These carbon cycle models are not utilized in APMT during a typical policy analysis as they are older LRFs that are not representative of current scientific understanding, but they are included in the model to provide flexibility to directly compare APMT to other SCMs.

The radiative forcing on climate derived for aviation-emitted CO_2 in APMT as well as all other SCMs except CICERO-1, is calculated explicitly based on the following simplified function as described by IPCC Third Assessment Report (Ramaswamy et al., 2001).

$$RF_{CO_2} = \alpha_{CO_2} \ln\left(C \diagup C_0\right) \tag{2.2}$$

Where RF_{CO_2} is the adjusted radiative forcing from CO_2 (Wm^{-2}) for a CO_2 concentration C (ppm) above the preindustrial concentration C_0 (278 ppm). The scaling parameter α_{CO_2} has the value of 5.35 Wm^{-2} ($= \frac{3.71}{\ln(2)} Wm^{-2}$).

To calculate the temperature change for a given change in radiative forcing, APMT has primarily used the energy balance model developed by Shine et al. (2005) with the purpose of presenting the global temperature potential concept. The Shine et al. energy balance model assumes the heat capacity of the earth resides in a 100 m deep ocean mixed-layer with a heat capacity of 4.2×10^8 $JK^{-1}m^{-2}$ with no deeper ocean layers. APMT has recently updated its energy balance model based on the results from this study and has now adopted the CICERO-1 energy balance model that will be explained in detail in the CICERO-1 section.

CICERO-1

CICERO-1 was developed to compare the relative physical climate effect of different transportation sectors (road, ship, air, and rail) over the next century (Berntsen and Fuglestvedt, 2008).

Like APMT, CICERO-1 employs the Joos et al. (1996) LRF to describe the relation between CO_2 emissions and atmospheric concentrations adopted from IPCC third assessment report (TAR). The coefficients are derived by calibration against the Bern carbon cycle model, but under a different baseline scenario than the LRFs used by APMT; namely, it is based on an instantaneous release of 40 GTC input into the preindustrial atmosphere (Joos, 2002). CICERO-1 uses a constant specific radiative forcing for CO_2 over time of 1.8×10^{-15} $W/m^2/Kg$ CO_2 (Caldeira and Kasting, 1993).

CICERO-1 uses a 2-box analytical energy balance model composed of an isothermal atmosphere/ocean-mixed-layer box of 70 meters and an isothermal deep ocean box 3000 meters (Berntsen and Fuglestvedt, 2008). Heat transfer between the two layers is represented by a constant advective water mass flux of 1.23×10^{-4} $kgm^{-2}s^{-1}$ from the mixed-layer to the deep ocean, and a turbulent diffusive heat transfer between layers with a diffusion coefficient of 4.4×10^{-5} m^2s^{-1}. The heat capacities for the ocean mixed-layer and deep ocean are $2.94\times10^{8}Jk^{-1}m^{-2}$ and 1.26×10^{10} $JK^{-1}m^{-2}$, respectively (Berntsen and Fuglestvedt, 2008). It is noted that the constant parameters used in CICERO-1 energy balance model were obtained by tuning to an ESM.

CICER0-2

CICERO-2 was implemented to estimate the climate effect of anthropogenic emissions, including the aviation sector, under different emission scenarios (Fuglesvedt and Berntsen, 1999; Skeie et al. 2009). The CICERO-2 carbon cycle is based on the approach by Joos et al. (1996) which simulates the dynamics of a three-box atmosphere-ocean-biosphere system. It uses process specific LRFs for each reservoir (ocean and biosphere) to express the decay of CO_2 impulse in each reservoir, and then calculates the CO_2 partial pressure at each reservoir as a function of total background carbon in each reservoir (Alfsen and Berntsen, 1999), and finally interconnects the

CO_2 partial pressure in ocean and biosphere to the CO_2 partial pressure in atmosphere by explicit treatment of atmosphere-ocean-biosphere mass transfer of CO_2 to account for the nonlinearities in the system. Therefore, its carbon cycle takes into account the nonlinearities in the system as it represents the change in atmospheric CO_2 as a function of total background carbon. The ocean LRF, which represents the mixed-layer carbon content, is calibrated against the HILDA model (Joos et al., 1996). The correlation between mixed-layer background inorganic carbon content and mixed-layer CO_2 partial pressure was calibrated against the three-dimensional Bern carbon cycle (Joos et al., 2001). CICERO-2 accounts for the biosphere response by considering the CO_2 uptake and release of terrestrial vegetation as a function of the CO_2 fertilization effect. The increase in the rate of photosynthesis, relative to preindustrial times, is considered to be proportional to the logarithm of the relative increase in atmospheric CO_2 concentration from its pre-industrial value of 278 ppm. The proportionality constant, known as the CO_2 fertilization factor, is 0.287. CICERO-2 accounts for the feedback of carbon on the carbon cycle through changes in biosphere fertilization and through changes in ocean chemistry.

CICERO-2 uses the hemispheric energy-balance-climate/upwelling-diffusion-ocean model developed by Schlesinger et al. (1992) to derive hemispheric and globally-averaged temperature changes. It is based on the energy exchange between the atmosphere, ocean mixed-layer, and deep ocean. The atmosphere is divided into two boxes in each hemisphere, one over land and one over ocean. The mixed-layer thickness is set to 70 meters and the deep ocean is composed of 40 layers with a uniform thickness of 100 meters. The ocean is subdivided horizontally into the polar region, where bottom water is formed and is recirculated to complete the thermohaline circulation, and the nonpolar region, where there is upwelling. In the nonpolar region, heat is transported upward by upwelling and downward by physical processes the effects of which are considered as an equivalent diffusion. Moreover, heat is also moved from the mixed-layer in the nonpolar region to the polar region, and from there it is transported to the bottom by downwelling. This heat is ultimately transported upward from the ocean floor in the nonpolar region. Vertical upwelling and thermal diffusion happen over the deep ocean with uniform upwelling velocity of $4 myr^{-1}$ and uniform vertical thermal diffusivity of $0.227\ m^2yr^{-1}$. CICERO-2 calculates the global mean temperature change and the individual change in temperature over sea and land in each hemisphere (Andronova and Schlesinger, 2001).

ISAM

ISAM was originally developed to estimate the past carbon budget given past CO_2 concentration, fossil carbon emission, and temperature records, and also to estimate the climate effect of anthropogenic emissions under different emission scenarios (Kheshgi and Jain, 2003). Different versions of ISAM were used to study the effect of CO_2 and climate change on ocean acidification and carbon sequestration in agricultural soils, and also to study the biophysical effect of bioenergy production. ISAM was used for future climate projections from emission scenarios in both the IPCC second assessment report (SAR) (Schimel et al., 1996) and third assessment report (TAR) (Ramaswamy et al., 2001).

The ISAM carbon cycle consists of a simplified one box atmosphere which is coupled to a six-box globally aggregated terrestrial biosphere sub-model that represents ground vegetation, non-woody tree parts, woody tree parts, detritus, mobile soil (turn-over time 75 years), resistant soil (turnover time 500 years); an ocean mixed-layer and a vertically resolved advective-diffusion deep ocean. Air-sea exchange is modeled by an air-sea exchange coefficient in combination with the buffer factor that summarizes the chemical re-equilibration of sea water with respect to CO_2 variations (Jain et al., 1995), and as such accounts for the nonlinearity in ocean chemistry at high CO_2 partial pressures. ISAM has a one-dimensional column ocean that is treated as a mixed-layer with a depth of 70 m, and a deep ocean with a depth of 4000 m that is composed of 40 layers. The transport in the ocean takes place through the thermohaline circulation and depends on upwelling velocity of 3.5 m/yr and eddy diffusivity of 4700 m^2/yr resulting from calibration to the estimated global-mean pre-anthropogenic depth-profile of ocean ^{14}C concentration (Jain et al., 1995). The increase in the rate of photosynthesis, relative to preindustrial times, is modeled to be proportional to the logarithm of the relative increase in atmospheric CO_2 concentration from its pre-industrial value of 278 ppm. The proportionality constant, known as the CO_2 fertilization factor, is 0.45. (Kheshgi and Jain, 2003).

ISAM uses an energy balance model that contains a vertically-integrated atmosphere box, a mixed-layer ocean box, an advective-diffusive deep ocean, and a thin slab representing land thermal inertia. The isothermal mixed-layer depth is 70 meters and is coupled to an advective-

diffusive deep ocean composed of 19 layers of varying thickness (Harvey and Schneider, 1985), with higher resolution near the surface due to the larger temperature gradient. Thermohaline circulation is represented by an advective heat transport between the layers. There is also a diffusive heat transfer term that accounts for small-scale vertical mixing. Thermal diffusivity and upwelling velocity are 0.216 m^2yr^{-1} and 4 myr^{-1}, respectively, and are constant with respect to ocean depth.

There is a coupling between the carbon cycle and the energy balance model in ISAM that accounts for the feedback of climate change on the carbon cycle. ISAM also accounts for carbon feedback on the carbon cycle through the changes in biosphere fertilization and oceanic CO_2 uptake.

LinClim

LinClim (Lim et al., 2007; Lee et al., 2009) is a simplified climate response model, which has expanded the approach presented in Sausen and Schumann (2000), to include the full suite of aviation-specific effects identified by IPCC (1999).

LinClim first derives aviation CO_2 emissions from fuel data. It then calculates CO_2 concentrations resulting from the aviation emissions by using the Hasselmann et al. (1997) LRF. The current version of LinClim uses fit parameters which approximates the results of the Maier-Reimer and Hasselmann (1987) carbon-cycle model.

The simplified expression published in IPCC (2007) is used to calculate CO_2 RF. However, in order to calculate the contribution of aviation CO_2 to RF, LinClim also requires background CO_2 concentration. Historical background CO_2 concentrations are obtained from IPCC observed concentrations, while future concentrations are obtained from other carbon-cycle models or published data. The aviation CO_2 RF is then assumed to be the difference between background RF and RF due to the difference between background and aviation concentrations. In this study, the background concentrations were obtained from the IPCC BERN data (IPCC, 2012).

The temperature response in LinClim is defined by a LRF derived by Hasselmann et al., (1993). The formulation has since been expanded to include the perturbation's efficacy (Lim et al., 2007). This LRF can be tuned to climate models running different types of experiments. There is no constraint on the number of degrees of freedom. Therefore, when tuned, the temperature response is able to approximate the full results of the parent climate model and type of experiment, fully capturing the simulations. At present, LinClim has been tuned to numerous climate models (ECHAM4, CNRM, UM, CMIP3 (phase 3 of the Coupled Model Intercomparison Project, IPCC, 2007) models), running different types of experiments (pulse, transient, $2xCO_2$ and $4xCO_2$). In this study, the temperature LRF has been tuned to reproduce the CMIP3 2xCO2 (equilibrium doubling of CO_2 experiment) behavior of the atmosphere-ocean general circulation model ECHAM5/MPI-OM (Roeckner et al., 2003).

MAGICC6

MAGICC was developed to emulate the results of ESMs and it was used in previous IPCC reports for various scenario analyses (Meinshausen et al., 2008). It combines the carbon cycle response calibration to 9 C4MIP (Coupled Carbon Cycle Climate Model Intercomparison Project) models and climate response calibration to 19 AOGCMs (Atmosphere/Ocean General Circulation Models) that were included in CMIP3.

The MAGICC6 carbon cycle consists of a homogenous atmosphere coupled to a three-box globally aggregated terrestrial biosphere sub-model that represents a living plant box and two dead biomass boxes of detritus and organic matter in soils; and an ocean sub-model. The detail of this carbon cycle is described in (Meinshausen et al., 2011), and same as CICERO-2 carbon cycle, it uses process specific LRFs that are interconnected in order to form a nonlinear carbon cycle model. The ocean sub-model in the MAGICC6 carbon cycle has the same applied analytical representation of LRF as used in CICERO-2 (Joos et al., 2001). However, the difference is that the mixed-layer LRF in MAGICC6 is calibrated against the 3-D-GFDL model (Sarmiento et al., 1992).

MAGICC6 accounts for the atmospheric CO_2 fertilization effect on net primary production. The increase in net photosynthesis due to the CO_2 fertilization effect is modeled as a linear combination of both a logarithmic form and a rectangular hyperbolic form. This is more realistic than the logarithmic form of the relative increase in atmospheric CO_2 concentration used in CICERO-2 and ISAM for both high and low CO_2 concentration as the net primary production does not rise without limit as CO_2 concentrations increase (Meinshausen et al., 2011).

MAGICC6 has an upwelling-diffusion energy model for each hemisphere. It has four boxes with zero heat capacity, one over land and one over the oceans in each hemisphere. The atmospheric boxes are coupled to the ocean mixed-layer in each hemisphere. The ocean sub-model is composed of a mixed-layer and 39 layers of deep ocean of the same thickness to the total depth of 5000 m. Ocean area, upwelling and diffusion throughout the oceans are temperature and depth dependent (Meinshausen et al., 2011). The assumption of constant upwelling and diffusion in the ocean sub-model can lead to an overestimate of the ocean heat uptake for higher warming scenarios if parameter values are based on calibration to lower warming scenarios. However, the temperature-dependent representation of upwelling and diffusion decreases the heat uptake due to thermal stratification and reduced vertical mixing in the higher warming scenarios. The MAGGIC6 energy model has time-varying effective climate sensitivities that are a function of climate state. The change in effective climate sensitivity over time results from the modification of land-ocean heat exchange. MAGICC6 accounts for the feedbacks of both carbon and climate on carbon cycle.

Summary of Carbon Cycles Used in the SCMs

APMT, CICERO-1 and LinClim calculate the CO_2 concentration resulting from an emission perturbation by using IRFs. However, their IRFs are different as they were calibrated against different parent carbon cycle model and/or under different emission scenarios. ISAM has a complex nonlinear carbon cycle that explicitly treats the CO_2 exchange process within the carbon cycle and CICERO-2 uses interconnected process specific IRFs with explicit treatment of air-sea and air-biosphere exchange of CO_2 (Joos et al., 1996, Alfsen and Berntsen, 1999) that forms a nonlinear carbon cycle. The ocean and biosphere IRFs in CICERO-2 express how the

CO_2 impulse is decayed within each reservoir, then the CO_2 partial pressure in each reservoir is calculated as a function of the total background carbon in that reservoir and finally the CO_2 partial pressure in each reservoir is related to the CO_2 partial pressure in atmosphere by explicitly solving for the atmosphere-ocean-biosphere CO_2 mass transfer. Therefore, CICERO-2 carbon cycle takes into account the nonlinearity in ocean chemistry and biosphere uptake at high CO_2 partial pressures since it represents the atmospheric change in CO_2 as a function of total background. Similarly, MAGICC6 uses a nonlinear carbon cycle composed of coupled process specific IRFs and is calibrated towards the combined responses of 9 C4MIP carbon cycle models.

Summary of Energy Balance Models Used in SCMs

APMT has primarily used the energy balance model developed by Shine et al. (2005) with the purpose of presenting the global temperature potential concept. Shine et al. energy balance model assumes that atmosphere only dose exchange heat with just a slab year of ocean of about 100 m and does not consider the heat transport to the deap ocean. APMT has recently updated its energy balance model based on the results from this study and has now adopted the CICERO-1 energy balance model that will be explained in detail in the CICERO-1 section. CICERO-1 uses a 2-box analytical energy balance model composed of an isothermal atmosphere/ocean-mixed-layer box of 70 meters and an isothermal deep ocean box of 3000 meters, and accounts for the heat transfer between the layers (Berntsen and Fuglestvedt, 2008). CICERO2, MAGICC6 and ISAM all have multi-layer ocean sub-models and they account for the heat transfer between the layers. CICERO-2 uses the hemispheric energy-balance-climate/upwelling-diffusion-ocean model developed by Schlesinger et al. (1992) to derive hemispheric and globally-averaged temperature changes. It is based on the energy exchange between the atmosphere, ocean mixed-layer, and deep ocean. The mixed-layer thickness is set to 70 meters and the deep ocean is composed of 40 layers with a uniform thickness of 100 meters. MAGICC6 has an upwelling-diffusion energy model for each hemisphere. It has four boxes with zero heat capacity, one over land and one over the oceans in each hemisphere. The atmospheric boxes are coupled to the ocean mixed-layer in each hemisphere. The ocean sub-model is composed of a mixed-layer and 39 layers of deep ocean of the same thickness to the total depth

of 5000 m. ISAM uses an energy balance model that contains a vertically-integrated atmosphere box, a mixed-layer ocean box, an advective-diffusive deep ocean, and a thin slab representing land thermal inertia. The isothermal mixed-layer depth is 70 meters and is coupled to an advective-diffusive deep ocean composed of 19 layers of varying thickness (Harvey and Schneider, 1985), with higher resolution near the surface due to the larger temperature gradient. LinClim energy balance model is an IRF based model that has been tuned to reproduce the CMIP3 2xCO2 (equilibrium doubling of CO_2 experiment) behavior of the atmosphere-ocean general circulation model ECHAM5/MPI-OM (Roeckner et al., 2003). More detailed descriptions of SCMs energy balance models are provided in the following sections.

Table 2.1 lists the main characteristics of each SCM sub-models. All of the SCM's simulations in this study were run using a single set of parameters (two sets in the case of APMT). Some of the SCMs used in this study (APMT and MAGICC6) are designed to produce a likely range of climate response. However, the intercomparison of SCMs' results presented here is not intended to show an absolute or likely range of climate response, but only how each SCM compares to other SCMs on a similar basis.

Tabel 2.1. Characteristic of each SCM sub-models.

Models	**Carbon Cycle Sub-model**	**Energy balance sub-model**	**Feedback between carbon cycle and energy balance sub-models**
APMT	LRF	1-Box	No
CICERO-1	LRF	2-Box	No
CICERO-2	Non-linear Process specific	hemispheric upwelling-diffusion-ocean model	No
ISAM	Non-linear Process specific	upwelling-diffusion-ocean model	Yes
LinClim	LRF	LRF tuned to ECHAM5/MPI-OM $2xCO_2$ experiment	No
MAGICC6	Non-linear Process specific	hemispheric upwelling-diffusion-ocean model	Yes

Results and Discussion

Intercomparison of Carbon Cycle Models

Carbon cycle is a complex series of processes through which all the carbon is cycled through different part of the Earth system. Carbon cycle is considered a nonlinear system due to the nonlinearities in ocean and biosphere uptake of CO_2. There is nonlinearity in ocean uptake as at high CO_2 partial pressure (above 50% of preindustrial level (Alfsen and Berntsen, 1999; Joos et al., 1996)), ocean uptake of atmospheric CO_2 decreases due to higher oceanic dissolved CO_2 concentration, and less CO_2 is available to be mixed down to the deep ocean by the thermohaline circulation. There is also nonlinearity in biosphere carbon uptake and it is usually assumed that biosphere uptake varies proportional to the logarithm of the atmospheric CO_2 partial pressure. Due to the nonlinearities in ocean and biosphere uptake of CO_2, aviation CO_2 effects over time are determined by calculating the effects of all the human-made sources (background scenario) and subtracting the effects of all the human-made sources excluding aviation. In this case the calculation of the aviation induced changes in CO_2 concentration is affected by the nonlinearities arising from to the growth of carbon emissions in the background scenario. Therefore, it is important for the carbon cycle models to do well in producing the background CO_2 concentration. Figure 2.1 shows the carbon cycle response of MAGICC6, CICERO-2, ISAM, and APMT to the IPCC A1FI and B1 SRES bounding CO_2 background emission scenarios relative to the IPCC AR4 mean and the ± 1 standard deviation (SD) range of CO_2 concentration projections (IPCC, 2007). The AR4 ± 1 SD range of CO_2 concentration was emulated by adjusting the MAGICC model version 4.2 (Wigley and Raper, 2001) to a set of carbon cycle models from the "C4MIP" project (hereafter called "± 1 SD range of AR4 CO_2 concentrations") (IPCC, 2007). LinClim and CICERO-1 results are not included in this figure as they do not treat background CO_2 emissions. Their linear carbon cycles (IRFs) models are applied only to aviation CO_2 emissions; background CO_2 emissions are not included in the calculations of the CO_2 concentration.

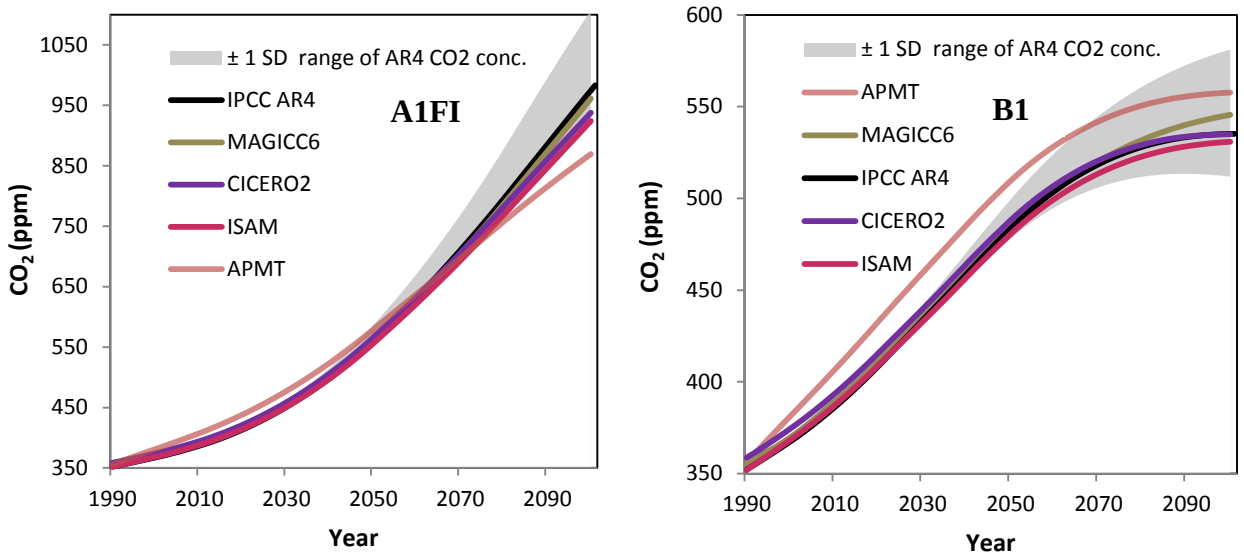


Figure 2.1. Simple climate model projections of CO_2 concentration for the IPCC SRES A1FI and B1 CO_2 emission scenarios. The mean and ±1 SD of the range of results from the IPCC AR4 projections [IPCC, 2007] are also shown.

The results indicate that the carbon cycle of all the SCMs but APMT produce a comparable CO_2 concentration. However, the APMT response to the B1 emission scenario is about 20 ppm higher than the average response from the other models and the mean CO_2 concentration reported in AR4. The APMT response to the A1FI emission scenario is higher than that of the other models and of the mean IPCC up to 2050, and is lower than the other models after 2070, amounting to about 80 ppm lower response at year 2100 compared with the averaged response of the other models. Moreover, results indicate that the projection of all the models but APMT falls within the ± 1 SD range of AR4 CO_2 concentration projection; however, the APMT results fall outside the AR4 ± 1 SD range for the majority of the simulated time horizon. The reason for such behavior is that APMT uses an IRF for its carbon cycle. The APMT IRF, which is suitable for describing the CO_2 perturbations within the linear region, does not perform as well outside this region (when the increase in atmospheric CO_2 concentration is approximately above 50% of the preindustrial level (Joos et al., 1996)). The results in Figure 2.1 indicate that all SCMs that use a nonlinear carbon cycle produce similar CO_2 concentrations.

Figure 2.2 shows the carbon cycle response of the SCMs to constant annual aviation

emissions of 654 Tg CO_2 starting at year 2000 (Fuglestvedt et al., 2008) and continuing to 2100, under A1FI, A2, A1B and B1 IPCC background emission scenarios. The results show that both APMT and CICERO-1 produce 4 and 3.8 ppm change in atmospheric CO_2 concentration by 2100, respectively, while LinClim produces about 4.8 ppm change in CO_2 by 2100. This is simply due to the fact that these SCMs have been tuned to different parent models and under different emission scenarios. For all other models the projection of CO_2 concentration at 2100 varies from about 4.3 to about 5.3 ppm. CICERO-2, MAGICC6 and ISAM all produce higher aviation-induced CO_2 concentrations relative to APMT, CICERO-1 and LinClim, and their projections of aviation-induced CO_2 concentration vary proportional to the growth in the background scenario. The larger the CO_2 emission spread is over time in the background emission scenario, the higher the divergence would be, since due to the nonlinearities in the carbon cycle, higher background carbon emissions would further lower the ocean and biosphere uptake of additional CO_2 emissions. The increase in spread over time shows the importance of the background scenario on projections of aviation-induced CO_2 concentration. CICERO-1 and LinClim's projection of aviation-induced CO_2 concentration is independent of the background emission scenarios as expected since they do not include the background CO_2 emissions in their calculations. Also, due to their use of IRFs carbon cycle models their projection of aviation-induced CO_2 concentration would have been independent of the background emission scenarios. APMT uses IRF as its carbon cycle that does not account for the nonlinear changes in ocean and biosphere carbon uptake as the background carbon increases. This would be true for any other carbon cycles that use an IRF (i.e. CICERO-1 and LinClim). Therefore, for carbon cycles that use IRF, the projection of future CO_2 concentration is independent of the growth rate in the background emission scenario. Results in Figure 2.2 indicate that regardless of the fact that aviation CO_2 emission might be small enough that such perturbation can be within a linear region for IRF to be applicable, due to the effect of background CO_2 emissions and nonlinearities in carbon cycle, a single IRF cannot be used to address the changes in future (~ beyond 50 years in future) CO_2 concentration induced by aviation.

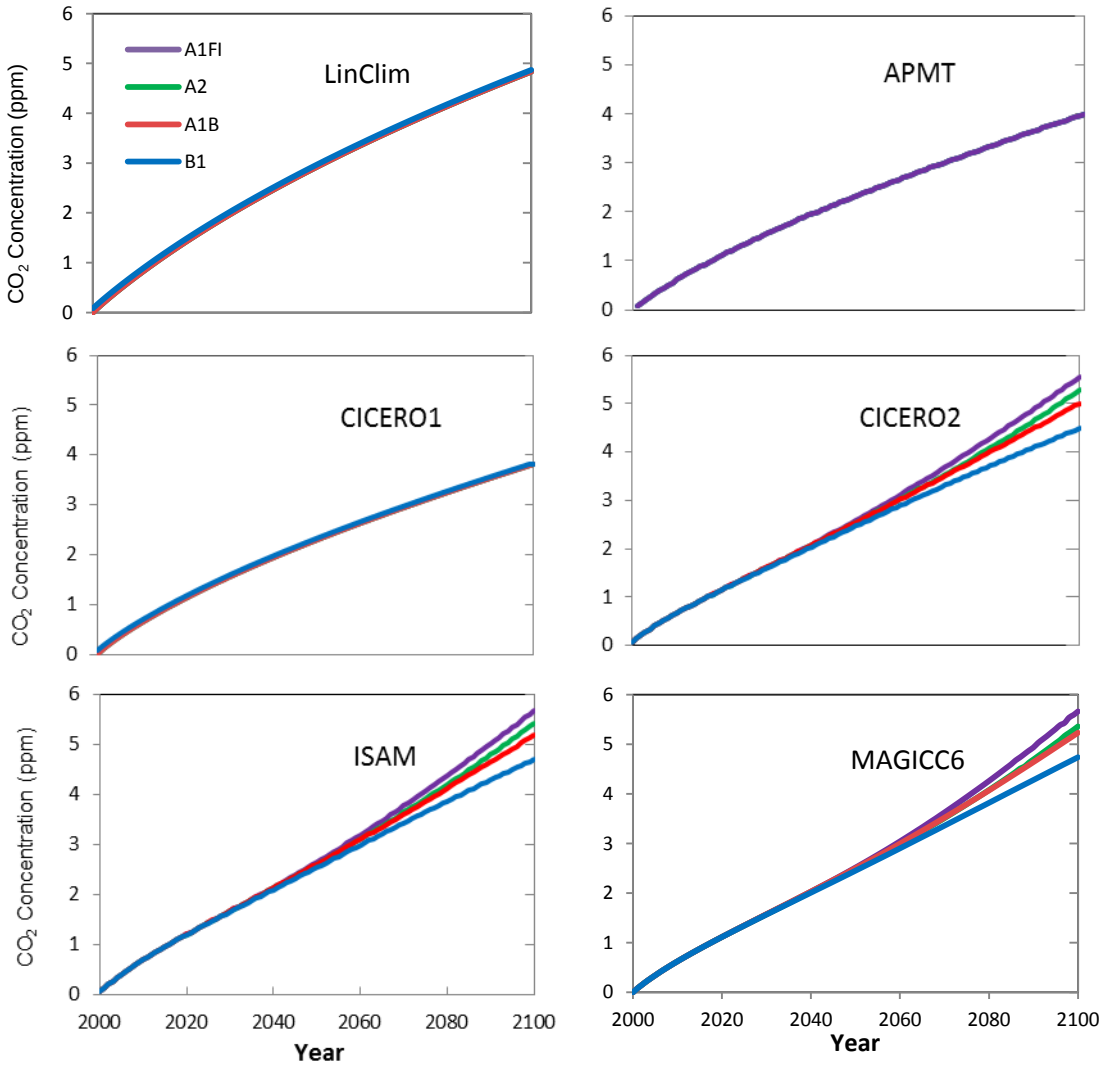


Figure 2.2. Simple climate model simulated CO_2 concentration for constant CO_2 emissions of 654 Tg/yr (starting in 2000) for different IPCC SRES background CO_2 emissions scenarios.

Results in Figure 2.2 indicate that CICERO-2, MAGICC6 and ISAM produce similar atmospheric CO_2 concentrations, despite the differences in their carbon cycles, as they all account for the nonlinearities in ocean chemistry and biosphere uptake at high CO_2 partial pressure. It is noted that some of the SCMs (i.e. MAGICC6 and ISAM) consider the temperature feedback on carbon cycle; but for the time scale and projected temperature change considered in this comparison, the temperature feedback due to incremental changes in aviation CO_2 has a

negligible effect on the results presented in this figure (at most 2.5% by 2100).

Figure 2.3 shows the changes in CO_2 concentration projected by the SCMs relative to IPCC analyses (IPCC, 1999) for the aviation Edh emission scenario, the high-growth scenario, starting at 1990 and continuing to 2050, with zero emissions afterward, and the IPCC A1B scenario as the background. The IPCC (1999) analyses of the future change in CO_2 concentration were obtained by adjusting the Wigley (1993) carbon cycle model to the results of ISAM (Jain et al., 1994) and Bern (Siegenthaler and Joos, 1992; Joos et al., 1996) models. The aviation Edh scenario was selected for this comparison since it is the upper bound aviation emission scenario and makes the model's responses to be more evident for the purpose of our comparison. Results show that the projected CO_2 concentration from APMT and CICERO-1 model that use IRF for their carbon cycle, drops off faster compared with other models when the emissions stop. LinClim that uses IRF with parameters tuned to the Hasselmann et al. (1997) carbon cycle model produces a higher response compared with APMT and CICERO-1 for the first 80 years and then its projected CO_2 concentration drops off as fast as APMT and CICERO-1 and falls below MAGICC6, CICERO-2 and ISAM by 2100.

The behavior of these IRFs points to the possibility of finding a particular IRF that provides a closer response to a reference line (in this case IPCC 1999 projections) for emission scenarios inside the original calibration space, but that would not agree as well for a scenario outside the original calibration range (Joos et al., 1996; Meinshausen et al., 2011). MAGICC6, CICERO-2 and ISAM models produce similar changes in atmospheric CO_2 concentration as they account for the nonlinearities in ocean chemistry and biosphere uptake. They also produce similar changes in atmospheric CO_2 concentration compared with IPCC (1999).

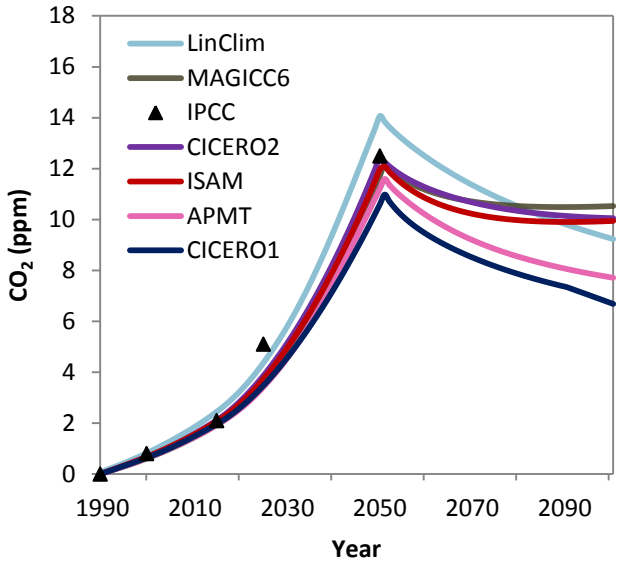


Figure 2.3. Changes in CO_2 concentrations derived for the APMT, CICERO1, CICERO2, ISAM, LinClim, and MAGICC6 simple models for the CO_2 emissions of Edh aviation scenario up to 2050 and zero emissions afterward and A1B as the background scenario. The IPCC projections [IPCC, 1999] are also shown. The IPCC projection used the IS92a background scenario.

Intercomparison of Energy Balance Models

Energy balance model estimates the change in the climate system temperature based on the change in the climate system radiaive forcing. In this section the capability of SCMs energy balance model to calculate the temperature change induced by aviation forcings are compared. For the intercomparison of the SCMs' energy balance models, all of the SCMs were run with climate sensitivity of 3 ^{o}C and a mixed-layer depth of 70 meters, which in most models was the default setting. APMT has a default mixed-layer depth of 100 meters, and was run with both a mixed-layer depth of 70 and 100 meters.

Figure 2.4 presents the temperature response of the SCMs energy balance models to total radiative forcing from IPCC AR4 A1FI and B1 bounding scenarios obtained from MAGICC model (version 4.2). The temperature responses of SCMs were compared with the AR4 median and the ± 1 SD range of AR4 temperature projections. The AR4 ± 1 SD range was emulated by

adjusting MAGICC model (version 4.2) to the combined results of C4MIP and the annual average temperature results of 17 coupled atmosphere-ocean general circulation models (AOGCMs) from the "CMIP3" project (hereafter called "± 1 SD range of AR4 temperature") (IPCC, 2007). The AR4 multi-model likely range for temperature (based on the full temperature range of the 17 AOGCMs that participated in the CMIP3 intercomparison project), is also shown in the grey bars in the right side of Figure 4 for the year 2100.

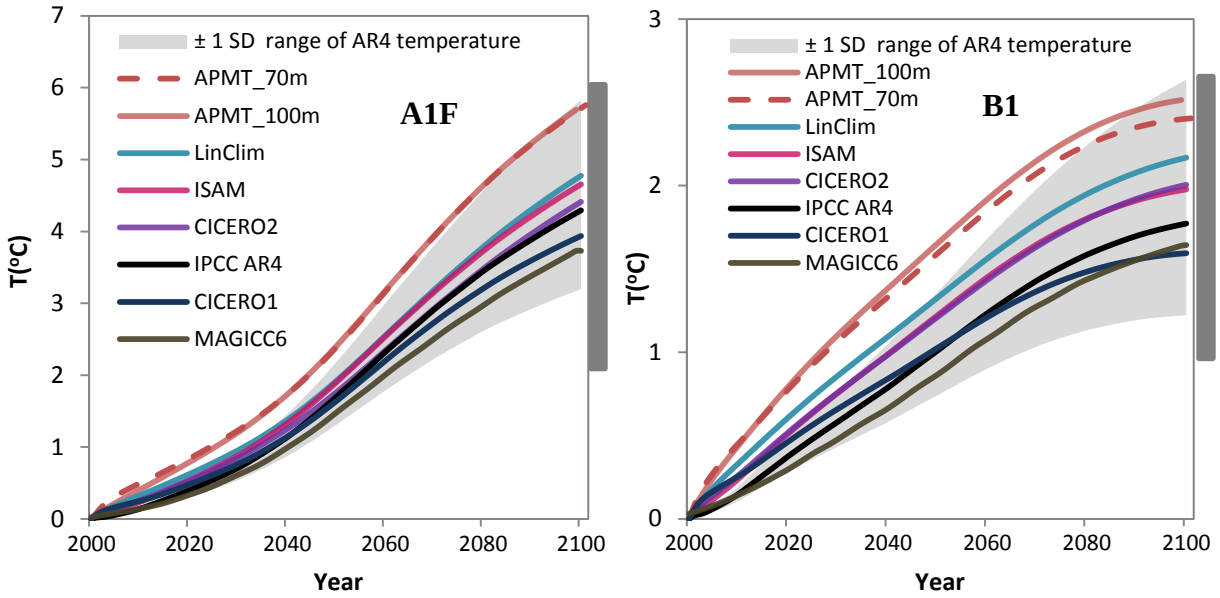


Figure 2.4. Temperature change (relative to year 2000) projected by APMT, ISAM, CICERO-2, CICERO-1, LinClim, MAGICC6 and IPCC for 2000 to 2100 in response to IPCC AR4 total radiative forcing (Wm^{-2}) (GHG plus direct and indirect aerosol effects) for the A1FI and B1 scenarios. The AR4 multi model likely ranges for the year 2100 are shown in the grey bars to the right of the figure.

APMT, CICERO-1, CICERO-2, LinClim and ISAM energy balance models were forced with RFs from the IPCC AR4 (IPCC, 2007) for total radiative forcing from 1990 to 2100. All the temperature responses in Figure 4 are relative to year 2000 and the MAGICC6 temperature response is for the respective IPCC AR4 emission scenario, not forced with RFs from the IPCC AR4. However, MAGICC6 calculated RFs for the respective scenarios are within the 2% of the IPCC AR4 RFs. All of the SCMs' temperature responses lie within the AR4 multi-model likely range for the year 2100 and except for APMT lie within the ± 1 SD range of AR4 temperature

projections (Figure 2.4). APMT, by virtue of using the Shine energy balance model (Shine et al., 2005), which considers heat transfer to mixed-layer ocean as the sole heat transfer mechanism in the climate system (single time scale), produces the largest temperature response for both the A1FI and B1 scenarios among other SCMs. It also produce the highest temperature change compared with the mean and the ± 1 SD range of AR4 temperature projections for both a mixed-layer depth of 70 and 100 meters, and lies at the outer edge or outside of the ± 1 SD range of AR4 temperature projections for most of the simulated time horizon. LinClim which uses the IRF with multiple time scales for the dominant heat transfer mechanisms in the climate system, tuned to ECHAM5 (Roeckner et al., 2003) gives a temperature change consistent with other SCMs that use energy balance models with upwelling-diffusion ocean sub-models.

Figure 2.5 shows the temperature change derived by the APMT, CICERO-1, CICERO-2, LinClim and ISAM models relative to the temperature change projected by IPCC (1999) by forcing their energy balance model with RFs from the Edh aviation forcing scenario starting at 1990 (IPCC, 1999). The RFs include all aviation forcings. The IPCC (1999) analyses of the future aviation-induced temperature change were obtained by adjusting the upwelling-diffusion, energy balance model of Wigley and Raper (1992) and Raper et al. (1996) to AOGCMs results. MAGICC6 temperature response is to the Edh emission scenario, not forced with RFs from the Edh scenario. The temperature responses in Figure 2.5 are relative to the year 2000. Forcings before 1990, which were included in the IPCC projection, were not considered in these simulations as there were not reported in IPCC 1999. However, the inclusion of pre-1990 forcings only changes the results slightly (at most 3% if we assume pre-1990 forcings were same as 1990 forcing), and does not affect our forthcoming conclusion that APMT produces noticeably higher warming (about 33%) compared with other SCMs by not including the heat transfer to deep ocean.

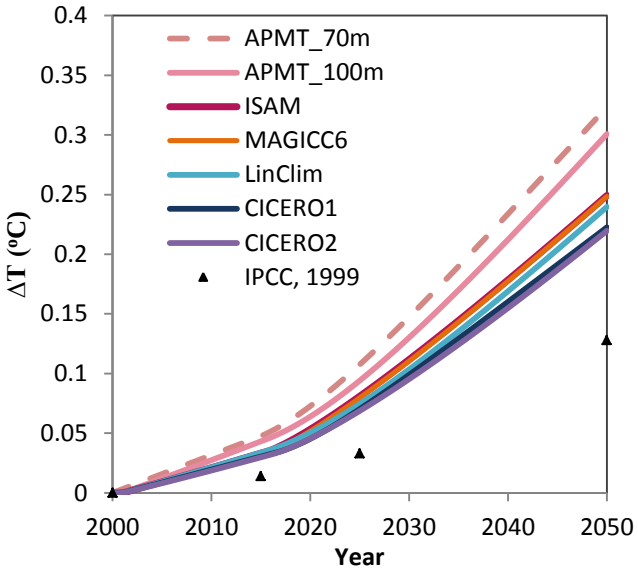


Figure 2.5. Changes in temperature derived by APMT, CICERO1, CICERO2, ISAM, LinClim and MAGICC simple models relative to IPCC projection [IPCC, 1999]. The SCMs were forced with radiative forcings for Edh aviation scenario from IPCC (1999).

All of the SCMs produce a higher temperature change relative to IPCC (1999). However, all of the SCMs but AMPT produce similar aviation-induced temperature change on the time scale of 10-50 years. Results in Figure 5 show that the CICERO-1 energy model with a 2-box ocean sub-model and the LinClim temperature IRF that is tuned to ECHAM5 can provide a similar response compared with ISAM and MAGICC6 that are energy balance models with upwelling-diffusion ocean sub-models. APMT produces 33% and 28% higher temperature changes than the other models for mixed-layer depth of 70 and 100 meters, respectively, due to using a one-box mixed-layer ocean sub-model. The APMT energy balance model with the mixed-layer depth of 70 meters produces about 5% higher temperature change at 2050 than if it were to use a mixed-layer depth of 100 meters.

Conclusions

In this study we compared the capability of six widely used SCMs that were each previously evaluated independently, to project climate effects associated with CO_2 emission from

aviation. This resulted in recognizing the factors that lead to similar performance in some SCMs and the factors that lead to some SCMs to be outliers in certain areas. This intercomparison resulted in recommendations about how best to represent carbon cycle and energy balance models in SCMs to gauge aviation-induced climate change.

Several factors come into play when choosing a simple climate model to quantify aviation effects on the climate. These factors are the reliability of the representation of the carbon cycle, non-CO_2 emissions effects and the representation of energy balance processes as well as the capability to project a possible range of future responses and the capability to assess the economic impacts of aviation. Among the models evaluated in this study, several are already designed to consider a full suite of aviation effects (APMT, CICERO-1, CICERO-2, LinClim and MAGICC6), while the ISAM model is not. CICERO-2, MAGICC6, and ISAM have a carbon cycle that addresses the nonlinearity in the ocean and terrestrial biosphere carbon uptake, and therefore are better suited for aviation scenarios outside the linear regime. MAGICC6 and CICERO-2 carbon cycles are simpler than ISAM's, however, since they use IRFs in combination with separate equations describing air-sea and atmosphere-biosphere CO_2 exchange, they extend the use of linear IRFs to the nonlinear domain and give a good approximation (to within 10%) of a more complex carbon cycle models.

All of the models, with the exception of the version of APMT used in this study, include either parameterized or explicit calculations of energy exchange within the deep ocean, and hence are expected to perform better for calculations of temperature change, including those from aviation effects. CICERO-1 and LinClim have the simplest energy models that address the heat exchange with the deep ocean. CICERO-1 has a 2 box-ocean sub-model but gives comparable results (to within 10%) to MAGICC6, ISAM, and CICERO-2 that have more complex energy models with upwelling-diffusion ocean sub-models. The LinClim energy balance model is based on an IRF tuned to the ECHAM5 coupled atmosphere ocean general circulation model and can also provide a relatively good (to within 8%) representation of energy balance models with an upwelling-diffusion ocean sub-model. The ultimate choice of SCMs depends on the type of application and the availability of suitable fit parameters for the particular type of application; but it would seem reasonable to include a carbon cycle capable for

addressing emission scenarios outside the linear regime and an energy balance model accounting for heat exchange within the deep ocean, as these greatly expand the applicable region in terms of background and future scenarios while adding little computational cost. However when calculating the impact of all aviation impacts (not just carbon cycle and energy balance models addressed here) it is important that the treatment of those processes is adequately represented. It is noted that depending on the type of application, the ultimate chose of SCMs also depends on their capability to provide a possible range of future aviation-induced climate responses, and also, the capability to calculate the economic impacts of aviation. Currently, among the SCMs we studied, APMT and MAGICC6 are the only ones currently set up to be able to do Monte Carlo simulations to produce a possible range of future aviation climate impacts, and AMPT is the only one capable of projecting aviation impacts from emissions to physical impacts to economic impacts.

BIBLIOGRAPGY

Alfsen, K. H., and T. Berntsen (1999), An efficient and accurate carbon cycle model for use in simple climate models, CICERO, Oslo, Norway.

Berntsen, T., J. S. Fuglestvedt (2008), Global temperature responses to current emissions from the transport sectors, *Proceedings of the National Academy of Sciences*, USA 105, 19154–19159.

Caldeira, K., J. F. Kasting (1993), Insensitivity of Global Warming Potentials to Carbon Dioxide Emission Scenarios, *Nature*, 366: 251-253.

Fuglesvedt, J. S., and T. Berntsen (1999), A simple model for scenario studies of changes in climate, Version 1.0, CICERO, Oslo, Norway, pp. 59.

Fuglestvedt, J. S., T. Berntsen, G. Myhre, K. Rypdal and R. B. Skeie (2008), Climate forcing from the Transport Sectors, *Proceedings of the National Academy of Sciences (PNAS)*, vol 105 (no. 2): pp. 454-458.

Hasselmann, K., R. Sausen, E. Maier-Reimer, R. Voss (1993), On the cold start problem in transient simulations with coupled atmosphere-ocean models, *Climate Dynamics*, Volume 9, Issue 2, 53 – 61.

Hasselmann, K., S. Hasselmann, R. Giering, V. Ocana, H. V. Storch (1997), Sensitivity Study of Optimal CO_2 Emission Paths Using a Simplified Structural Integrated Assessment Model (SIAM), *Climatic Change*, Volume 37, Issue 2, 345 – 386.

Hooss, G., R. Voss, K. Hasselmann, E. Maier-Reimer, F. Joos (2001), A nonlinear impulse response model of the coupled carbon cycle-climate system (NICCS)", *Climate Dynamics*, Volume 18, Issue 3 – 4, 189 – 202.

IPCC (2007), Climate Change 2007: The Physical Science Basis, In: Solomon, S., D. Qin, M. Manning, Z. Chen, M. Marquis, K.B. Averyt, M.Tignor and H.L. Miller (Eds.), Contribution of Working Group I to the Fourth Assessment Report of the IPCC, Cambridge University Press, Cambridge, United Kingdom and New York, NY, USA.

IPCC (1999), Aviation and the global atmosphere, Penner, J. E., D.H. Lister, D.J. Griggs, D.J. Dokken, M. McFarland, (Eds.), Intergovernmental Panel on Climate Change. Cambridge University Press, Cambridge, UK.

IPCC (2012), http://www.ipcc-data.org/ancilliary/tar-bern.txt.

Jain, A. K., and X. Yang (2005), Modeling the effects of two different land cover change data sets on the carbon stocks of plants and soils in concert with CO_2 and climate change. *Global Biogeochemical Cycles*, 19, GB2015, doi:10.1029/2004GB002349.

Jain, A. K., H. S. Kheshgi, and D. J. Wuebbles (1994), Integrated science model for assessment of climate change, UCRL-JC-116526, Lawrence Livermore Nat. Lab., Livermore, Calif.

Jones, C. et al. (2011), The HadGEM2-ES implementation of CMIP5 centennial simulations, *Geoscientific Model Development*, 4, 543–570, doi:10.5194/gmd-4-543-2011.

Joos, F., M. Bruno, R. Fink, T. F. Stocker, U. Siegenthaler, C. LeQue´re ´, and J. L. Sarmiento (1996), An efficient and accurate representation of complex oceanic and biospheric models for anthropogenic carbon uptake, *Tellus*, 48B, 397–417.

Joos, F., I. C. Prentice, S. Sitch, R. Meyer, G. Hooss, G. K. Plattner, S. Gerber, K. Hasselmann (2001), Global warming feedbacks on terrestrial carbon uptake under the IPCC emission scenarios, *Global Biogeochemical Cycles*,15, pp. 891–907.

Joos, F., (2002) http://unfccc.int/resource/brazil/carbon.html.

Kheshgi, H. S., A. K. Jain, R. Kotamarthi, D. J. Wuebbles (1999), Future atmospheric methane concentrations in the context of the stabilization of greenhouse gas concentrations, *Journal of Geography Research*, 104, 19,183-19,190.

Kheshgi, H. S., and A. K. Jain (2003), Projecting future climate change: Implications of carbon cycle model intercomparison, *Global Biogeochemical Cycles*, 17(2), 1047, doi: 10.1029/2001GB001842.

Lee, D. S. , D. W. Fahey, P. M. Forster, P. J. Newton, R. C. N. Wit, L. L. Lim, B. Owen, R. Sausen (2009), Aviation and global climate change in the 21st century, *Atmospheric Environment*, doi:10.1016/j.atmosenv.2009.04.024.

Li, S., A. J. Jarvis, D. Leedal (2009), Are response function representations of the global carbon cycle ever interpretable?, *Tellus*, 61B:361–371.

Lim, L., D. S. Lee, R. Sausen, M. Ponater (2007), Quantifying the effects of aviation on radiative forcing and temperature with a climate response model, Proceedings of an International Conference on Transport, Atmosphere and Climate (TAC). Office for Official Publications of the European Communities, Luxembourg, ISBN 92-79-04583-0, pp. 202–207.

Maier-Reimer, E., and K. Hasselmann (1987), Transport & storage of CO_2 in the ocean - an inorganic ocean-circulation carbon cycle model. *Climate Dynamics*, 2, 63 - 90.

McCarthy, J., (2010), Aviation and climate change, in G. Blumenthal (ed.), Aviation and climate change (USA: Nova Science Publishers, Inc.).

Mahashabde, A., et al. (2011), Assessing the environmental impacts of aircraft noise and emissions, *Progress in Aerospace Sciences*, 47, 1, 15-52.

Marais, K., S. P. Lukachko, M. Jun, A. Mahashabde, and I. A. Waitz (2008), Assessing the impact of aviation on climate, *Meteorologische Zeitschrift*, 17(2): 157-172.

Marten, A. L., (2011), Transient Temperature Response Modeling in IAMs: The Effects of Over Simplification on the SCC, *Economics*: The Open-Access, Open-Assessment E-Journal.

Meinshausen, M., S. C. B. Raper and T. M. L. Wigley (2008), Emulating IPCC AR4 atmosphere-ocean and carbon cycle models for projecting global-mean, hemispheric and land/ocean temperatures: MAGICC 6.0, *Atmospheric Chemistry and Physics Discuss*, 8, 6153–6272.

Meinshausen, M., S. C. B. Raper, and T. M. L. Wigley (2011), Emulating coupled atmosphere-ocean and carbon cycle models with a simpler model, MAGICC6 – Part 1: Model description and calibration, *Atmospheric Chemistry and Physics*, 11, 1417–1456, doi:10.5194/acp-11-1417.

Ramaswamy, V., O. Boucher, J. Haigh, D. Hauglustaine, J. Haywood, G. Myhre, T. Nakajima, G. Y. Shi, S. Solomon (2001), Intergovernmental Panel on Climate Change: Chapter 6. Radiative Forcing of Climate Change, In: Climate Change 2001: The Scientific Basis (J. T. Houghton, et al. eds, Cambridge, U.K.: Cambridge University Press).

Raper, S. C. B., T. M. L. Wigley, and R. A. Warrick (1996), Global sea level rise: Past and future. Sea-Level Rise and Coastal Subsidence: Causes, Consequences and Strategies, J. Milliman and B. U. Haq, Eds., *Kluwer Academic*, 11–45.

Roeckner, E, G. Baeuml, L. Bonventura, R. Brokopf, M. Esch, M. Giorgetta, S. Hagemann, I. Kirchner, L. Kornblueh, E. Manzini, A. Rhodin, U. Schlese, U. Schulzweida, and A. Tompkins (2003), The atmospheric general circulation model ECHAM5. PART I: Model description, Report 349, Max Planck Institute for Meteorology, Hamburg, Germany.

Sausen, R., U. Schumann (2000), Estimates of the Climate Response to Aircraft CO_2 and NOx Emissions Scenarios, *Climatic Change*, 44, 1-2, 27-58, DOI 0.1023/A:1005579306109.

Schimel, D., D. Alves, I. Enting, M. Heimann, F. Joos, D. Raynaud and T. Wigley (1996), CO_2 and the carbon cycle, in Climate Change 1995: The Science of Climate Change: Contribution of WGI to the Second Assessment Report of the IPCC, edited by J.T. Houghton et al., pp. 65-86, cambridge University Press, New York.

Sarmiento, J. L., J. C. Orr, and U. Siegenthaler (1992), A perturbation simulation of CO_2 uptake in an ocean general circulation model, *Journal of Geography Research*, 97, 3621–3645, 6163, 6204.

Shine, K. P., J. S. Fuglestvedt, K. Hailemariam, N. Stuber (2005), Alternatives to the global warming potential for comparing climate impacts of emissions of greenhouse gases, *Climatic Change*, Volume 68, Issue 3, Feb, Pages 281 - 302, DOI 10.1007/s10584-005-1146-9.

Siegenthaler, U. and F. Joos (1992), Use of a simple model for studying oceanic tracer distributions and the global carbon cycle, *Tellus, 44B*, 186-207.

Schlesinger, M. E., X. Jiang, and R. J. Charlson (1992), Implications of anthropogenic atmospheric sulphate for the sensitivity of the climate system, Reprinted form Climate Change and Energy Policy, American Institute of Physics, New York.

Skeie, R. B., J. S. Fuglestvedt, T. Berntsen, M. Lund Tronstad, G. Myhre and K. Rypdal (2009), Global temperature change from the transport sectors: Historical development and future scenarios, *Atmospheric Environment*, 43 (39), pp. 6260-6270.

Thompson, M. V. and J. T. Randerson (1999), Impulse response functions of terrestrial cycle models: method and application, *Global Change Biology*, 5:371–394.

van Vuuren, D. P., J. Lowe, E. Stehfest, L. Gohar, A. F. Hof, C. Hope, R. Warren, M. Meinshausen, G. K. Plattner (2009), How well do integrated assessment models simulate climate change? Climatic Change. doi:10.1007/s10584-009-9764-2.

Warren, R., M. Mastrandrea, C. Hope, and A. Hof (2010), Variation in the climatic response to SRES emissions scenarios in integrated assessment models, *Climatic Change*, 102(3): 671{685. doi:10.1007/s10584-009-9769-x.

Wigley, T. M. L. and S. C. B. Raper (1992), Implications for climate and sea level of revised IPCC emissions scenarios, *Nature*, 357, 293–300.

Wigley, T. M. L. (1993), Balancing the carbon budget: Implications for projections of future carbon dioxide concentration changes, *Tellus*, 45B, 409–425.

Wigley, T. M. L. and S. C. B. Raper (2001), Interpretation of high projections for global-mean warming, *Science*, 293, 451–454.

CHAPTER 3: AVIATION 2006 NOx-INDUCED EFFECTS ON ATMOSPHERIC OZONE AND OH IN COMMUNITY EARTH SYSTEM MODEL (CESM)

Abstract

The interactions between atmospheric chemistry and ozone (O_3) in the upper troposphere and lower stratosphere (UTLS) present one of the major uncertainties in understanding the effects of aviation on climate. In this study, the latest atmospheric model components, CAM4 and CAM5, from the Community Earth System Model (CESM), developed primarily at NCAR, are used to evaluate the effects that aircraft nitrogen oxides (NOx) emissions have on ozone and the background chemistry in the UTLS. CAM4 and CAM5 both have extensive tropospheric and stratospheric chemistry with about 133 species and 330 photochemical reactions. Updates to CAM5 include a new modal aerosol module (MAM) whereby CAM4 uses a bulk aerosol module. To examine the impact of this update on the aviation NOx induced ozone distribution, results from the CAM5 simulation were compared to the CAM4 simulation. NOx emissions for 2006 were obtained from the inventory of the AEDT (Aviation Environmental Design Tool) global commercial aircraft emissions. Being the first study with CAM5 that runs the model with full chemistry, it is important to confirm that the background atmosphere is represented accurately, therefore a set of diagnostic tests were done to evaluate the performance of each of the models in simulating the background ozone and other relevant chemical species in the troposphere and lower stratosphere. The comparison of simulated O_3 concentration to ozonesonde measurements at representative levels in the troposphere and different regions indicate that the average percent difference in O_3 concentration for all locations is 13% in CAM5 and 18% in CAM4. Results show a localized increase in aviation-induced O_3 concentrations at aviation cruise altitudes that stretches from 40^oN to the North Pole. The results indicate a higher production of aviation NOx-induced ozone in CAM5 compared to CAM4 with the annual mean tropospheric O_3 perturbation of 1.0 ppb for CAM4 and 1.3 ppb for CAM5. Aviation emissions further result in increasing OH concentrations and an increase in the methane (CH_4) loss rates and therefore reduced the methane lifetimes in CAM4 and CAM5 by 1.40% and 1.86%, respectively. Aviation NOx

emissions are associated with a change in global mean O_3 radiative forcing (RF) of 36.5 and 43.9 mWm^{-2} in CAM4 and CAM5, respectively. While, there are differences in the simulated O_3 concentration and background atmosphere between the two models due to the different representation of the background atmosphere, the differences are smaller than current estimates of the uncertainty in aviation effects on ozone.

Introduction

The aviation industry has grown rapidly since its nascence, at a rate of 9% per year for passenger traffic between 1960 and 2000 (IPCC, 1999) and is one of the fastest growing transportation sectors (IPCC, 2008). Despite several international economic and other setbacks over the last few decades, including large price increases for fuel, and a global recession, the aviation industry continues to experience growth. The 2013 FAA forecast calls for an annual average increase of 2.2% per year in U.S. passenger carrier growth over the next twenty years. The growth is predicted to be slightly greater for the first five years under the assumption of a faster U.S. economic growth rate (FAA, 2013). As such, it is crucial to assess the potential impacts that aviation will have on future climate.

Aviation affects climate in various ways. The main concerns to climate result from the emissions of carbon dioxide (CO_2) and nitrogen oxides (NOx), which influence the gas-phase chemistry. Other aviation induced impacts result from the emissions of H_2O, and the emission of sulphate and soot particles, which influence the formation of contrail-cirrus clouds and change the cloudiness by acting as cloud condensation nuclei (Gettelman et. al., 2012). The resulting effects of these emissions modify the chemical properties of the upper troposphere and lower stratosphere and the cloud microphysics that affect the Earth's climate system radiative forcing. For the majority of effects, the radiative forcing is positive; however, sulphate particles, which reflect incoming shortwave radiation, and the reduction of CH_4 induced by the increase in OH concentration cause a negative radiative forcing (Lee et al., 2009). The indirect effect of aerosols on cirrus clouds may on the other hand result in a negative anomaly of the radiative forcing due to the reduction of outgoing long-wave radiation trapped by those clouds (Gettelman et al., 2012). This study will focus on the aviation NOx-induced effects.

There have been many previous studies that examined the effect of aviation NOx emissions on the chemical composition of the atmosphere (Derwent et al., 1999; Fuglestvedt et al., 1999; Wild et al., 2001; Derwent et al., 2001; Stevenson and Doherty, 2004; Köhler et al., 2008; Hoor et al., 2009; Koffi et al., 2010; Hodnebrog et al., 2011). Other recent studies have examined the factors that control the production of NOx-induced ozone (O_3). Stevenson and Derwent (2009) found that the O_3 and CH_4 response to NOx emissions varies regionally, and are most sensitive in regions with low background NOx concentrations. Several studies analyzed the impact of the location and time of the emissions (Derwent et al., 2000; Stevenson et al., 2004). Wild et al. (2012) studied the impact of sunlight while Shine et al. (2005) and Berntsen et al. (2005) investigated the effects of atmospheric mixing. However, as reported in Holmes et al. (2011), model-based estimates of aviation NOx-induced changes in O_3 vary by up to 100%; largely because of differences between models in the ratios of NO : NO_2 and OH : HO_2, background NOx levels, location and time of emissions, the amount of sunlight, and in atmospheric mixing (Holmes et al., 2011). Recent studies by Olsen et al. (2013) and Brasseur et al. (2013) compare aviation NOx-induced changes in ozone and the background atmosphere from a set of climate-chemistry models and found considerable differences between the models as well.

In this study, we examined the effect of aviation NOx emissions on the background atmosphere using the latest versions of the CESM model, the Community Atmosphere Model with Chemistry, Version 4 (CAM4) and Version 5 (CAM5). While the calculated effects in CAM4 and CAM5 will provide a new reference for the aviation NOx-induced effects in comprehensive climate-chemistry models, they also provides a measure for the effect that improvements in treating aerosol processes could have on the aviation NOx-induced effects. The main difference between CAM4 and CAM5 is the representation of aerosols in each model. CAM4 uses a bulk aerosol module as described in Lamarque et al. (2012), while CAM5 uses a modal aerosol module (MAM) based on Liu et al. (2012). The significance of MAM is its capability of simulating aerosol size distribution and both internal and external mixing between aerosol components while treating aerosol processes and properties in a physically-based manner (Liu et al., 2012).

This paper is organized as follow. The next section details CAM4 and the updates to the aerosol representation made for CAM5; the following sections discuss a chemistry diagnosis based on observations from ozonesondes; the emissions and simulation setup; the model results and the conclusion.

Model Description

CAM4 and CAM5 (Community Atmosphere Model versions 4 and 5) are the atmospheric component models for the Community Earth System Model (CESM) (http://www.cesm.ucar.edu/). The details of the physics of the CAM4 and CAM5 models have been discussed extensively in other studies before (e.g. Neale et al., 2011; Gent et al., 2011; Lamarque et al., 2012). The released version of CAM4 and the development version of CAM5 (cesm1_2_beta08_chem) were used in this study.

Both models use the same gas-phase chemical mechanisms including tropospheric and stratospheric chemistry with about 133 species and 330 photochemical reactions (Lamarque et al., 2012). A complete list of species and reactions can be found in Lamarque et al. (2012).

A major difference between the model is that CAM4 uses a bulk aerosol module with one lognormal distribution for all aerosols (Lamarque et al., 2012) while CAM5 uses a new modal aerosol module (MAM) (Lui et al., 2012). MAM was developed with two versions, one with seven lognormal modes (MAM7) and one with three lognormal modes (MAM3) (Liu et al., 2012; Lamarque et al., 2012). Here, we use the more complete version with seven lognormal modes (MAM7). MAM simulates the size distribution of aerosols, both internal and external mixing of aerosols, chemical and optical properties of aerosols and various complicated aerosols processes (Liu et al., 2012). Cloud microphysical processes are represented by a prognostic, two-moment formulation for cloud droplets and cloud ice. Mass and number concentrations of cloud droplets and cloud ice follow the Morrison and Gettelman (2008) parameterization. The gamma function is employed to determine liquid and ice particle sizes (Gettelman et al., 2008). The evolution of liquid and ice particles in time are affected by grid-scale advection, convective detrainment, and turbulent diffusion. Activation of cloud droplets are a function of aerosol size distribution, aerosol chemistry, temperature and vertical

velocity (Neale et al., 2011). The cloud macrophysics scheme imposes full consistency between cloud fraction and cloud condensate. Liquid cloud fraction is based on a triangular distribution of total relative humidity. Ice cloud fraction is based on Gettelman et al. (2010) that allows supersaturation via a modified relative humidity over ice and the inclusion of the ice condensate amount. The aerosols-cloud scheme has the ability to simulate full aerosol-cloud interactions such as cloud droplet activation by aerosol, precipitation processes due to particle size dependence and explicit radiative interaction of cloud particles. Further details on CAM5-chem can be found on the NCAR website (http://www.cesm.ucar.edu/models/cesm1.0/cam/).

The University of Illinois Radiative Transfer Model (UIUC RTM) was used offline to calculate the forcing associated with aviation NOx-induced short-term O_3. Earlier versions of the UIUC RTM have been used in previous research (e.g., Jain et al., 2000; Naik et al., 2000; Youn et al., 2009; Patten et al., 2011). The UIUC RTM calculates the flux of solar and terrestrial radiation across the tropopause. The solar model includes 18 spectral bins from 0.2 to 0.5 microns and includes absorption by H_2O, O_3, O_2, CO_2, clouds and the surface. Scattering processes by clouds, gas-phase molecules, and the surface are included as well. The terrestrial radiation calculation uses a narrow band model of absorptivity and emissivity that covers wave numbers from 0 to 3000 cm^{-1} at a resolution of 10 cm^{-1} for H_2O, CFC-11, and CFC-12 and of 5 cm^{-1} for all other gases. The infrared absorption parameters for gases are obtained from the HITRAN 2004 database (Rothman et al., 2005). Surface albedo and emissivity are based on observations, while clouds are based on the International Satellite Cloud Climatology Project.

Aviation NOx Emissions and Simulation Setup

Both models were run at a horizontal resolution of 1.9° latitude x 2.5° longitude and were configured with 56 vertical levels covering from the surface up to ~2 hPa. To reduce year-to-year climate variability in the model simulations and to be able to detect the aviation NOx signal, specified dynamics ("off-line" mode) simulations were performed. In these simulations, changes in the chemical constituents do not affect the dynamics. The models were nudged with observed meteorology data from the year 2005. Both were run in offline mode driven with 2005 meteorology from the GEOS DAS v5.1. The aviation emissions for 2006 used in this study are from the AEDT aviation emissions scenarios (Wilkerson et al., 2010; Olsen et al,

2012). The background emissions of non-aviation short-lived species (e.g., NOx, volatile organic compounds (VOCs)) were obtained from the IPCC RCP4.5 scenario (van Vuuren et al., 2011). The monthly surface concentrations of longer-lived species, e.g., CO_2, CH_4, chlorofluorocarbons (CFCs), and nitrous oxide (N_2O), were specified as boundary conditions based on the IPCC RCP4.5 scenario. To analyze the effect of aviation NOx emissions on the background atmosphere, two simulations are performed in each model. One simulation considers all NOx emissions including aviation NOx, and the other simulation has no aviation NOx (control run). The difference between these two simulations corresponds to the changes induced by aviation NOx. The simulations were run for 7 years to reach steady-state with data from the 7^{th} year used in this analysis.

Results and Discussions

Chemistry Diagnosis

Due to the radiative importance of ozone in troposphere and stratosphere, simulated ozone in the control runs at representative altitudes is evaluated using a present-day ozonesonde climatology (Tilmes et al., 2012). This climatology includes observations for the years 1995-2011 and covers averaged ozone profiles for 41 different ozonesonde stations that are grouped into 12 regions. For our comparisons, we evaluate ozone at four pressure levels covering the troposphere and lower stratosphere (50, 250, 500, and 900 hPa) over the 12 areas, which are grouped into three larger regions (Tropics, Mid-Latitudes, and High Latitudes), as shown Figure 3.1. Model results are interpolated to all the stations within each region, and averaged over each region. The comparison between model and observations is illustrated in Taylor-like diagrams for each of the corresponding pressure levels and regions (Tilmes et al., 2012). The models are verified against ozonesonde measurements due to the importance of ozone in tropospheric chemistry. CAM4 has been previously verified against ozone observations (e.g., Lamarque et al., 2012). More extensive comparison of the simulated ozone against ozonesonde was performed running NCAR CAM chemistry diagnostic package and results are provided in Appendix A. The same conclusion on models performance as was drawn in the Taylor-like diagrams was obtained from these analyses.

The models are in good agreement at 50 hPa, but for most locations, the models overestimate the observed ozone concentration. While CAM4 overestimates ozone at all locations, CAM5 underestimates ozone at the NH Poles, Canada, and Western Europe. CAM4 and CAM5 perform best in NH High Latitudes and Mid-Latitudes (with the exception of Japan). The average percent difference for all locations in generated ozone at 50 hPa is 13.8% in CAM5 and 14.4% in CAM4. With the exception of the W-Pacific/E-Indian Ocean in CAM4 and the Atlantic/Africa region in CAM5, both models resolve the seasonal correlation quite well at 50 hPa. The average seasonal correlation with ozone cycle as described in ozonesonde measurements is 0.83 in CAM5 and 0.84 in CAM4. Overall, both models are similar in representing ozone at 50 hPa.

At 250 hPa, CAM5 performs better than CAM4 with a smaller percent difference in generated ozone. At all locations, CAM4 gives a higher ozone concentration than CAM5. This difference is due to the dissimilar aerosol configurations in both models. For NH High Latitudes, both models greatly underestimate ozone (18-26%). In the mid-latitudes and tropics, both models overestimates ozone, a result that was also found in Lamarque et al. (2012), who noted that this result is an indication of a model estimated tropopause that is lower than observed. The seasonal correlation is good for most locations, with the exception of the W-Pacific/E-Indian Ocean, NH Sub Tropic, Equatorial America, Atlantic/Africa regions. On average, both models are in general agreement with a 0.75 correlation in both CAM5 and CAM4, indicating a good representation of the seasonal ozone cycle.

Of the four pressure levels studied, the models most accurately estimate ozone at the 500 hPa level. The absolute difference in generated ozone is within 11.7% for both models. For nine of the twelve locations evaluated at this pressure level, CAM5 underestimates ozone. CAM4, on the other hand, overestimates ozone at all but one location. Overall, CAM5 appears to perform better than CAM4 due to a lower percent difference in ozone (6.0% in CAM5 compared to 11.7% in CAM4). The seasonal correlation is very good for both models; 0.80 in CAM5 and 0.82 in CAM4.

On average, both models perform well in the lowest level (900 hPa), although there are several outliers. Both models overestimate the ozone concentration in the Western

Europe and Canada regions. Additionally, both models also underestimate ozone in the SH Mid-Latitude and SH Polar regions. At all other locations, however, the estimated ozone is very accurate. For four of the locations, CAM5 underestimates ozone, while CAM4 overestimates ozone at all locations. The percent difference is also lower in CAM5 (10.0% compared to 15.7% in CAM4), indicating a better representation of ozone by the model. Additionally, with the exception of the Equatorial Americas region in CAM4 and the Japan region for both models, the seasonal correlation is excellent (0.81 in CAM5 and 0.81 in CAM4).

Overall, both models represent ozone well (on average to within 13% in CAM5 and 18% in CAM4 of all the locations) in the troposphere and stratosphere. The seasonal cycle is also very accurate in the models. In general CAM4 tends to overestimate ozone, more so than CAM5, which occasionally underestimates ozone—especially at lower levels. CAM5, however, appears to be slightly better at estimating ozone than CAM4.

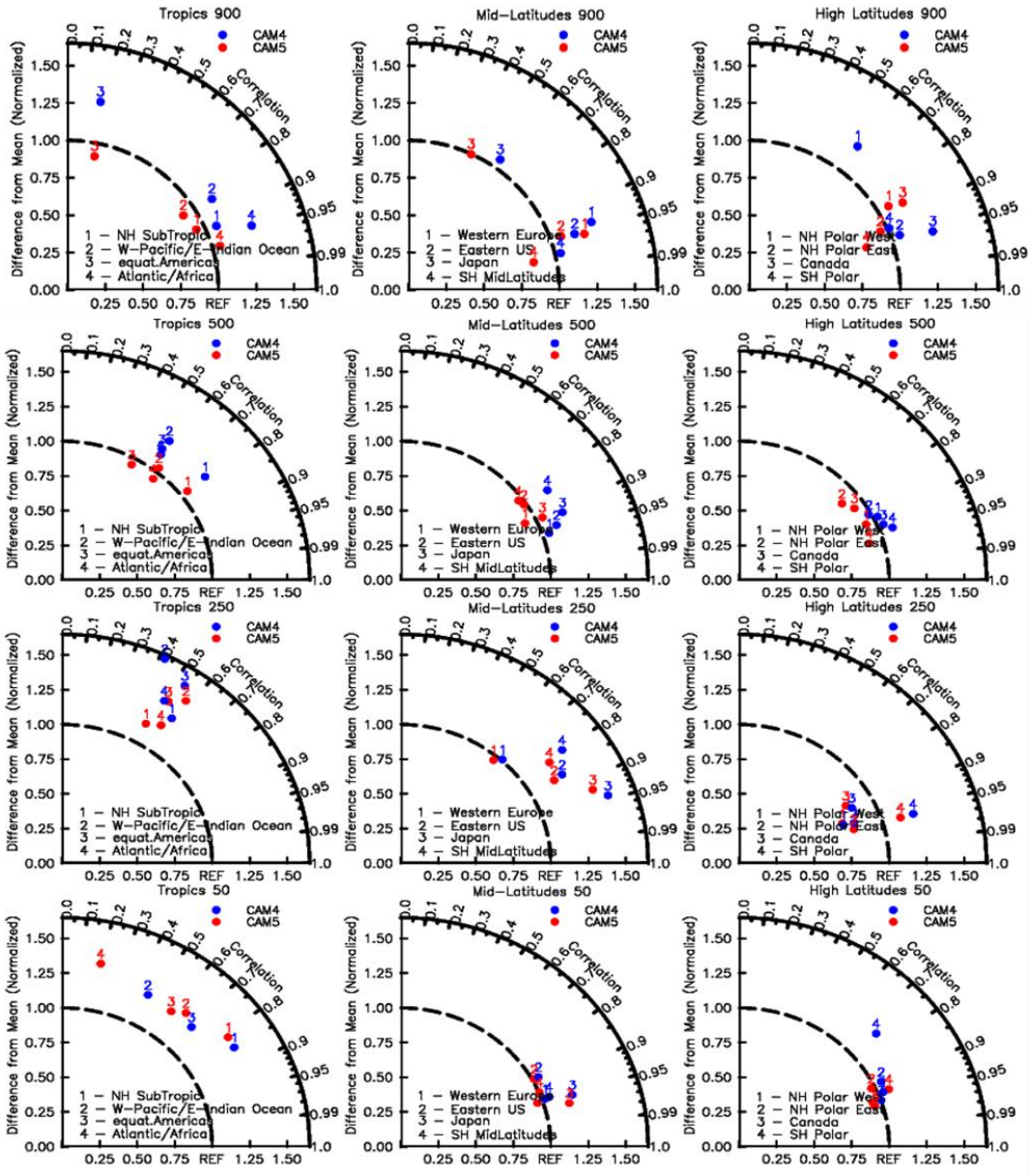


Figure 3.1. Taylor diagram of model ozone against ozonesonde climatology for 4 pressure levels and three latitudinal regions. REF along the abscissa denotes the observations while the radial distance describes the normalized bias. The correlation for the seasonal cycle is described along the angle.

Spatial distribution of NOx emissions

The AEDT NOx emission data used as the input to the models run had a hourly temporal resolution and the spatial distribution of aviation NO_X emissions for 2006 is shown in Figure 3.2 which amounts to the total of 2.7 Tg (NO_2)/yr. As is shown in Figure 3.2, there are three maxima, one in the eastern United States, one in eastern Asia and one in Europe. The local maximum in the eastern U.S. contributes approximately 0.0136 Tg to the global emissions of NO_2 while the local maxima in Europe contributes 0.0154 Tg. Additionally, the maximum location in Asia contributes 0.0123 Tg to the global total. The main source of NO_X emissions fall between 30° and 60°N latitude.

Figure 3.3 shows the seasonal distribution of aviation 2006 NOx emissions. As shown in Figure 3.3, aviation NOx emissions have a different seasonal distribution with the highest amount of emissions released in the summer time.

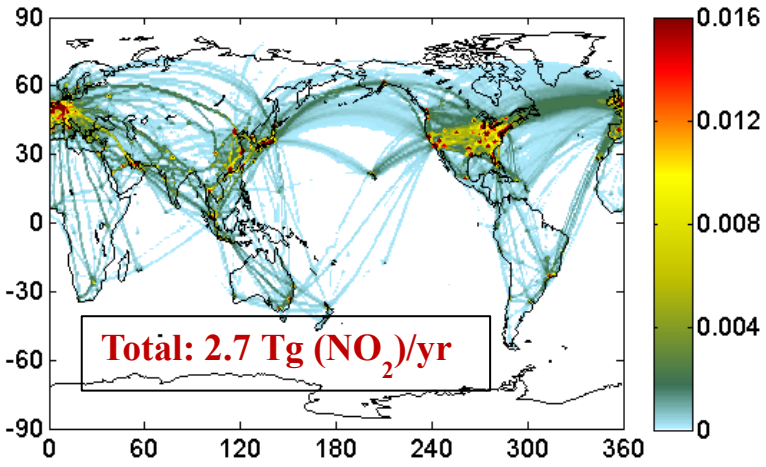


Figure 3.2. Spatial distribution of aviation NOx emissions for 2006.

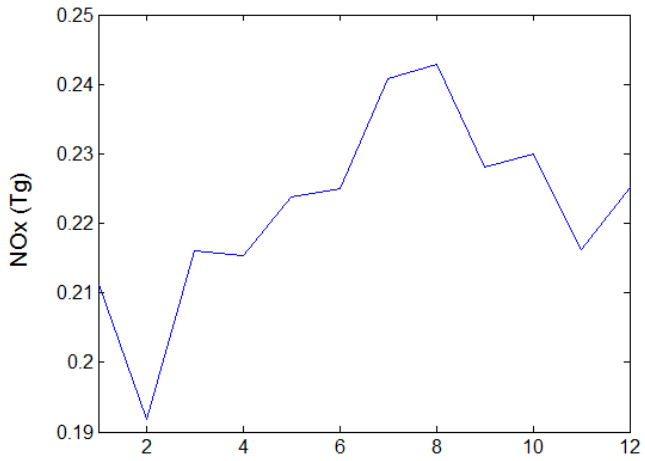


Figure 3.3. Seasonal distribution of aviation NOx emissions for 2006.

Ozone

Figure 3.4 shows the aviation NOx-induced annual vertical profile of O_3 production and loss as calculated by CAM5 (red) and CAM4 (blue). Both models illustrate that the maximum rate of ozone production peaks in the upper troposphere/lower stratosphere (UT/LS) region where the greatest amount of aircraft induced NO_X emissions are. As we analyze the results from the model runs, the following ozone production (P) and loss (L) equations are used to describe the observed trend. Ozone is produced in the troposphere mainly through the following chemical reactions (Sillman, 2012):

P1	$VOC + OH \overset{O_2}{\rightarrow} RO_2 + H_2O$
P2	$CO + OH \overset{O_2}{\rightarrow} HO_2 + CO_2$
P3	$RO_2 + NO \overset{O_2}{\rightarrow} secondary\,VOC + HO_2 + NO_2$
P4	$HO_2 + NO \rightarrow OH + NO_2$
P5	$NO_2 + h\nu \rightarrow NO + O$
P6	$O + O_2 + M \rightarrow O_3 + M$

Ozone destruction in the troposphere, on the other hand, is given by the following reactions (Sillman, 2012):

L1	$NO + O_3 \rightarrow NO_2 + O_2$
L2	$O_3 + h\nu \xrightarrow{H_2O} 2OH + O_2$
L3	$HCHO + h\nu \xrightarrow{2O_2} 2HO_2 + CO$
L4	$HO_2 + HO_2 \rightarrow H_2O_2 + O_2$
L5	$RO_2 + HO_2 \rightarrow ROOH + O_2$
L6	$OH + NO_2 \rightarrow HNO_3$

At the UT/LS altitudes, the rate of ozone loss decreases due to the increase in HO_2 reacting with NO (as in equation P4). This process creates NO_2 which further increases O_3 production (equations P5 and P6). Part of the excess ozone that is created in the UT/LS region is transported to lower altitudes. As shown in Figure 3, the rate of ozone loss begins to increase and peaks around 500 hPa. At this altitude, as described by equation L2, excess ozone transported from the UT/LS region in the presence of water vapor, reacts to form hydrogen oxide radicals (HOx), and therefore increasing ozone loss. Additional reductions in net O_3 production are caused by the increased HOx reacting with NOx near the surface, resulting in the conversion of NOx to HNO_3 (equation L6).

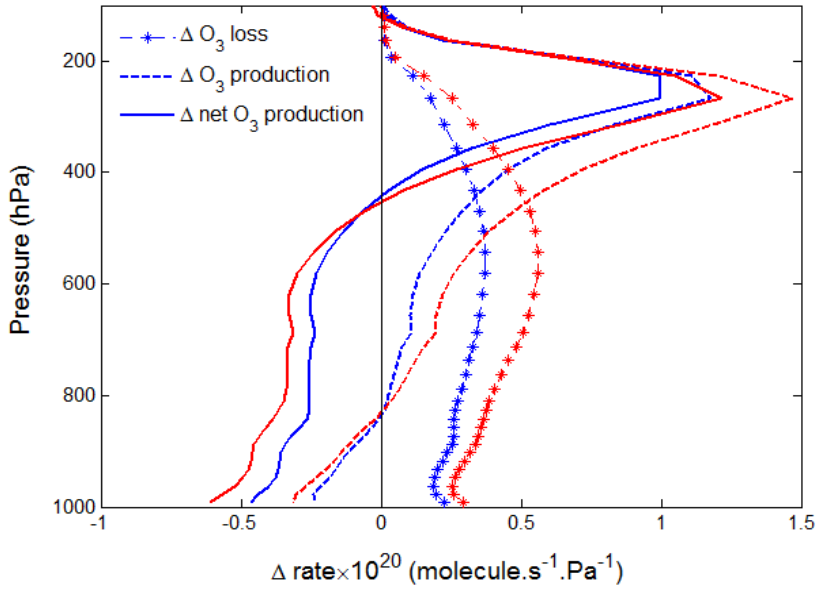


Figure 3.4. Vertical profile describing the aviation NOx-induced change in the rate of O_3 production with height (results are shown in red for CAM5 and in blue for CAM4). Net rate of ozone production (solid line), the gross rate of ozone production (dashed line), and the rate of ozone loss (dotted line) are shown. Production and loss rates are calculated as a zonal and meridional average for the year 2006.

The models are in good agreement for the ozone production in the UT/LS region. Compared to CAM4, the net rate of ozone production in CAM5 is higher at cruise altitudes and slightly lower in lower altitudes. The maximum net production of ozone is 1.2×10^{20} molecules.s^{-1}.Pa^{-1} in CAM5 and 1.0×10^{20} molecules.s^{-1}.Pa^{-1} in CAM4. CAM4 estimates a maximum rate of production at 1.2×10^{20} molecules.s^{-1}.Pa^{-1} while CAM5 estimates a rate of 1.5×10^{20} molecules.s^{-1}.Pa^{-1}. At lower altitudes, CAM5 gives a greater rate of ozone loss than CAM4. Both models show a peak in ozone loss rate around 600 hPa which peaks to about 0.6×10^{20}molecules.s^{-1}.Pa^{-1} in CAM5, and to about 0.4×10^{20} molecules.s^{-1}.Pa^{-1} in CAM4. Overall, as was observed in Figure 3.1 (as confirmed through comparisons with ozonesonde data) and shown in Figure 3.4, CAM5 is more efficient in producing ozone than CAM4 in most of the atmosphere.

Global burdens

To explore the cause of higher O_3 production in CAM5, we compare the tropospheric burden of HOx, NOx and NOy (all the nitrogen containing compounds in the gas phase) in both CAM4 and CAM5. Table 3.1 compares the annual mean tropospheric burden of HOx, NOx, NOy and the ratios of OH : HO_2 and NOx : NOy in both CAM4 and CAM5 for both the control run and aviation NOx-perturbed run. Table 3.1 shows the burden of HOx, NOx, NOy and the ratios of OH : HO_2 and NOx : NOy between 200-400 hPa and between 30-60°N (where most aircraft fly) in both CAM4 and CAM5 for both the control and aviation NOx-perturbed run. As shown in Table 3.1, the ratio of OH : HO_2 is about 24% higher in CAM5 perturbed run which in turn results in higher ozone production as OH is the main deriver of the initial reaction of the ozone production sequence (P1) and as it implies higher NO to NO_2 conversion (P4). Also the ratio of NOx : NOy is about the same between the models, however, the NOy burden is about 16% higher in the CAM5 perturbed run than in CAM4 perturbed run which indicates lower conversion of NOy to aerosol phase. This indicates that more NOx would be available in the CAM5 perturbed run to trigger the ozone formation reactions and hence it would results in higher ozone production in CAM5. The detail discussion of the magnitude and the pattern of aviation NOx-induced changes in ozone and HOx are discussed in the coming paragraphs.

Table 3.1. Annual mean burden of HOx, NOx, NOy and the ratios of OH : HO_2 and NOx : NOy between 200-400 hPa and between 30-60°N in both CAM5 and CAM4 for both the control run (_c) and aviation NOx-perturbed run (_p).

	OH (kg)	HO_2 (kg)	HOx (kg)	OH/HO_2	NOx (kgN)	NOy (kgN)	NOx/NOy
CAM4_c	9.61E+03	7.95E+05	8.04E+05	1.21E-02	4.54E+06	4.48E+07	0.10
CAM4_p	1.09E+04	7.57E+05	7.67E+05	1.44E-02	6.39E+06	5.28E+07	0.12
CAM5_c	1.30E+04	8.79E+05	8.92E+05	1.47E-02	4.80E+06	4.85E+07	0.10
CAM5_p	1.47E+04	8.25E+05	8.40E+05	1.78E-02	7.03E+06	6.13E+07	0.11

The aviation NOx-induced ozone perturbation is shown in Figure 3.5. Model results from CAM5 are shown on the top panel while CAM4 is on the bottom. The left column shows the mean zonal ozone perturbation for January while the right column shows July. As shown in Figure 3.5, CAM5 produces a greater amount of ozone in the UT/LS region for both months.

While, the pattern and the localized maximums of ozone perturbation that happens around 200 hPa in NH is about the same between both CAM4 and CAM5. The tropospheric mean change in O_3 is higher in CAM5 than CAM4 for both January and July. In July CAM5 generates an aviation NOx-induced tropospheric mean ozone perturbation of 1.2 ppb (compared to 1.0 in CAM4). In Jan CAM5 generates an aviation NOx-induced tropospheric mean ozone perturbation of 1.3 ppb (compared to 1.1 in CAM4).

As exhibited in Figure 3.5, in both model, the UT/LS ozone perturbation is much greater in July than in January. This is due to the difference in the length of daylight between July and January and more intense photochemistry and partially due to the higher aviation NOx emissions in July (as seen in in Figure 3.3). The increased length of daylight allows for a higher volume of photolysis of NO_2 to occur, which generates atomic oxygen that reacts with O_2 to create O_3 (equations P5 and P6). Also note the differences in ozone perturbations in the lower troposphere between January and July. In the summer, the ozone perturbation at lower altitudes is weaker due in part to the greater surface deposition (Hodnebrog et al., 2011) and also due to the shorter photochemical lifetime of ozone through increased water vapor (and hence more HOx giving increased ozone loss) (Hodnebrog et al., 2011). It is also noted that, in July, both models show the maximum ozone impact increasing towards high latitudes in the NH. A similar result was found by Hoor et al. [2009] who showed a maximum zonal mean ozone perturbation centered around 75° N during June.

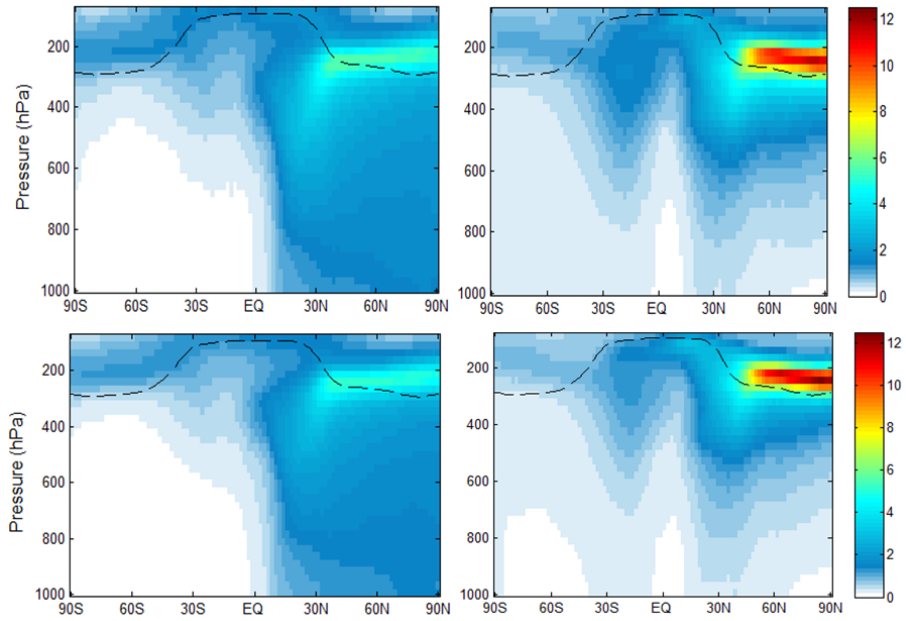


Figure 3.5. Zonal mean perturbations of ozone (ppb) during January (left) and July (right). CAM5 is in the top panel, while CAM4 is on the bottom. The dashed line indicates the tropopause.

As seen in both January and July for both CAM5 and CAM4, a mid-latitudinal perturbation extends from 400 hPa down towards lower altitudes. This feature agrees with past studies by Hoor et al. (2009), Koffi et al. (2010), and Hodnebrog et al. (2011). Hoor et al. (2009) notes that during the summer, the boundary layer mixing and convective transport into the free troposphere is more vigorous.

Figure 3.6 shows the yearly mean ozone column. As shown in Figure 3.6, ozone changes are relatively zonally well mixed, however, several 'hotspots' in both CAM5 and CAM4 exist just north of the Mediterranean and off the western coast of Europe. A more uniform spread is seen over Europe, the western half of Asia, the Atlantic Ocean and a small strip at about 45°N in the Pacific Ocean. These hotspots are stronger in CAM5 than CAM4. As expected, the ozone impact is very small in the SH. A sharp gradient in O_3 appears in the NH subtropics, as was also seen in previous studies. However, the ozone concentration continues to increase, with the maximum values between 30 and 60° N. Hoor et al. (2009) and Hodnebrog et al. (2011) found a similar distribution.

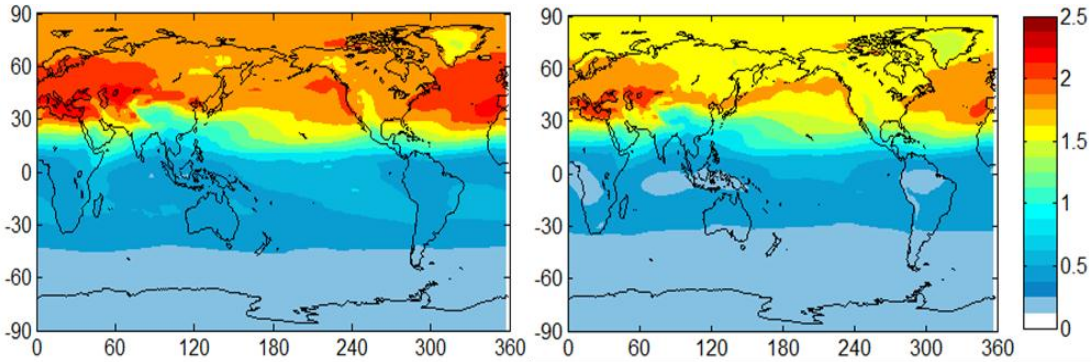


Figure 3.6. Yearly mean perturbations of the ozone column (ΔDU) based on 2006 aircraft NOx emissions. CAM5 is on the left, while CAM4 is on the right.

HOx

The hydroxyl radical (OH) plays a very large role in the creation of atmospheric ozone. It is the primary oxidizing agent of the troposphere. It is responsible for removing greenhouse gases such as CH_4, CO, HCFCs, and others. Production of OH by O_3 is given by equation L2. Figure 3.7 shows the model generated zonal mean annual production of OH in the troposphere. Due to the short lifetime of OH, the zonal mean estimate represents the locations of emissions, but is also strongly affected by incoming solar radiation, the amount of water vapor, the background levels of pollution and the lifetime of the emitted species (Hodnebrog et al., 2012).

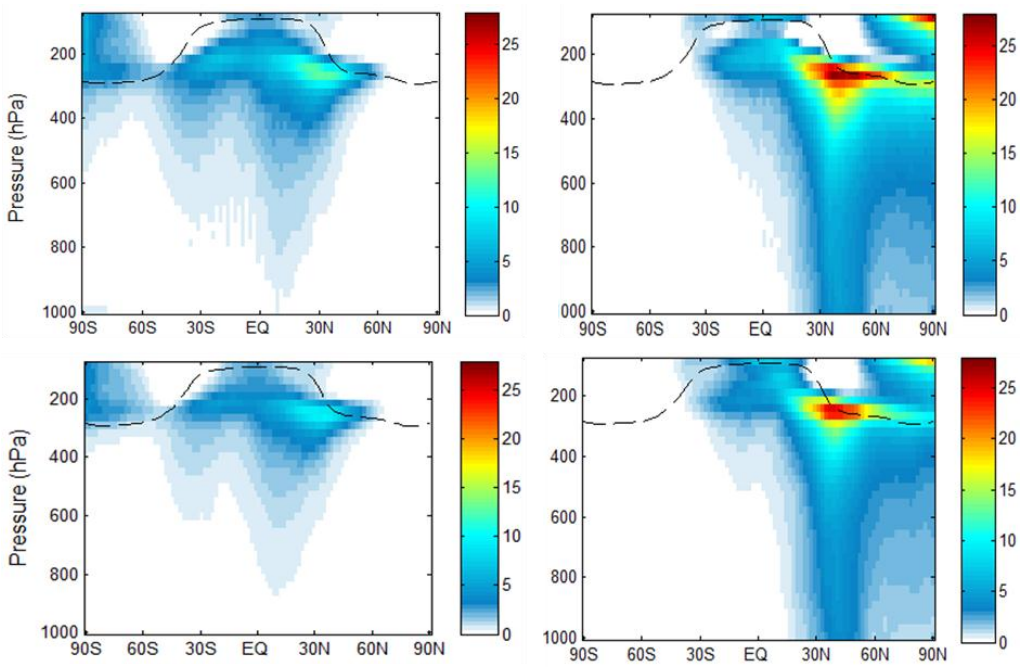


Figure 3.7. OH concentration (10^{-4} Δmolec cm^{-3}) during January (left) and July (right). CAM5 is in the top panel, while CAM4 is on the bottom. The dashed line indicates the tropopause.

Similar to ozone, the impact of aviation emitted NO_X on tropospheric OH production is largest in July. This increase in OH during the summer months is also due to the enhanced photochemistry in the summer. Aircraft emissions have the largest zonal mean ozone impact in the UT/LS region above mid-latitudes in the NH. However, the OH perturbation is more concentrated about mid-latitudes (~40°N) relative to the O_3 perturbation, which stretched from 40°N to the Poles. The more southern position of OH is due to the increased humidity and the lower solar zenith angle, which are essential to produce excited oxygen atom ($O(^1D)$) and hence higher OH concentration. This result agrees well with recent studies by Hoor et al. (2009) and Hodnebrog et al. (2011). Additionally, there is a greater perturbation of OH extending towards lower altitudes over mid-latitudes than there was of O_3. This is due to the increased production of HO_x (HO_x = OH + HO_2) in the mid-troposphere at the expense of O_3. Additionally, both models derive changes in OH extending from 400 hPa down to the surface for latitudes above 40°N. This feature is much weaker in January when the UV actinic flux necessary to OH production is much smaller in the NH.

It also appears that the production of aviation NOx-induced OH is higher in CAM5 compared to CAM4. This in fact is a result of higher O_3 production in CAM5 compared to CAM4 due to the improvements in aerosol module in CAM5 which undergoes photolysis and produce OH. In July CAM5 generates an aviation NOx-induced tropospheric mean OH perturbation of 1.4×10^4 molecules.cm^{-3} (compared to 9.1×10^3 in CAM4). In January CAM5 generates an aviation NOx-induced tropospheric mean OH perturbation of 9.7×10^3 molecules.cm^{-3} (compared to 6.4×10^3 in CAM4).

Figure 3.8 shows the HO_2 perturbation as generated by CAM5 and CAM4. Areas that experience an increase in HO_2 concentrations are shown in red and areas that experience HO_2 loss are shown in blue. The decrease in HO_2 concentration happens because aviation-induced NO_x increases OH levels by shifting the HO_x balance in favor of OH production, given by equation P4 (Stevenson et al., 2004; Berntsen et al., 2005; Köhler et al., 2008), and as such results in HO_2 loss at cruise region. As expected, the areas of HO_2 loss correspond to the areas the experienced an increase in OH concentrations in Figure 3.7.

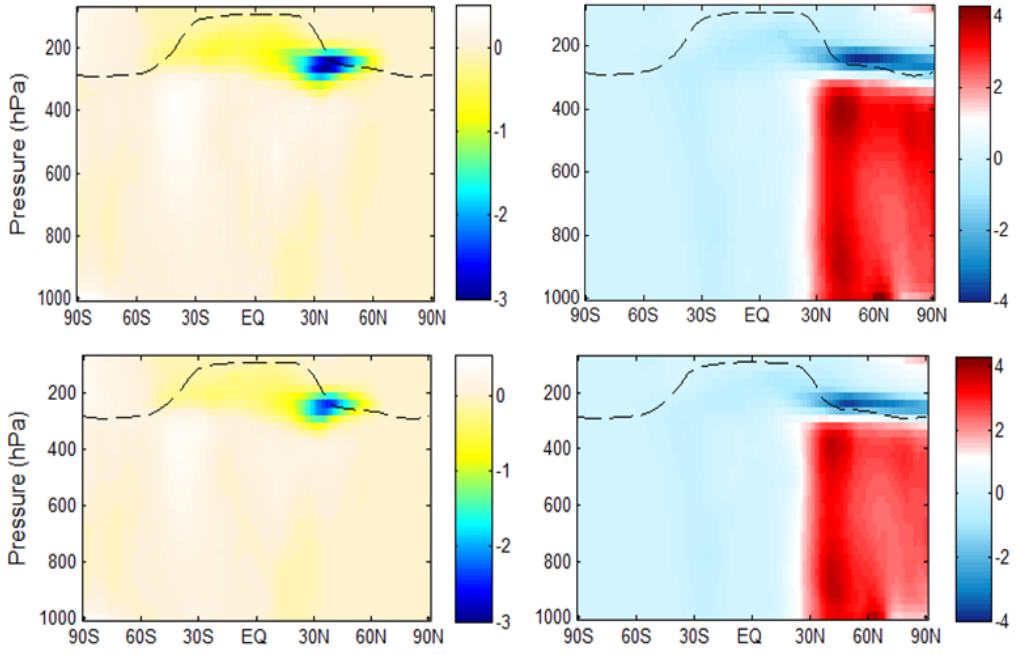


Figure 3.8. As in Figure 3.6, but for HO_2 (10^{-6} Δmolec cm^{-3}).

In January, there is a greater rate of HO_2 consumption in the UT/LS region in CAM5 than there is in CAM4 due to higher OH production. Following equation P4, this HO_2 is reacting with aircraft emitted NO to give OH and NO_2. Similarly, the rate of HO_2 consumption is also greater in the UT/LS region during July in CAM5 as well. When comparing Figure 3.8 with Figure 3.7, the locations of maximum HO_2 loss correspond with the locations of maximum OH concentration, indicating that reaction P4 in a significant reaction in OH production in the UT/LS region. At lower altitudes in July, the transported ozone is photolyzed in the presence of water vapor, thus increasing HO_X ($HO_X = HO_2 + OH$).

CH_4

The hydroxyl radical OH also plays a large role in the atmospheric methane concentrations due to its role as an oxidizing agent. CH_4 is one of the principle sinks of OH in the troposphere. As the OH concentration is effected by aircraft emissions, so is the methane concentration and its lifetime.

Figure 3.9 shows the aviation-induced annual zonal averaged CH_4 loss rate for CAM5 (left) and CAM4 (right). In both CAM4 and CAM5, the methane loss is mostly confined to the NH at a more southern location of the perturbed OH (between 30-60°N). This predominately occurs due to the increase in the methane-OH reaction rate constant with larger temperatures at lower altitudes. As such, in both models the position of the maximum CH_4 loss is below the cruise altitude. As shown in Figure 3.9, the CH_4 loss is higher in CAM5 compared to CAM4 which is the result of higher production of aviation-induced OH. Table 3.2 shows the reduction in methane lifetimes as calculated for both CAM4 and CAM5.

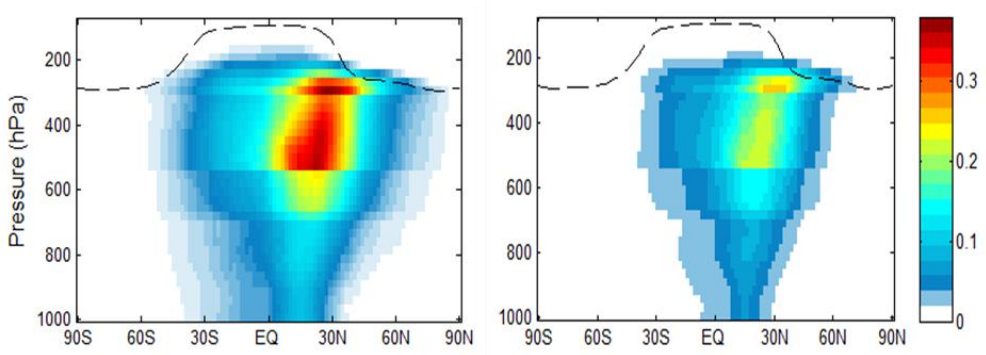


Figure 3.9. Annual zonal averaged CH_4 loss (mol/s) induced by aviation NOx emissions. CAM5 is on the left, CAM4 is on the right. The dashed line indicates the tropopause.

Table 3.2. CH_4 lifetimes as calculated by CAM4 and CAM5 for the control run and for the NOx perturbation run. The relative change between runs is displayed in the right-most column.

CH4 lifetime (yr)	Control run	Perturbed run	Rel change (%)
CAM5	7.35	7.21	1.90
CAM4	8.83	8.71	1.40

Table 3.2 shows the global annual average CH_4 lifetimes as calculated by CAM4 and CAM5 for the background (control) run and the NOx-perturbed run. The change in CH_4 lifetime is also presented as the percent change in lifetime. The reduction in CH_4 lifetime calculated in CAM5 and CAM4 is 1.90% (2.32%/[TgN/yr^{-1}]) and 1.40% (1.71%/[TgN/yr^{-1}]), respectively, excluding the feedback of changes in methane concentration on its lifetime. The CAM4 result falls within the -1.4±0.4 (%/[TgN/yr^{-1}]) to -1.6±0.37 (%/[TgN/yr^{-1}]) range reported by Hodnebrog et al. (2011) using different emissions and an ensemble of six different atmospheric chemistry models. The CAM5 simulated change in CH_4 lifetime falls outside the range reported by Hodnebrog et al. (2011) and near its upper end. Inclusion of the aviation-induced methane feedback on its lifetime further decreases the lifetime by a factor of 1.4. The higher reduction of CH_4 lifetime in CAM5 is the result of higher increase in the aviation-induced OH concentration in CAM5 as was shown in Figure 3.6.

Radiative Forcings

The aviation NOx-induced O_3 RFs were calculated as the difference of the radiation imbalance between the NOx-perturbed and control simulations at the tropopause calculated with the UIUC RTM, excluding the effects of stratospheric adjustment. Figure 3.10 shows the yearly averaged ozone RF for CAM5 (left) and CAM4 (right). Both models show the greatest RF in the NH between 30-60°N. As expected, O_3 RF from aviation is low in the SH. The greatest RF values in the SH are over the SH tropical Pacific Ocean and are most likely due to air traffic between Australia and the United States. Interestingly, radiative forcing values over Asia are relatively low, given the amount of NO_X emissions from this area. Additionally, it appears that the maximum radiative forcing from Europe's emissions has shifted to the Mediterranean, indicating that these aircraft emissions have a maximum impact downwind of the source. These results agree well with Hodnebrog et al. (2011).

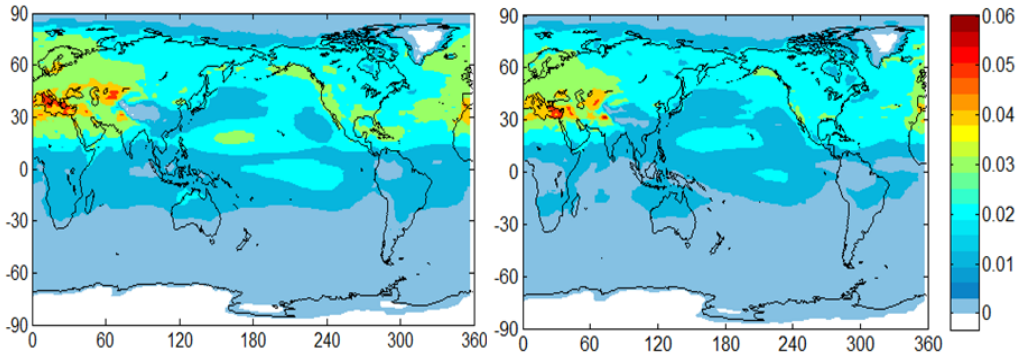


Figure 3.10. Yearly mean radiative forcing (mWm^{-2}) from O_3 due aviation NOx emissions. CAM5 is on the left, CAM4 is on the right.

The associated global mean ozone RF is 43.9 and 36.5 mWm^{-2} in CAM5 and CAM4, respectively. CAM5 has a greater annual ozone RF, since as noted earlier, CAM5 produced a greater ozone perturbation than CAM4 which largely accounts for the differences in radiative forcings.

Conclusion

Based on our model results, it appears that CAM5 and CAM4 simulate background ozone to within 13% and 18%, respectively, compared to ozonesonde. Based on comparison with ozonesonde observations, CAM5 does better at determining the ozone distribution in the troposphere and lower stratosphere, in relationship to the improvements made in its aerosol treatments.

As found in previous studies, the maximum effect from aircraft NO_X emissions on ozone is in the NH Upper Troposphere/Lower Stratosphere region. This is due to the high frequency of subsonic aircraft flying in this region. The aircraft-induced ozone perturbation is greater in the NH summer due to the enhanced photochemistry. The ozone perturbation mixes towards lower altitudes in January due to the shorter photochemical lifetime of ozone and the faster surface deposition rate in July. The results show a more localized and higher production of aviation NOx-induced ozone in CAM5 that generates an aviation NOx-induced tropospheric mean ozone perturbation of 1.2 ppb in July (compared to 1.0 in CAM4) and 1.3 ppb in Jan (compared to 1.1 in CAM4).

The hydroxyl perturbations are located at a more southern location of the position of maximum aviation-induced changes in ozone and at lower latitudes. This, however, is due to the lower zenith angle and increased humidity which are essential to produce excited oxygen atom ($O(^1D)$) and hence higher OH concentration. Overall, the aviation NOx-induced change in OH is higher in CAM5 in accordance with higher ozone production. The induced changes in OH concentration increase the methane (CH_4) loss rate and reduce its lifetime by 1.90% and 1.40% in CAM5 and CAM4, respectively.

Results indicate a global mean O_3 RF of 43.9 and 36.5 mWm^{-2} in CAM5 and CAM4, respectively. Both models agree that the maximum O_3 radiative forcing is between 30-60°N. However, it is interesting to note that it appears that the maximum RF is realized downwind of a local maximum NO_X source.

The evaluation of aviation NOx-induced effect in CAM5 is the first evaluation of these effects in a 3-D climate-chemistry model that simulates the size distribution of aerosols, both internal and external mixing of aerosols, chemical and optical properties of aerosols and various complicated aerosols processes. Since the only difference between the CAM5 and CAM4 simulations were the representation of aerosols, the difference in their simulated aviation NOx-induced effects highlights the importance of the aerosols treatment. These results suggest the modal versus bulk representation of aerosols has a profound effect on quantifying the effect of aviation emissions on ozone. More detailed analysis is required to explore the effects of aerosol representation on aviation NOx-induced effects to a greater extent. It is noted that while the simulated change in ozone is relatively different between the two models, it is considerably smaller than the current estimates of the uncertainty in aviation effects on ozone.

BIBLIOGRAPHY

Arnold, F., J. Scheid, T. Stilp, H. Schlager, and M. E. Reinhardt (1992), Measurements of jet aircraft emissions at cruise altitude I: The odd-nitrogen gases NO, NO2, HNO2 and HNO3, *Geophysical research letters*, 19 (24), pp. 2421-2424.

Beck, J. P., C. E. Reeves, F. A. De Leeuw, and S. A. Penkett (1992), The effect of aircraft emissions on tropospheric ozone in the northern hemisphere, *Atmospheric Environment, Part A. General Topics*, 26 (1), pp. 17-29.

Berntsen, T. K., J. S. Fuglestvedt, M. M. Joshi, K. P. Shine, N. Stuber, M. Ponater, R. Sausen, D. A. Hauglustaine, and L. Li (2005), Response of climate to regional emissions of ozone precursors: Sensitivities and warming potentials, Tellus, 57B(4), 283 – 304.

Borucki, W. J., R. C. Whitten, V. R. Watson, H. T. Woodward, C. A. Riegel, L. A. Capone, and T. Becker (1976), Model predictions of latitude-dependent ozone depletion due to supersonic transport operations, *AIAA Journal*, 14 (12), pp. 1738-1745.

Brasseur, G. P., J.-F. Müller and C. Granier (1996), Atmospheric impact of NO_x emissions by subsonic aircraft: A three-dimensional model study, *Journal of Geophysical Research*, 101 (D1), pp. 1423–1428.

Brasseur, P. G., B. Weber, R. Damoah, , A. R. Douglass, M. Z. Jacobson, H. Lee, Q. Liang, S. C. Olsen, L. D. Oman, L. Ott, S. Pawson, H. Selkirk, A. Sokolov, R. S. Stolarski, N. Unger, D. J. Wuebbles (2013), Model Intercomparison of Ozone Sensitivity to NOx emissions in the vicinity of the extratropical tropopause, *Geophysical Research Letters.*

Climatic Impact Assessment Program (CIAP), Report of findings, The effects of stratospheric pollution by aircraft, Rep. DOT-TST-75-50, U.S. Dep. of Transp., Washington, D.C., 1974.

Collins, W. J., N. Bellouin, M. Doutriaux-Boucher, N. Gedney, P. Halloran, T. Hinton, J. Hughes, C. D. Jones, M. Joshi, S. Liddicoat, G. Martin, F. O'Connor, J. Rae, C. Senior, S. Sitch, I. Totterdell, A. Wiltshire, and S. Woodward (2011), Development and evaluation of an Earth-system model – HadGEM2, *Geoscientific Model Development Discussion*, 4, pp. 997-1062

Crutzen, P. J. (1972), SST's: A Threat to the Earth's Ozone Shield, *Ambio*, 1 (41).

Dameris, M., V. Grewe, I. Köhler, R. Sausen, C. Bruhl, J. U. Grooss, and B. Steil (1998), Impact of aircraft NOx emissions on tropospheric and stratospheric ozone. Part II: 3-D model results, *Atmospheric Environment*, 32, pp. 3185–3199.

Derwent, R. G. (1982), Two-dimensional model studies of the impact of aircraft exhaust emissions on tropospheric ozone, *Atmospheric Environment*, 18 (8), pp. 1997-2007.

Derwent, R.G., W.J. Collins, C.E. Johnson, and D.S. Stevenson (2001), Transient behavior of tropospheric ozone precursors in a global 3-D CTM and their indirect greenhouse effects, *Climatic Change*, 49 (4), pp. 463-487.

Emmons, L. K., S. Walters, P. G. Hess, J.-F. Lamarque, G. G. Pfister, D. Fillmore, C. Granier, A. Guenther, D. Kinnison, T. Laepple, J. Orlando, X. Tie, G. Tyndall, C. Wiedinmyer, S. L. Baughcum, and S. Kloster (2010), Description and evaluation of the Model for Ozone and Related chemical Tracers, version 4 (MOZART-4), *Geoscientific Model Development*, 3, pp. 43–67.

Fitcher, C., S. Marquart, R. Sausen, and D. S. Lee (2005), The impact of cruise altitude on contrails and related radiative forcing, *Meteorologische Zeitschrift*, 14 (4), pp. 563 – 572.

Flatøy, F., and Ø. Hov (1996), Three-dimensional model studies of the effect of NO x emissions from aircraft on ozone in the upper troposphere over Europe and the North Atlantic, *Journal of Geophysical Research*, 101 (D1), pp. 1401-1422.

Fuglestvedt, J. S., T. Berntsen, I. S. A. Isaksen, M. Huiting, X.-Z. Liang, and W.-C. Wang (1999), Climatic forcing of nitrogen oxides through changes in tropospheric ozone and methane; global 3D model studies, *Atmospheric Environment*, 33, pp. 961-977.

Gauss, M., G. Myhre, G. Pitari, M. J. Prather, I. S. A. Isaksen, T. K. Berntsen, G. P. Brasseur, F. J. Dentener, R. G. Derwent, D. A. Hauglustaine, L. W. Horowitz, D. J. Jacob, M. Johnson, K. S. Law, L. J. Mickley, J.-F. Müller, P.-H. Plantevin, J. A. Pyle, H. L. Rogers, D. S. Stevenson, J. K. Sundet, M. van Weele, and O. Wild (2003), Radiative forcing in the 21st century due to ozone changes in the troposphere and the lower stratosphere, *Journal of Geophysical Research: Atmospheres*, 108 (D9), pp. 1984–2012.

Gauss, M., I. S. A. Isaksen, D. S. Lee, and O. A. Søvde (2006), Impact of aircraft NOx emissions on the atmosphere – tradeoffs to reduce the impact, *Journal of Atmospheric Chemistry and Physics*, 6, pp. 1529-1548.

Gent, P. R., G. Danabasoglu, L. J. Donner, M. M. Holland, E. C. Hunke, S. R. Jayne, D. M. Lawrence, R. B. Neale, P. J. Rasch, M. Vertenstein, P. H. Worley, Z.-L. Yang, and M. Zhang (2001), The community climate system model version 4. *Journal of Climate*, 24 (19), pp. 4973-4991.

Gettelman, A., H. Morrison, and S. J. Ghan (2008), A new two-moment bulk stratiform cloud microphysics scheme in the NCAR Community Atmosphere Model (CAM3), Part II: Single-column and global results, *Journal of Climate*, 21 (15), pp. 3660–3679.

Gettelman, A., X. Liu, D. Barahona, U. Lohmann, and C. Chen (2012), Climate impacts of ice nucleation, *Journal of Geophysical Research*, 117, D20201, doi:10.1029/2012JD017950.

Gettelman, A., X. Liu, S. J. Ghan, H. Morrison, S. Park, A. J. Conley, S. A. Klein, J. Boyle, D. L. Mitchell, and J.-LF Li (2010), Global simulations of ice nucleation and ice supersaturation with an improved cloud scheme in the Community Atmosphere Model, *Journal of Geophysical Research*, 115 (D18).

Hesstvedt, E. (1974), Reduction of Stratospheric Ozone from Highflying Aircraft, Studied in a Two-dimensional Photochemical Model with Transport, *Canadian Journal of Chemistry*, 52, p. 1592.

Hodnebrog, Ø., T. K. Berntsen, O. Dessens, M. Gauss, V. Grewe, I. S. A. Isaksen, B. Koffi, G. Myhre, D. Olivié, M. J. Prather, J. A. Pyle, F. Stordal, S. Szopa, Q. Tang, P. Velthoven, J. E. Williams, and K. Ødemark (2011), Future impact of non-land based traffic emissions on atmospheric ozone and OH – an optimistic scenario and a possible mitigation strategy, *Journal of Atmospheric Chemistry and Physics*, 11, pp. 11293–11317.

Holmes, C. D., Q. Tang, Q., and M. J. Prather (2011), Uncertainties in climate assessment for the case of aviation NO, *Proceedings of the National Academy of Sciences, U.S.A.*, 108, pp. 10997–11002.

Hoor, P., J. Borken-Kleefeld, D. Caro, O. Dessens, O Endresen, M. Gauss, V. Grewe, D. Hauglustaine, I. S. A. Isaksen, P. Jöckel, J. Lelieveld, E. Meijer, D. Olivie, M. Prather, C. Schnadt Poberaj, J. Staehelin, Q. Tang, J. van Aardenne, P. van Velthoven, and R. Sausen (2009), The Impact of Traffic Emissions on Atmospheric Ozone and OH: results from QUANTIFY, *Journal of Atmospheric Chemistry and Physics*, 9, pp. 3113-3136.

Horowitz, L. W., S. Walters, D. L. Mauzerall, L. K. Emmons, P. J. Rasch, C. Granier, X. Tie, J.-F. Lamarque, M. G. Schultz, G. S. Tyndall, J. J. Orlando, and G. P. Brasseur (2003), A global simulation of tropospheric ozone and related tracers, Description and evaluation of MOZART, version 2, *Journal of Geophysical Research*, 108 (D24), p. 4784.

IPCC (1999), Aviation and the global atmosphere, In: J. E Penner, D.H. Lister, D.J. Griggs, D.J. Dokken, M. McFarland (Eds.), Intergovernmental Panel on Climate Change. Cambridge University Press, Cambridge, UK.

Isaksen, I. S. A., C. Granier, G. Myhre, T. K. Berntsen, S. B. Dalsøren, M. Gauss, Z. Klimont, R. Benestad, P. Bousquet, W. Collins, T. Cox, V. Eyring, D. Fowler, S. Fuzzi, P. Jöckel, P. Laj, U. Lohmann, M. Maione, P. Monks, A. S. H. Prevot, F. Raes, A. Richter, M. Rognerud, B., Schulz, M., Shindell, D., Stevenson, D. S., Storelvmo, T., Wang, W.-C., van Weele, and D. Wuebbles (2009), Atmospheric composition change: climate–chemistry interactions, *Atmospheric Environment*, 43(33), pp. 5138-5192.

Johnson, C. (1992), Impact of aircraft and surface emissions of nitrogen oxides on tropospheric ozone and global warming, *Nature*, 355, pp. 69-71.

Johnson, C. E., and R. G. Derwent (1996), Relative radiative forcing consequences of global

emissions of hydrocarbons, carbon monoxide and NOx from human activities estimated with a zonally-averaged two-dimensional model, *Climatic Change*, 34 (3-4), pp. 439-462.

Johnston, H. S. (1971), Reduction of Stratospheric Ozone by Nitrogen Oxide Catalysts from Supersonic Transport Exhaust, *Science*, 173, p.517.

Kinnison, D. E., D. R. Marsh, R. R. Garcia, F. Vitt, S. Tilmes, M. J. Mills, J.-F. Lamarque, L. K. Emmons, J. J. Orlando, A. Gettelman, H.-L. Liu, V. Yudin, M. Park, W. Randel, L. L. Pan, M. Brakebusch, C. E. Randall, and P. Hess (2011), Description and evaluation of the Whole Atmosphere Community Climate Model (WACCM): Chemistry Update, in preparation.

Kinnison, D. E., G. P. Brasseur, S. Walters, R. R. Garcia, D. A. Marsh, F. Sassi, B. A. Boville, L. Harvey, C. Randall, L. Emmons, J.-F. Lamarque, P. Hess, J. Orlando, G. Tyndall, X. X. Tie, W. Randel, L. Pan, A. Gettelman, C. Granier, T. Diehl, U. Niemeier, and A. J. Simmons (2007), Sensitivity of chemical tracers to meteorological parameters in the MOZART-3 chemical transport model, *Journal of Geophysical Research*, 112 (D20).

Koffi, B., S. Szopa, A. Cozic, D. Hauglustaine, and P. van Velthoven, P. (2010), Present and future impact of aircraft, road traffic and shipping emissions on global tropospheric ozone, *Journal of Atmospheric Chemistry and Physics*, 10 (11), pp. 681-711.

Köhler, M.O., G. Radel, O. Dessens, K. P. Shine, H. L. Rogers, O. Wild, and J. A. Pyle (2008), Impact of perturbations to nitrogen oxide emissions from global aviation, *Journal of Geophysical Research*, 113 (D11).

Lamarque, J.-F. , L. K. Emmons, P. G. Hess, D. E. Kinnison, V. Tilmes, V. Vitt, V. Heald, E. A. Holland, P. H. Lauritzen, J. Neu, J. J. Orlando, P. Rasch, and G. Tyndall (2011), CAM-chem: Description and evaluation of interactive atmospheric chemistry in CESM, *Geoscientific Model Development Discussions*, 5, pp. 369 - 411.

Lee, D. S., D. W. Fahey, P. M. Forster, P. J. Newton, R. C. N. Wit, L. L. Lim, B. Owen, and R. Sausen (2009), Aviation and global climate change in the 21st century, *Atmospheric Environment*, 43, pp. 3520 – 3537.

Liang, Q., J. M. Rodriguez, A. R. Douglass, J. H. Crawford, J. R. Olson, E. Apel, H. Bian, D. R. Blake, W. Brune, M. Chin, P. R. Colarco, A. da Silva, G. S. Diskin, B. N. Duncan, L. G. Huey, , D. J. Knapp, D. D. Montzka, J. E. Nielsen, S. Pawson, D. D. Riemer, A. J. Weinheimer, and A. Wisthaler, (2011), Reactive nitrogen, ozone and ozone production in the Arctic troposphere and the impact of stratosphere-troposphere exchange, *Journal of Atmospheric Chemistry and Physics*, 11, 13181-13199.

Liu, X., R. C. Easter, S. J. Ghan, R. Zaveri, P. Rasch, X. Shi, J.-F. Lamarque, A. Gettelman, H. Morrison, F. Vitt, A. Conley, S. Park, R. Neale, C. Hannay, A. Ekman, P. Hess, N. Mahowald, W. Collins, M. Iacono, C. Bretherton, and M. Flanner (2012), Toward a Minimal

Representation of Aerosol Direct and Indirect Effects: Model Description and Evaluation, *Geosci entific Model Development Discussion*, 4, 3485-3598, doi:10.5194/gmdd-4-3485-2012.

McElroy, M. B., S. C. Wofsy, J. E. Penner, and J. C. McConnell (1974), Atmospheric Ozone: Possible Impact of Stratospheric Aviation, *Journal of the Atmospheric Sciences*, 31, p. 287.

Meinshausen, M., S. C. B. Raper, and T. M. L. Wigley (2011), Emulating coupled atmosphere-ocean and carbon cycle models with a simpler model, MAGICC6 – Part 1: Model description and calibration, *Journal of Atmospheric Chemistry and Physics*, 11, pp. 1417–1456.

Morrison, H., and A. Gettelman (2008), A new two-moment bulk stratiform cloud microphysics scheme in the NCAR Community Atmosphere Model (CAM3), Part I: Description and numerical tests, *Journal of Climate*, 21 (15), pp. 3642–3659.

Neale, R. B., J. Richter, S. Park, P. H. Lauritzen, S. J. Vavrus, P. J. Rasch, and M. Zhang (2011), The Mean Climate of the Community Atmosphere Model (CAM4) in forced SST and fully coupled experiments, *Journal of Climate*, Submitted.

Neu, J. L., and M. J. Prather (2011), Toward a more physical representation of precipitation scavenging in global chemistry models: cloud overlap and ice physics and their impact on tropospheric ozone. *Journal of Atmospheric Chemistry and Physics Discussions*, 11, pp. 24413–24466.

Olsen, S. C., and D. J. Wuebbles (2012), Comparison of global 3-D aviation emissions datasets, *Journal of Atmospheric Chemistry and Physics*, 12, pp. 16885 – 16992.

Olsen, S. C., G. P. Brasseur, D. J. Wuebbles, S. Barrett, H. Dang, S. D. Eastham, M. Z. Jacobson, A. Khodayari, H. Selkirk, A. Sokolov, N. Unger (2013), Comparison of model estimates of the effects of aviation emissions on atmospheric ozone and methane, submitted to *Geophysical Research Letters.*

Price, C., J. Penner and M. Prather (1997), NOx from lightning: Global distribution based on lightning physics, *Geophysical Research Letter, Res*., 102, pp. 5929–5941.

Ridley, B., K. Pickering, and J. Dye (2005), Comments on the parameterization of lightning-produced NO in global chemistry-transport models, *Atmospheric Environment*, 39, pp. 6184–6187.

Roof, C., A. Hansen, G. G. Fleming, T. Thrasher, A. Nguyen, C. Hall, E. Dinges, R. Bea, F. Grandi, B. Y. Kim, S. Usdrowski, and P. Hollingsworth (2007), Aviation Environmental Design Tool (AEDT) System Architecture AEDT-AD-01.

Sillman, S., 2012. Overview: Tropospheric ozone, smog and ozone-NOx-VOC sensitivity. [online] University of Michigan. Available from: http://www-personal.umich.edu/~sillman/Sillman-webOZONE.pdf [Accessed 11 April 2012].

Stevenson, D. S., R. M. Doherty, M. G. Sanderson, W. J. Collins, C. E. Johnson, and R. G. Derwent (2004), Radiative forcing from aircraft NOx emissions: Mechanisms and seasonal dependence, *Journal of Geophysical Research,* 109 (D17).

Tilmes, S., J.-F. Lamarque, L. K. Emmons, A. Conley, M. G. Schultz, M. Saunois, V. Thouret, A. M. Thompson, S. J. Oltmans, B. Johnson, and D. Tarasick (2011), Technical Note: Ozonesonde climatology between 1995 and 2011: Description, Evaluation and Applications, *Atmospheric Chemistry and Physics*, 12, 7475-7497, 2012, doi:10.5194/acp-12-7475-2012.

Voulgarakis, A., N. H. Savage, O. Wild, G. D. Carver, K. C. Clemitshaw, and J. A. Pyle (2009), Upgrading photolysis in the p-TOMCAT CTM: model evaluation and assessment of the role of clouds, *Geoscientific Model Development*, 2 (1), pp. 59-72.

Walcek, C. J., R. A. Brost, J. S. Chang, and M. L. Wesely (1986), SO_2, sulfate and HNO_3 deposition velocities computed using regional land use and meteorological data, *Atmospheric Environment*, 20, pp. 946–964.

Walmsley, J. L. and M. L. Wesely (1996), Modification of coded parameterizations of surface resistances to gaseous dry deposition, *Atmospheric Environment*, 30, pp. 1181–1188.

Wesely, M. L. and B. B. Hicks (2000), A review of the current status of knowledge on dry deposition, *Atmospheric Environment*, 34, pp. 2261–2282.

Wild, O., M. J. Prather, and H. Akimoto (2001), Indirect long-term global cooling from NOx emissions, *Geophysical Research Letters*, 28, pp. 1719-1722.

Wilkerson, J.T., M. Z. Jacobson, A. Malwitz, S. Balasubramanian, R. Wayson, G. Fleming, A. D. Naiman, and S. K. Lele (2010), Analysis of emission data from global commercial aviation: 2004 and 2006, *Journal of Atmospheric Chemistry and Physics*, 10, pp. 6391–6408.

CHAPTER 4: EVALUATION OF AVIATION NOx-INDUCED RADIATIVE FORCINGS FOR 2005 AND 2050

Abstract

Aviation NOx emissions lead to the production of ozone (O_3) in the troposphere and lower stratosphere. This O_3 increase results in a reduction of methane (CH_4) which causes a longer-term reduction in O_3 concentrations and lower stratospheric water vapor (SWV). Most prior studies have not fully accounted for these latter two effects. Here we report new evaluations of aviation NOx-induced radiative forcing (RF) from these factors and compare them with previously published analyses of aviation NOx effects on climate. To do so, we evaluate the aviation NOx-induced steady-state RFs using the three-dimensional (3-D) global climate-chemistry Community Atmosphere Model (CAM), CAM4. We then determine time dependent transient RFs by utilizing a parameterization based on the specific RFs (RFs per unit of NOx emission) calculated in the 3-D model simulations. In this context, transient RF refers to the time-dependent forcing driven by time-dependent emissions data considering the lifetime of the perturbed species, and steady-state RF refers to the steady-state focing due to the repeated emissions of a particular year. The net aviation NOx-induced transient RFs calculated for the year 2005 NOx emissions, for 2050 Scenario1 and 2050 Baseline NOx emissions are 17.1, 31.1 and 96.2 mWm^{-2}, respectively. The 2050 Scenario1 assumes a 2% per annum fuel efficiency due to technological and operational improvements and the 2050 Baseline assumes no technological or operational improvements. For aviation NOx-induced effects we find that the net transient RFs differ from the linearly scaled specific RFs (specific RFs multiplied by NOx emissions) by +22% for 2005, and +10% and +36% for 2050 Scenario1 and Baseline projections, respectively. These results indicate the importance of accounting for the transient CH_4, long-term ozone and stratospheric water vapor changes when reporting aviation NOx-induced RF changes and interpreting results of 3-D steady state simulations of the NOx-O_3 effects.

Introduction

Aviation emissions alter the chemistry of the atmosphere and the Earth's energy balance. Radiative forcing (RF) is a measure of the net change in the Earth's energy balance at the tropopause. The aviation sector contributed about 5% of the total human-contributed RF on the climate in 2005 (Lee et al., 2010). Aviation emissions of CO_2 and NOx, and aviation-induced cloudiness (contrails and induced cirrus formations) are the main contributors to this RF. Other aviation effects are currently thought to be a small fraction of the total aviation-induced RF (Lee et al., 2010; IPCC, 1999). In this paper, we focus on calculations of aviation NOx-induced effects.

Aircraft emitted nitrogen oxides (NOx) affect the climate in several ways. At commercial aircraft cruise altitudes in the upper troposphere and lower stratosphere, aviation NOx emissions increase ozone (O_3) production and concentrations. This O_3 increase is associated with an increase in radiative forcing on climate (e.g., IPCC, 1999; Wuebbles et al., 2007; Lee et al., 2009). At these altitudes, aviation NOx emissions are about four times more efficient in producing O_3 than NOx emissions at the Earth's surface (Hodnebrog et al., 2011). Some of the O_3 produced by aviation NOx emissions photolyze to produce excited oxygen atoms that then react with water vapor to produce OH. Additionally, NOx emissions increase the OH level by shifting the HOx balance in favor of OH (Stevenson et al., 2004; Berntsen et al., 2005). In the troposphere, OH is the dominant sink for methane (CH_4); therefore an increase in OH increases the loss of CH_4 and thus decreases its concentration. Since CH_4 is a potent greenhouse gas (with a lifetime of ~10 years), this decrease in CH_4 is associated with a decrease in the CH4 RF (IPCC, 1999; Prather et al., 2001; Wuebbles et al., 2007; Lee et al., 2009). As CH_4 is also a major precursor to O_3 formation in the free troposphere, its reduction results in a longer-term response (decrease) in O_3 that decays in proportion to the changes in CH_4 over time. Thus a single pulse of aviation NOx can result in a short-term increase in O_3, which decays with a lifetime (e-folding time) of a few months, and a longer-term decrease in CH_4 and O_3, which decays with a lifetime of ~ 10 years (Wild et al., 2001). Also, since water vapor is an end-product of CH_4 oxidation, a decrease in CH_4 results in a decrease in stratospheric water vapor (SWV). Both the long-term decrease in O_3 and SWV, induced by changes in CH_4 are associated with a decrease in RF (e.g.,

Prather et al., 2001). The decrease in water vapor due to the decrease in CH_4 occurs both in the troposphere and stratosphere; however, the change in water vapor due to CH_4 oxidation in the troposphere is insignificant (as such a change is small compared to the large variation of the background water vapor in the troposphere), but is significant in the stratosphere where ~ 25±5% of the net increase in the background stratospheric water vapor mixing ratio is due to the background CH_4 oxidation during 1980–2010 (Hurst et al., 2011). The positive RF associated with the short-term NOx-induced O_3 production is to some extent offset by the negative RFs associated with aviation NOx emissions leading to a relatively large uncertainty associated with the overall net NOx-induced RF. It is generally reported that the net effect is positive (IPCC, 1999; Holmes et al., 2011).

The production of O_3 due to additional NOx emissions depends on the background atmosphere (e.g., Kohler et al., 1997; Jacob, 1999), which is quite inhomogeneous; therefore three-dimensional (3-D) chemistry-climate models are necessary to quantify NOx-induced effects. However, even using 3-D models, there are relatively large differences between the calculated aviation NOx-induced effects due to differences in model chemistry schemes and the treatment of physical processes, including transport and other factors (IPCC 1999; Stevenson et al., 2004; Kohler et al., 2008; Holmes et al., 2011; Olsen et al., 2012). Ideally, aviation NOx-induced effects would be calculated using 3-D models in a transient manner with time-dependent emissions and full consideration of the couplings and lifetimes of the perturbed species. However, it is inherently computationally demanding to run a 3-D model due to the detailed representation of physical and chemical processes. In addition, the calculation of transient effects in 3-D models adds further computational expense, as it requires accounting for changes in historical emissions. Therefore, in 3-D chemistry-climate models, usually the steady-state response of the system to the perturbation at a given year is calculated.

Steady-state response refers to a model's response once non-changing conditions relative to the background atmosphere have been reached for annually repeating emissions. This is a one way to evaluate the importance of emissions at a given year. To avoid the computational cost of calculating transient aviation NOx-induced transient RFs in 3-D models, in this study as in most other studies (Berntsen and Fuglestvedt, 2008; Marais et al., 2008; Mahashabde et al., 2011),

after the aviation NOx-induced specific steady-state RFs (steady-state RFs per unit of NOx emission) are calculated for a reference year in a 3-D model, they are used to calculate the annual global mean transient response of the system for any given time in the past or future. In general, NOx-induced effects have a non-linear dependence on the NOx concentrations. However, on the scale on which the aviation NOx emissions influence the background atmosphere, its induced effects depends linearly on the aviation NOx emission rate (Grewe et al., 1999; IPCC, 1999; Sausen and Schumann, 2000). Therefore, in the case of aviation NOx-induced effects, a simple parameterization such as linear scaling the global mean specific RFs calculated from the steady-state 3-D model simulation by total annual NOx emissions is utilized to analyze the steady-state RFs caused by perturbations at other years. Furthermore, by including the lifetime of the perturbed species in the analyses, we calculate transient RFs. Parameterizations of this type are usually employed in simple climate models (SCMs). SCMs use parameterization to represent the complex physical processes that are otherwise explicitly solved in 3-D models, and usually present global average values for the physical quantities of interest with a yearly temporal resolution (Harvey et al., 1997; Marais et al., 2008; Mahashabde et al., 2011; Khodayari et al., 2013). Because of this, SCMs are essential tools for exploring policy options and trade-offs when using a 3-D model to explore the climate effects of numerous different scenarios would be too computationally demanding. (Harvey et al., 1997; Marais et al., 2008; Mahashabde et al., 2011; Khodayari et al., 2013).

For short-lived species (species with lifetimes less than one year), transient RFs for a given year are nearly equal to the product of the specific RFs and the NOx emissions for that year. This is because short-lived species reach steady-state rapidly and their effects do not last more than a very short time beyond their release year. However, this is not the case for long-lived species such as CO_2 and CH_4. Therefore transient RFs and steady-state RFs should not be used interchangeably for aviation NOx-induced CH_4, plus the long-term O_3 and SWV effects induced by the changes in CH_4. In this study, we investigate the difference between linearly scaled aviation NOx-induced steady-state RFs and transient RFs. To further investigate the difference between these two types of RFs, we compare a set of steady-state RFs that were previously reported by Lee et al. (2009) as representative of the most recently available analysis of aviation NOx-induced projected effects to the equivalent transient RFs calculated in this study. Lee et

al.'s (2009) steady-state RFs were solely calculated by linear scaling of the specific RFs by NOx emission for a given year. The linearly scaled approach assumes steady-state condition and that everything has a relatively short lifetime (< 1 year). The use of transient RFs instead of the linearly scaled steady-state RFs is particularly important for quantifying aviation NOx-induced effects. This is because aviation NOx emissions result in three relatively long-lived effects (CH_4, SWV and long-term O_3) that together contribute significantly to the overall RF due to aviation NOx emissions.

The following section describes the model and the data used to calculate aviation NOx-induced effects. The following section provides an overview of the methodology used to calculate aviation NOx-induced steady-state and transient effects. The calculated steady-state reference year forcings are presented in the following section. The last two sections present the calculated transient RFs and quantify the difference between transient RFs and linearly scaled steady-state RFs and the concluding remarks.

Data and Model

The representative 3-D global chemistry-climate model, namely the Community Atmosphere Model (CAM), CAM4 (Neale et al., 2011and Gent et al., 2011) was used for this study. The CAM4 simulations used an interactive troposphere-stratosphere gas-phase chemistry that included 133 species and 330 photochemical reactions (CAM4) (Lamarque et al., 2012). CAM4 (version 1.0.3) has 56 vertical levels covering up to about 2hPa, with a horizontal resolution of approximately 2.5° (longitude) × 1.9° (latitude).

Three dimensional time-dependent aviation NOx emission data for 2006 and for 2050 were used to simulate the aviation NOx-induced effects for 2006 and 2050. The data were provided by the Volpe National Transportation Systems Center and were computed using the Federal Aviation Administration's Aviation Environmental Design Tool (AEDT) (Roof et al., 2007). Two different 2050 emissions were used for 2050 projections, which are based on the FESG consensus demand forecast (FESG, 1998). The first, the 2050 Baseline emissions (~4 TgN/yr), assumes no technological or operational improvements in aviation activity and the second, the

2050 Scenario1 emissions (~1.6 TgN/yr), assumes a 2% per annum fuel efficiency due to technological and operational improvements. The emissions have a spatial resolution of 1^o (latitude) by 1^o (longitude) by 150 m altitude and an hourly temporal resolution.

All the simulations in this study were driven with 2005 meteorology data based on the Goddard Earth Observing System (GEOS) Data Assimilation System (DAS) v5.1 (Rienecker et al., 2008), and have the same spatial resolution as CAM4, and six hours temporal resolution. The monthly surface concentration of long-lived species and the most important source gases for inorganic chlorine and bromine compounds were prescribed as boundary conditions based on the IPCC (2007) evaluation of their concentrations suing the corresponding RCP 4.5 emission scenarios. The concentration of all other species is simulated in the model using its corresponding IPCC RCP 4.5 emission scenario for the appropriate year.

The University of Illinois Radiative Transfer Model (UIUC RTM) was used offline to calculate the forcing associated with aviation NOx-induced short-term O_3. UIUC RTM calculates fluxes of solar and terrestrial radiation across the tropopause. Earlier versions of the UIUC RTM have been used in previous research (e.g., Jain et al., 2000; Naik et al., 2000; Youn et al., 2009; Patten et al., 2011). The solar model includes 18 spectral bins from 0.2 to 0.5 microns and it includes absorption by H_2O, O_3, O_2, CO_2, clouds and the surface as well as scattering processes by cloud, gas-phase molecules, and the surface. The terrestrial radiation calculation utilizes a narrow band model of absorptivity and emissivity that covers the wave numbers from 0 to 3000 cm^{-1} at the resolution of 10 cm^{-1} for H_2O, CFC-11, and CFC-12 and of 5 cm^{-1} for other gases. The infrared absorption parameters for gases are obtained from HITRAN 2004 database (Rothman et al., 2005). Surface albedo and emissivity are based on observations, while clouds are based on the International Satellite Cloud Climatology Project.

Methodology

We calculated the aviation NOx-induced changes in short-term O_3 concentration from the difference in steady-state responses of CAM4 between a simulation including aviation emissions (perturbed) and one that does not (background). Since CH_4 was prescribed as a lower boundary

condition in the simulations, the tropospheric mean change in steady-state CH_4 concentration was calculated from the change in its lifetime with respect to reaction with tropospheric OH derived from CAM4 simulations (Fuglestvedt et al., 1999) as shown in Equation 4.1:

$$\Delta[CH_4]_{ss} = [CH_4]_{ref,ss} \times \left(-1.4\left(\frac{\Delta\tau}{\tau_{ref}}\right)\right). \quad (4.1)$$

A feedback factor of 1.4 was used to account for the CH_4 feedback on its own lifetime (Fuglestvedt et al., 1999). Here τ_{ref} denotes the lifetime of CH_4 versus reaction with OH in the non-perturbed simulation, $\Delta\tau$ the change in CH_4 lifetime between the non-perturbed simulation and the NOx-perturbed simulation, $[CH_4]_{ref,ss}$ the tropospheric mean CH_4 concentrations in the non-perturbed simulation and $\Delta[CH_4]_{ss}$ the tropospheric mean change in steady-state CH_4 concentration.

The tropospheric mean CH_4-induced change in long-term O_3 in Dobson unit (DU) was calculated based on the tropospheric mean steady-state changes in CH_4 concentration following the approach described in Prather et al., (2001) and Naik et al., (2005):

$$(O_3)_{long-term_3} = \frac{\Delta[CH_4]}{[CH_4]} \times \frac{0.64}{0.1}\,\text{DU}. \quad (4.2)$$

Here $\Delta[CH_4]$ denotes the tropospheric mean steady-state change in CH_4 concentration, and $[CH_4]$ the tropospheric mean background concentration of CH_4 calculated from the non-perturbed simulation.

The aviation NOx-induced short-term O_3 RFs were calculated as the difference of the radiation imbalance between the perturbed and non-perturbed simulations at the tropopause calculated with the UIUC RTM, not including the effects of stratospheric adjustment. The reference year steady-state RFs for CH_4 were calculated based on scaling the CH_4 specific RF of 0.37 $Wm^{-2}ppm^{-1}$ reported in Forster et al., 2007, by the tropospheric mean changes in steady-state CH_4 concentration calculated by Equation 4.1. The reference year steady-state RFs for long-term O_3 were calculated based on scaling the long-term O_3 specific RF of 0.036 $Wm^{-2}DU^{-1}$ reported in

Myhre et al., 2011, by the tropospheric mean CH_4-induced changes in ozone calculated with Equation 4.2. The change in SWV steady-state RF was calculated by scaling the change in CH_4 steady-state RF by 21% (Myhre et al., 2007).

The relationship between aviation NOx emissions and NOx-induced steady-state RFs is nearly linear (Grewe et al., 1999; IPCC, 1999; Sausen and Schumann, 2000). Due to this linearity, in SCMs that present global average values and have annual temporal resolution, the global mean aviation NOx-induced steady-state RFs for any given year have often been calculated assuming linear scaling of the global mean specific RFs calculated from 3-D models by the total NOx emissions for that year (Equation 4.3) (Marais et al., 2008; Lim et al., 2007; Sausen and Schumann, 2000). The same relationship was also assumed in IPCC (1999). Using this approach the aviation NOx-induced steady-state RFs for a given year may be expressed as

$$\Delta F_{ss}(t) = \frac{\Delta F_{ss(ref\ year)}}{Q_{NOx(ref\ year)}} \times Q_{NOx(t)}, \tag{4.3}$$

where ΔF denotes the global mean RF for different aviation NOx-induced compounds, SS means steady-state, Q_{NOx} is the total aviation NOx emissions and $(\frac{\Delta F_{ss}(ref\ year)}{Q_{NOx(ref\ year)}})$ is the steady-state RF per unit of NOx emissions. The steady-state RF_{ss} for the reference year is obtained from 3-D Chemical Transport Models (CTMs) or Climate Chemistry Models (CCMs).

However this method assumes an instantaneous adjustment for all species to aviation NOx emissions. While for short-lived species, e. g., short-term O_3, this approximation is reasonable, it is not for the RFs associated with the longer-lived CH_4 related effects. For such effects, the transient RF should be calculated using a method that accounts for the lifetime of the species. This applies to the reduction of CH_4, the additional long-term reduction of O_3 which responds with same lifetime as CH_4 (IPCC, 2007; Hoor et al., 2009), and the reduction of SWV induced by the reduction of CH_4. Using the specific RFs calculated based on the 3-D model simulations, we calculated the transient RFs for short-term production of O_3, the reductions in CH_4 and longer-term O_3 by considering the evolution of their RFs in the form of a convolution integral assuming a first-order exponential decay of RFs based on their perturbation lifetime, and accounting for

the emissions history of aviation NOx. We used the following mathematical equations to describe the decay of NOx-induced specific RFs as was proposed by Fuglestvedt et al. (2010).

$$\Delta SF_{CH4,O3}(t) = \Delta SF^{SS}_{CH4,O3}\left(1 - \exp\left(-\frac{t}{\alpha_s}\right)\right) \qquad for\ t \leq 1 \qquad (4.4)$$

$$\Delta SF_{CH4,O3}(t) = \Delta SF^{SS}_{CH4,O3}\left(1 - \exp\left(-\frac{1}{\alpha_s}\right)\right)\exp\left(-\frac{\mathrm{t}-1}{\alpha_s}\right) \qquad for\ t > 1 \qquad (4.5)$$

Here α_s is the lifetime of the effect (for CH_4 is effectively the adjustment time which is the CH_4 lifetime adjusted for its feedback on its lifetime), ΔSF denotes the NOx-induced specific RFs (mWm^{-2}/TgN) and SS indicates "steady-state".

A lifetime of 0.27 years was chosen for short-term production of O_3 following the suggestion by Fuglestvedt et al. (2010). Similar to Fuglestvedt et al. (2010), we find that the results are not sensitive to small variations around this value. An adjustment time of 10.7 years (Hoor et al. 2009) was assumed for CH_4 RF and its induced long-term O_3 RFs. Results are also insensitive to small variations around this value. Three different NOx emissions time series were used for transient RF calculation. The aviation NOx emissions time series used for the calculation of NOx-induced RFs were produced using fixed-year emissions for 1940-1999, 2000, 2005, 2020 and 2050. The pre-1999 aviation NOx emissions (1940-1999) were obtained from Sausen and Schumann (2000), emissions for the year 2000 from IEA fuel estimates (Lee et al. 2009), emissions for 2005 and 2020 from the regional forecast of the traffic growth as described in Lee et al. (2009) and emissions for 2050 from two alternative AEDT future projections, Scenario1 and Baseline. Between these fixed-year emissions, linear interpolation was used to derive a continuous time series of emissions. The time series of NOx emissions for which NOx emissions for 2050 were obtained from AEDT Scenario1 and AEDT Baseline projections are hereafter referred to as "Baseline-based" and "Scenario1-based", respectively.

In the absence of any estimate for the lifetime of SWV and the large uncertainty in its changes, the SWV transient RF induced by the changes in CH_4 was calculated by scaling the changes in CH_4 transient RFs by 21% (Myhre et al., 2007).

Aviation NOx-Induced Steady-State RFs

Table 4.1 shows the absolute and relative changes in tropospheric mean concentration of short-term O_3, and the aviation NOx-induced change in CH_4 lifetime derived from the CAM4 simulations for 2006, 2050 Baseline and 2050 Scenario1 aviation NOx emissions. The change in short-term O_3 concentration varies from 0.79 ($DU(O_3)/TgN$) for the 2006 NOx emissions to 0.65 ($DU(O_3)/TgN$) for the 2050 Baseline NOx emissions. These changes are either within or fall at the higher end of the 0.6±0.15 ($DU(O_3)/TgN$) range reported in literature (e.g., Penner et al., 1999; Stordal et al., 2006; Hoor et al., 2009, Holmes et al., 2011). The relative change in CH_4 lifetime varies from about -1.59 (%/[TgN/yr^{-1}]) for the 2050 Baseline NOx emissions to about -1.88 (%/[TgN/yr^{-1}])) for the 2050 Scenario1 NOx emissions. These results fall within the -1.4±0.4 (%/[TgN/yr^{-1}]) to -1.6±0.37 (%/[TgN/yr^{-1}]) range reported by Hodnebrog et al. (2011) using different emissions and an ensemble of six different atmospheric chemistry models. Although some of these studies used different CH_4 boundary conditions the impact of these differences has a relatively small effect (up to 2%) (Hodnebrog et al., 2011).

Table 4.1. The absolute and relative changes in Aviation NOx-induced tropospheric short-term O_3 and the absolute and relative change in CH_4 lifetime for the 2006, 2050 Scenario1, and 2050 Baseline aviation NOx emissions calculated from the CAM4 simulations.

Year emission	NOx (TgN/yr^{-1})	Short-term O_3 ($DU/[TgN/yr^{-1}]$)	Short-term O_3 (%) ($\%/[TgN/yr^{-1}]$)	$\Delta\tau_{CH4}$ (yr)	$\Delta\tau_{CH4}$
2006	0.82	0.79	1.91%	-0.12	-1.65
2050 Scenario1	1.6	0.78	3.68%	-0.27	-1.88
2050 Baseline	4.0	0.65	6.51%	-0.57	-1.59

Table 4.2 shows the tropospheric mean steady-state changes in CH_4 and long-term O_3 concentration calculated using Equations 4.1 and 4.2. The relative change in CH_4 concentration varies from about -2.3 (%/TgN) to -2.6 (%/TgN). These changes are higher than the -1.7±0.35 (%/TgN) range reported in previous studies (IPCC, 1999; Stordal et al., 2006; Hoor et al., 2009, Holmes et al., 2011). The change in long-term O_3 varies from about 3.4 ($DU/ppm\ (CH_4)$) to 3.6

(DU/ppm (CH_4)). These changes are within the range reported in the science literature, 3.5±1.0 (DU/ppm (CH_4)) (Prather et al., 2001; Fiore et al., 2008; Holmes et al., 2011).

Table 4.2. Aviation NOx-induced tropospheric mean steady-state changes in CH_4 and long-term O_3 for 2006, 2050 Scenario1, and 2050 Baseline aviation NOx emissions.

Year emission	NOx (TgN/yr^{-1})	CH_4 (ppb)	CH_4 (%/[TgN/yr^{-1}])	long-term O_3 (DU/ppm(CH_4))
2006	0.82	-32.8	-2.3%	3.7
2050 Scenario1	1.6	-76.4	-2.6%	3.4
2050 Baseline	4.0	-161.3	-2.2%	3.5

Table 4.3 shows the aviation NOx-induced steady-state RFs for 2006, 2050 Scenario1, and 2050 Baseline aviation NOx emissions. Results indicate that short-term O_3 forcing is the dominant component of the aviation NOx-induced forcing and that overall aviation NOx-induced changes exert a positive forcing on climate. As shown in Table 3, the increase in aviation NOx-induced forcings is consistent with the increase in the aircraft NOx emissions.

Table 4.3 Aviation NOx-induced steady-state RFs calculated from the CAM4 model simulations and the UIUC RTM for the 2006, 2050 Scenario1, and 2050 Baseline aviation NOx emissions.

Year emission	NOx (TgN/yr^{-1})	RF (mWm^{-2})				
		Short-term O_3	CH_4	Long-term O_3	SWV*	Net
2006	0.82	36.5	-12.1	-4.4	-2.6	17.4
2050 Scenario1	1.6	70.5	-28.3	-9.4	-5.9	26.9
2050 Baseline	4.0	143.0	-59.7	-20.3	-12.5	50.5

*SWV: Stratospheric water vapor

Figure 4.1 shows the aviation NOx-induced steady-state RF components for the NOx emissions presented in Table 3. There is a nearly linear relationship between aviation NOx-induced steady-state RF components and NOx emissions (Figure 4.1). However, as it is shown for the case of short-term O_3, the linear relationship is a better fit at small values of the NOx

emissions indicating non-linear response at high aviation NOx emissions (2050 Baseline emissions).

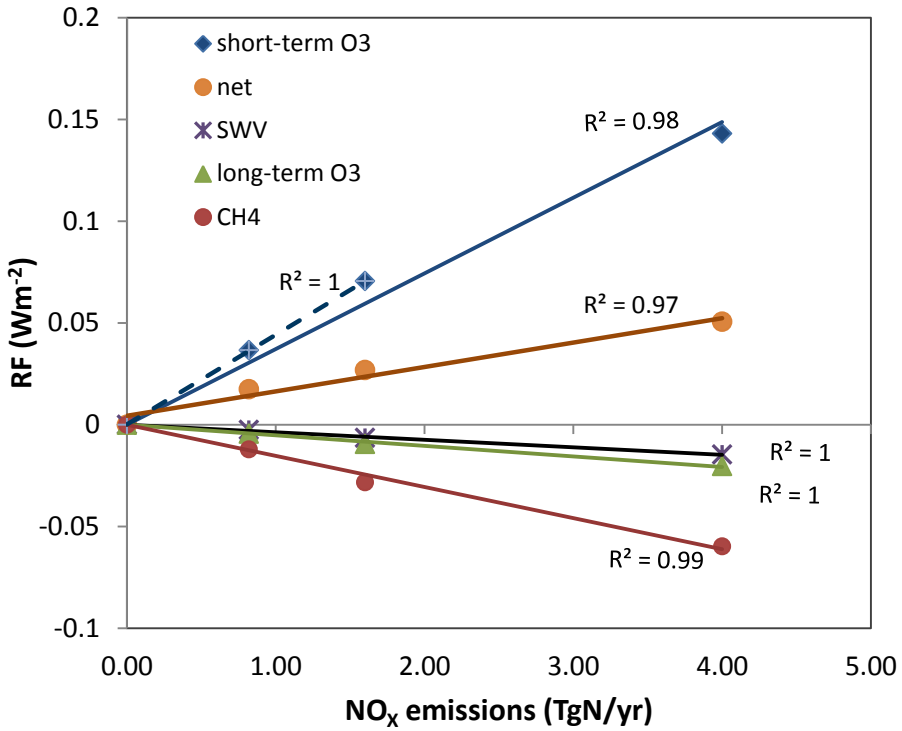


Figure 4.1 Steady-state RFs for short-term O_3 (blue line), SWV (purple line), long-term O_3 (green line), CH_4 (red line) and net (orange line) calculated from the CAM4 simulations and the UIUC RTM for the 2006, 2050 Scenario1 and 2050 Baseline NOx emissions.

The specific RFs for the aviation NOx-induced compounds in this study were calculated from the slope of corresponding lines on Figure 4.1. For this study we use specific RFs calculated from the 2006 (~0.82 TgN/yr) and 2050 Scenario 1, (~1.6 TgN/yr) data points, since the non-linearity associated with the high NOx emissions of 2050 Baseline (~4.0 TgN/yr) is not representative of most aviation emissions over our time of interest.

Table 4.4 shows the specific steady-state RFs calculated in this study relative to those reported in Sausen and Schumann (2005) (which were updates to the IPCC (1999) best estimate) and Holmes et al. (2011) which were based on an ensemble of previous published studies published since the IPCC report on aviation (1999). The specific steady-state short-term O_3 and CH_4 RFs based on these CAM4 results are about 33% and 8% higher in magnitude, respectively, than those reported in Sausen and Schumann (2005) (these values were also used in Lee et al. (2009)). These specific RFs are within the mean ± standard deviation (SD) range of previous reported specific RFs for CH_4 and long-term O_3 reported in Holmes et al. (2011) but higher than the Holmes et al.'s reported mean ± SD range for short-term O_3. Generally, the uncertainty in aviation NOx-induced effects is large (Holmes et al., 2011) and the model evaluations of these effects sometimes vary by up to 100% due to the differences in model chemistry schemes, transport, and other factors (Holmes et al., 2011).

Table 4.4 Aviation NOx-induced specific RFs calculated based on the CAM4 model results and the UIUC RTM compared to those reported in Sausen and Schumann (2005) and Holmes et al. (2011).

Model	Specific RFs (mWm^{-2}/TgN)			
	Short-term O_3 SWV	CH_4	long-term O_3	
CAM4 (this study)	44.2	-17.0	-5.8	-3.6
Sausen and Schumann (2005)	33.2	-15.8	—	—
Holmes et al. (2011)	27.3±9.7	-16.1±5.6	-6.6±3.3	—

Aviation NOx-Induced Transient RFs

Figure 4.2a shows the time series of aviation NOx emissions used to derive the transient and linearly scaled RFs for the Scenario1-based and Baseline-based scenarios. The solid line corresponds to "Scenario1-based" NOx emissions time series and the dashed line corresponds to "Baseline-based" emission time series. The time series of the net aviation NOx-induced transient and linearly scaled RFs associated with the use of Scenario1-based and Baseline-based NOx emissions time series are shown in Figure 4.2b. The "Scenario1-based" and "Baseline-based" transient RFs were obtained using the specific RFs obtained from CAM4 and the RTM. The

comparison of transient RFs to linearly scaled RFs in Figure 4.2b indicates that the differences between transient and linearly scaled RFs are larger for high growth emission scenarios.

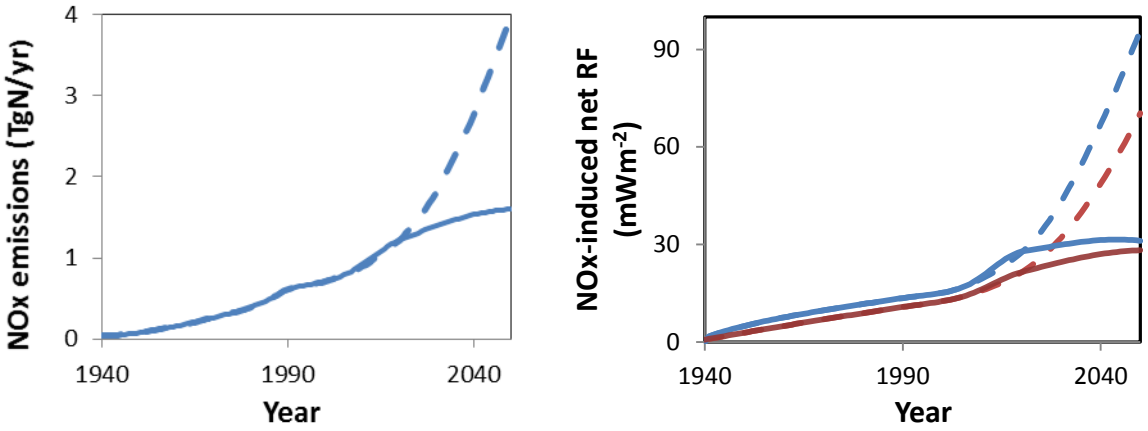


Figure 4.2. (a) Time series of aviation NOx emissions for the Baseline-based (dashed line) and Scenario1-based (solid-line) scenarios. (b) Aviation NOx-induced transient (blue) and linearly scaled (red) RFs for the Baseline-based (dashed lines) and Scenario1-based (solid lines) scenarios.

To illustrate the difference between transient RFs and linearly scaled RFs, the transient RFs for 2005 and 2050 are compared to the their corresponding linearly scaled RFs. Table 4.5 presents the individual components and net of aviation NOx-induced transient RFs for the years 2005 and 2050 Scenario1 and 2050 relative to the linearly scaled RFs using the specific RFs obtained from CAM4 and the RTM. The comparison of the results presented in Table 4.5 points to the effects of accounting for the lifetime effects of perturbed species into RF calculations. The transient RFs and the linearly scaled RFs are nearly the same for short-term O_3 (to within 4%). Therefore, short-term O_3 transient RF can be approximated with its steady-state RF. However, the transient RFs for CH_4, long-term O_3 and SWV are about 20%, 17% and 18% lower in magnitude, respectively than the linearly scaled RFs in 2005. The transient RFs for the long-term effects (i.e. CH_4, long-term O_3 and SWV) are about 7% and 30% lower in magnitude than the linearly scaled RFs for the 2050 Scenario1 and the 2050 Baseline NOx emissions, respectively. The net aviation NOx-induced transient RFs for the 2005, the 2050 scenario1 and the 2050 Baseline NOx emissions are about 22% , 10% and 36% higher, respectively, than the net of the linearly scaled RFs.

The inclusion of the long-term O_3 and SWV transient RFs lowers the net aviation-induced transient RFs by about 26%, 31% and 21% in 2005 and 2050 for the Scenario1-based Baseline-based NOx emissions, respectively. Therefore, long-term O_3 and SWV are important components of aviation NOx-induced RFs.

In order to examine the impact of transient versus linearly scaled RFs on previous studies, we compared the Lee et al.'s (2009) reported RFs that were calculated by linear scaling to their corresponding transient RFs. The transient RFs were calculated using the same emission scenario and specific RFs as in Lee et al. (2009), and taking into account the lifetime of the perturbed species.

Table 4.5 Aviation NOx-induced transient RFs calculated using the specific RFs obtained in this study in comparison with RFs obtained by linear scaling of the specific RFs obtained from CAM4 and the RTM.

		RF (mWm^{-2})				
Transient RFs						
Year emission	NOx (TgN/yr^{-1})	Short-term O_3	CH_4	long-term O_3	SWV	Net
2005	0.79	34.0	-10.8	-3.8	-2.3	17.1
2050 Scenario1-based	1.6	70.5	-25.4	-8.7	-5.3	31.1
2050 Baseline-based	4.0	170.3	-47.8	-16.3	-10.0	96.2
Linearly scaled steady-state RFs						
2005	0.79	34.9	-13.5	-4.6	-2.8	14.0
2050 Scenario1	1.6	70.6	-27.3	-9.3	-5.7	28.3
2050 Baseline	4.0	176.6	-68.3	-23.2	-14.4	70.7

Table 4.6 presents the linearly scaled RFs reported in Lee et al. (2009) for the years 2005 and 2050 in comparison to their corresponding transient RFs. Lee et al. (2009) adopted the specific RFs reported in Sausen and Schumann (2005) and used IPCC A1t1 scenario (IPCC, 1999) for obtaining 2050 NOx emissions. The A1t1 scenario is consistent with the IPCC SRES

A1 emission scenario and includes future improvements in aircraft technology as described in Henderson et al., (1999).

Results in Table 4.6 show that linear scaling of the specific RFs, as in Lee et al. (2009), results in CH_4 RFs that are about 25% for 2005 and 36% for 2050 higher than the transient RFs for the Alt1 scenario. The Lee et al. (2009) study didn't report long-term O_3 and SWV RFs. Our findings suggest that not including the lifetime of the effects in the RF calculations could significantly affect the evaluation of the net aviation NOx-induced RF.

Table 4.6. Aviation NOx-induced transient RFs and linearly scalded steady-state RFs calculated using specific RFs from Sausen and Schumann (2005)

		RF (mWm^{-2})				
Transient RFs, specific steady-state RFs from Lee et al. (2009)						
Year emission	NOx (TgN/yr^{-1})	Short-term O_3	CH_4	long-term O_3	SWV	Net
2005	0.79	25.6	-10.0	–	–	15.6
2050 A1t1	3.2	105.8	-38.3	–	–	67.6
Linearly scaled steady-state RFs, Lee et al. (2009)						
2005	0.79	26.3	-12.5	–	–	13.8
2050 A1t1	3.2	109.8	-52.1	–	–	57.7

Conclusions

The new evaluations of net aviation NOx-induced RFs presented here include the major aviation NOx-induced effects: short-term O_3, CH_4, long-term O_3, and SWV. These effects have not been considered all together in earlier studies. The net aviation NOx-induced transient RFs calculated for 2005, 2050 Scenario1-based and 2050 Baseline-based NOx emissions are 17.1, 31.1 and 96.2 mWm^{-2}, respectively. The inclusion of long-term O_3 and SWV RFs decreases the net aviation-induced RFs by about 26%, 31% and 21% for 2005, 2050 Scenario1 and 2050 Baseline NOx emissions, indicating they are important components of aviation NOx-induced RFs on climate.

The magnitudes of aviation NOx-induced RFs calculated by correctly accounting for the perturbed species lifetimes are lower for CH_4, long-term O_3 and SVW which tend to have negative RFs. Since the dominant aviation NOx-induced RF is due to short-term $O_{3,}$ which is associated with positive RF, and its transient and steady-state RF are about the same, the calculation of transient RFs instead of linearly scaled steady-state RFs results in a higher net aviation NOx-induced RF. The net aviation NOx-induced transient RFs for 2005, 2050 Scenario1-based and 2050 Baseline-based NOx emissions are about 22% , 10% and 36% higher, respectively, than the net of the linearly scaled steady-state RFs. Since three out of the four aviation NOx-induced changes (i.e. CH_4, long-term O_3 and SVW) are long-term changes, correctly accounting for the lifetime effects of these changes is important in the evaluation of the net aviation NOx- induced effects.

BIBLIOGRAPGY

Berntsen, T., J. S. Fuglestvedt (2008), Global temperature responses to current emissions from the transport sectors, Proceedings of the National Academy of Sciences, USA 105, 19154–19159.

Berntsen, T. K., J. S. Fuglestvedt, M. M. Joshi, K. P. Shine, N. Stuber, M . Ponater, R. Sausen, D. A. Hauglustaine, and L. Li (2005), Response of climate to regional emissions of ozone precursors, Sensitivities and warming potentials, *Tellus*, B 57:283–304.

Briegleb, B. P. (1992a), Delta-Eddington approximation for solar radiation in the NCAR Community Climate Model, *Journal of Geophysical Research*, 97, 7603–7612.

Briegleb, B. P. (1992b), Longwave band model for thermal radiation in climate studies, *Journal of Geophysical Research*, 97, 11,475–11,485.

FESG, (1998). Report 4. Report of the Forecasting and Economic Analysis Sub-Group (FESG): Long-Range Scenarios. International Civil Aviation Organization Committee on Aviation Environmental Protection Steering Group Meeting, Canberra, Australia, January 1998, 131 pp.

Forster P, et al. (2007), Changes in atmospheric constituents and in radiative forcing, In: Solomon S, et al., editors. Climate Change 2007: The Physical Science Basis Fourth Assessment Report of the Intergovernmental Panel on Climate Change. Cambridge, UK: Cambridge Univ Press; pp. 129–234.

Fiore, A.M., J.J. West, L.W. Horowitz, V. Naik, M.D. Schwarzkopf (2008), Characterizingthe tropospheric ozone response to methane emission controls and the benefits to climate and air quality, *Journal of Geophysical Research*, 113, D08307. doi:10.1029/2007JD009162.

Fuglestvedt, J.S., K.P. Shine, T. Berntsen, J. Cook, D.S. Lee, A. Stenke, R.B. Skeie, G.J.M. Velders, and I.A. Waitz (2010), Transport impacts on atmosphere and climate: metrics, *Atmospheric Environment*, 44, 4648–4677.

Fuglestvedt, J. S., et al. (1999), Climatic forcing of nitrogen oxides through changes in tropospheric ozone and methane: Global 3D model studies, *Atmospheric Environment*, 33:961–977.

Gent, P. R., et al. (2011), The Community Climate System Model version 4, *Journal of Climate*, 24, 4973–4991.

Gregory, J. M., and P. M. Forster (2008), Transient climate response estimated from radiative forcing and observed temperature change, *Journal of Geophysical Research*, 113, D23105, doi:10.1029/2008JD010405.

Grewe, V., M. Dameris, R. Hein, I. Koehler, and R. Sausen (1999), Impact of Future SubsonicAircraft NOx Emissions on the Atmospheric Composition, *Journal of Geophysical Research*, 26, 47–50.

Harvey, D., et al. (1997), An Introduction to Simple Climate Models Used in the IPCC Second Assessment Report, IPCC Technical Paper 2 [Houghton, J.T., L.G. Meira Filho, D.J. Griggs, and K. Maskell (eds.)]. IPCC, Geneva, Switzerland.

Henderson, S. C., et al. (1999), Aircraft emissions: current inventories and future scenarios. In 'Aviation and the Global Atmosphere', Intergovernmental Panel on Climate Change, Eds, J. E. Penner, D. H. Lister, D. J. Griggs, D. J. Dokken, M. McFarland, Cambridge University Press, UK.

Holmes, C. D., Q. Tang, and M. J. Prather (2011), Uncertainties in climate assessment for the case of aviation NO, *Proceedings of the National Academy of Sciences*, U.S.A., 108, 10 997–11 002, doi:10.1073/pnas.1101458108, 2011.

Hoor, P., et al. (2009), The Impact of Traffic Emissions on Atmospheric Ozone and OH: results from QUANTIFY, *Atmospheric Chemistry and Physics*, 9:3113-3136.

Hodnebrog, Ø., T. K. Berntsen, O. Dessens, M. Gauss, V., Grewe, I. S. A. Isaksen, B. Koffi, G.,Myhre, D. Olivié, M. J. Prather, J. A. Pyle, F. Stordal, S. Szopa, Q. Tang, P. Velthoven, J. E. Williams, and K. Ødemark (2011), Future impact of non-land based traffic emissions on atmospheric ozone and OH – an optimistic scenario and a possible mitigation strategy, *Atmospheric Chemistry and Physics*, 11, 11 293–11 317, doi:10.5194/acpd-11-11293-2011, www.atmos-chem-phys.net/11/11293/2011/, 2011.

Hurst, D.F., S.J. Oltmans, H. Vömel, K.H. Rosenlof, S.M. Davis, E.A. Ray, E.G. Hall, and A.F. Jordan (2011), Stratospheric water vapor trends over Boulder, Colorado: Analysis of the 30 year Boulder record., *Journal of Geophysical Research*, 116, D02306, doi:10.1029/2010JD015065.

IPCC, (1999), Aviation and the global atmosphere 1999, Penner, J., Lister, D.H., Griggs, D.J., Dokken, D.J., McFarland, M. (Eds.), Intergovernmental Panel on Climate Change. Cambridge University Press, Cambridge, UK.

IPCC, (2001), Climate change 2001: the scientific basis. In: Houghton, J.T., Ding, Y., Griggs, D.J., Noguer, M., van der Linden, P.J., Dai, X., Maskell, K., Johnson, C.A. (Eds.), Contribution of Working Group I to the Third Assessment Report of the Intergovernmental Panel on Climate Change. Cambridge University Press, UK.

IPCC, (2007), Climate change 2007, The physical science basis. In: Solomon, S., Qin, D., Manning, M., Marquis, M., Averyt, K., Tignor, M.M.B., Miller, H.L., Chen, Z. (Eds.), Contribution of Working Group I to the Fourth Assessment Report of the Intergovernmental Panel on Climate Change. Cambridge University Press, UK.

Jacob, D. J., (1999), Introduction to Atmospheric Chemistry, Princeton University Press: Princeton, NJ.

Jain, A. K., B. P. Briegleb, K. Minschwaner, and D. J. Wuebbles (2000), Radiative forcings and global warming potentials of 39 greenhouse gases, *Journal of Geophysical Research*, 105, 20,773–20,790, doi:10.1029/2000JD900241.

Khodayari, A., D. J. Wuebbles, S. Olsen, J. S. Fuglestvedt, T., Berntsen, M. T., Lund, I., Waitz, P. Wolfe, P. M. Forster, M., Meinshausen, D. S. Lee and L. L. Lim (2013), Intercomparison and evaluation of the capabilities of simplified climate models to project the CO_2 effects of aviation on climate, Atmospheric Environment, 75, 321-328.
http://dx.doi.org/10.1016/j.atmosenv.2013.03.055.

Kohler, I., R. Sausen and R. Reinberger (1997), Contributions of aircraft emissions to the atmospheric NOx content, *Atmospheric Environment*, 31, 1801—1818.

Kohler, M.O., Radel, G., Dessens, O., Shine, K.P., Rogers, H.L., Wild, O., Pyle, J.A., (2008), Impact of perturbations to nitrogen oxide emissions from global aviation, *Journal of Geophysical Research*, 113, D11305. doi:10.1029/2007JD009140.

Lamarque, J. F., L. K., Emmons, P. G., Hess, D. E., Kinnison, S. Tilmes, V. Vitt, V. Heald, E. A. Holland, P. H. Lauritzen, J. Neu, J. J. Orlando, P. Rasch, and G.Tyndall (2012), CAM-chem: Description and evaluation of interactive atmospheric chemistry in CESM, *Geoscientific Model Development*, 5, 369–411, doi:10.5194/gmd-5-369-2012, 2012.

Lee, D. S., et al. (2010), Transport impacts on atmosphere and climate: Aviation, *Atmospheric Environment*, 44:4678–4734.

Lee, D. S., D. W. Fahey, P. M. Forster, P. J. Newton, R. C. N. Wit, L.L., Lim, B. Owen, R. Sausen (2009), Aviation and global climate change in the 21st century, *Atmospheric Environment*, doi:10.1016/j.atmosenv.2009.04.024.

Lim, L., D.S. Lee, R. Sausen, M. Ponater, (2007), Quantifying the effects of aviation on radiative forcing and temperature with a climate response model, Proceedings of an International Conference on Transport, Atmosphere and Climate (TAC). Office for Official Publications of the European Communities, Luxembourg, ISBN 92-79-04583-0, pp. 202–207.

Mahashabde, A., P. Wolfe, A. Ashok, C. Dorbian, Q. He, A. Fan, et al. (2011), Assessing the environmental impacts of aircraft noise and emissions. Progress in Aerospace Sciences, 47, 15-52.

Marais, K., S. P. Lukachko, M. Jun, A. Mahashabde, and I. A. Waitz (2008), Assessing the impact of aviation on climate, *Meteorologische Zeitschrift*, 17(2): 157-172.

Meinshausen, M., S. C. B. Raper, and T. M. L. Wigley (2011), Emulating coupled atmosphere-ocean and carbon cycle models with a simpler model, MAGICC6 – Part 1: Model description and calibration, *Atmospheric Chemistry and Physics*, 11, 1417–1456, doi:10.5194/acp-11-1417.

Myhre, G., J. S. Nilsen, L. Gulstad, K. P. Shine, B. Rognerud, I. S. A. Isaksen (2007), Radiative forcing due to stratospheric water vapour from CH_4 oxidation, *Geophysical Research Letters*, 34 (1), L01807. doi:10.1029/2006GL027472.

Myhre, G., K. P. Shine et al (2011), Radiative forcing due to changes in ozone and methane caused by the transport sector, *Atmospheric Environment*, 45(2):387–394

Naik, V., A. K. Jain, K. O. Patten, and D. J. Wuebbles (2000), Consistent sets of atmospheric lifetimes and radiative forcings on climate for CFC replacements: HCFCs and HFCs, *Journal of Geophysical Research*, 105, 6903–6914, doi:10.1029/1999JD901128.

Naik, V., D. Mauzerall, L. Horowitz, M. D. Schwarzkopf, V. Ramaswamy, and M.,Oppenheimer (2005), Net radiative forcing due to changes in regional emissions of tropospheric ozone precursors, *Journal of Geophysical Research*,110, D24306, doi:10.1029/2005JD005908.

Neale, R. B., J. Richter, S. Park, P. H. Lauritzen, S. J. Vavrus, P. J. Rasch, and M. Zhang, (2011), The Mean Climate of the Community Atmosphere Model (CAM4) in forced SST and fully coupled experiments, Submitted, *Journal of Climate*.

Patten, K. O., Khamaganov, V. G., Orkin, V. L., Baughcum, S. L., Wuebbles, D. J., (2011), OH reaction rate constant, IR absorption spectrum, ozone depletion potentials and global warming potentials of 2-bromo-3,3,3-trifluoropropene, *Journal of Geophysical Research*, 116, D24307.

Prather, M., et al. (2001), Atmospheric chemistry and greenhouse gases, in Climate Change 2001: The Scientific Basis, edited by J. T. Houghton et al., pp. 239– 287, Cambridge Univ. Press, New York.

Rienecker, M. M., et al (2008), The GEOS-5 Data Assimilation System-Documentation of versions 5.0.1, 5.1.0, and 5.2.0. NASA/TM-2008-104606, Vol. 27, Technical Report Series on Global Modeling and Data Assimilation, 118 pp. (available at http://gmao.gsfc.nasa.gov/systems/geos5/)

Rothman, L. S., et al. (2005), The HITRAN 2004 molecular spectroscopic database, *Journal of Quantitative Spectroscopy and Radiative Transfer*, 96, 139–204, doi:10.1016/j.jqsrt.2004.10.008.

Roof, C., A. Hansen, G. G. Fleming, T. Thrasher, A. Nguyen, C. Hall, E. Dinges, R. Bea, F. Grandi, B. Y. Kim, S. Usdrowski, and P. Hollingsworth (2007), Aviation Environmental Design Tool (AEDT) System Architecture AEDT-AD-01.

Sausen, R., and U. Schumann (2000), Estimates of the climate response to aircraft CO_2 and NOx emissions scenarios, *Climatic Change*, 44, 27–58.

Sausen, R., I. Isaksen, V. Grewe, D. Hauglustaine, D.S. Lee, G. Myhre, M.O. Kohler, G. Pitari U. Schumann, F. Stordal, and C. Zerefos (2005), Aviation radiative forcing in 2000: an update of IPCC (1999), *Meteorologische Zeitschrif,* 114, 555–561.

Olsen, S. C., G. P. Brasseur, D. J. Wuebbles, S. R. H. Barrett, H. Dang, S. D. Eastham, M. Z. Jacobson, A. Khodayari, H. Selkirk, A. Sokolov, N. Unger (2012), Comparison of model estimates of the effects of aviation emissions on atmospheric ozone and methane, Submitted, Geophysical Research Letters.

Stevenson, D.S., R.M. Doherty, M.G. Sanderson, W.J. Collins, C.E. Johnson, R.G. Derwent (2004), Radiative forcing from aircraft NOx emissions: mechanisms and seasonal dependence, *Journal of Geophysical Research,* 109, D17307. doi:10.1029/2004JD004759.

Stordal, F., M. Gauss, G. Myhre, E. Mancini, D. A. Hauglustaine, M. O. Kohler, T. Berntsen, E.J.G. Stordal, D. Iachetti, G. Pitari, and I. S. A. Isaksen (2006), TRADEOFFs in climate effects through aircraft routing: forcing due to radiatively active gases, *Atmospheric Chemistry and Physics*,. 6, 10733–10771.

Wild, O., M.J. Prather, H. Akimoto (2001), Indirect long-term global radiative cooling from NOx emissions, *Geophysical Research Letters,* 28, 1719–1722.

Youn, D., K. O. Patten, J. T. Lin, and D. J. Wuebbles (2009), Explicit calculation of indirect global warming potentials for halons using atmospheric models, *Atmospheric Chemistry and Physics*, 9, 8719–8733, doi:10.5194/acp-9-8719-2009.

CHAPTER 5. AVIATION NOx-INDUCED CH_4 EFFECT: FIXED MIXING RATIO BOUNDARY CONDITIONS VERSUS FLUX BOUNDARY CONDITION

Abstract

The effect of aviation NOx emissions on the atmospheric methane (CH_4) concentration and its lifetime is evaluated. Most past studies of aviation NOx emissions effects on ozone and methane have traditionally used fixed mixing ratio boundary conditions for CH_4 to decrease the computational requirements, and then apply corrections for using a flux boundary condition. In addition, those studies that have accounted for the feedback of CH_4 on itself have assumed a factor of 1.4 as the effect of the change in response time for CH_4. Modeling studies using flux boundary conditions are used to examine the validity of these assumptions. The latest version of the National Center for Atmospheric Research Community Earth System Model (CESM), with the CAM5 atmospheric model, was used for this study. NOx emissions for 2006 were obtained from the inventory of the AEDT (Aviation Environmental Design Tool) global commercial aircraft emissions. Results show a 31.4 ppb change in CH_4 concentration when using the parameterization and 1.4 feedback factor, and 28.9 ppb change when the concentration was directly calculated in the model. The model calculated value for CH_4 feedback on its own lifetime agrees well with the 1.4 feedback factor. Systematic comparisons between the separate runs yielded an 8.6% difference in calculating CH_4 concentration using the correlation approach. Therefore, it is concluded that the estimation technique that is based on one-box model calculations; is good to within ~10% in CAM5 that is a three-dimensional (3-D) model and decreases the computational requirements by nearly a factor of 8.

Introduction

Methane (CH_4) plays an important role in atmospheric chemistry and as a greenhouse gas that can affect climate. Since pre-industrial times (~1750), the atmospheric CH_4 concentration has increased about 150% and it accounts for 20% of the change in radiative forcing on climate from all long-lived greenhouse gases, excluding water vapor over that time period (UNEP,

2001). Aviation emissions of nitrogen oxides (NOx) and NOx emissions in general can affect atmospheric concentrations of CH_4 as an indirect result of their effect on concentrations of ozone in the upper troposphere and lower stratosphere (UTLS). Resolving the resulting effects of aviation NOx emissions on ozone and methane remains an important issue towards understanding the effects of aviation emissions on climate. Many studies have shown that the effect of aviation NOx emissions at cruise altitudes (~200 – 300 hPa in the UTLS) increases the production of ozone (O_3) in this region (Derwent et al., 1999; Fuglestvedt et al., 1999; Stevenson and Doherty, 2004; Köhler et al., 2008; Hoor et al., 2009; Koffi et al., 2010; Hodnebrog et al., 2011; Khodayari et al., 2013 and others). Additionally, these studies also show that increased concentrations of O_3 will increase the atmospheric concentrations of hydroxyl (OH). OH is a major sink for CH_4 in the troposphere and stratosphere, and thus decreases its concentration, while also affecting the response time of CH_4 that is basically shortening CH_4 lifetime due to OH restoration as a results of decrease in CH_4 concentration (Prather, 1994; Wild and Prather, 2001; IPCC, 2007).

The lifetime of methane has been evaluated in many studies. IPCC (2001) and (2007) reported a methane lifetime of 9.6 years against reaction with OH which has been evaluated with contemporary chemistry-transport models (CTMs) (Prather et al., 2001). The same contemporary of CTMs from the IPCC TAR (Prather et al., 2001) calculated a consistent feedback factor with a range of 1.33 – 1.45 (average 1.4). The feedback factor of 1.4 has been widely accepted and used (IPCC, 2001; Holmes et al., 2011). This feedback factor lengthens the duration of the CH_4 perturbation (CH_4 response time) to 12 years (IPCC, 2007). Due to the near decadal lifetime of methane, in order to directly calculate the changes in its atmospheric concentration and response time, models using CH_4 flux boundary condition must run for more than 40 years to reach steady-state. This is often too computationally expensive; therefore, most past studies of aviation NOx emissions effects on ozone and methane have traditionally used fixed mixing ratio boundary conditions for CH_4, and then apply corrections (parameterization) for using a flux boundary condition. As described in Equation 5.1, the parameterization assumes that the change in CH_4 concentration is proportional to the change in CH_4 lifetime obtained from the simulations with fixed mixing ratio boundary conditions for CH_4 multiplied by a feedback factor that describes CH_4 feedback on its own lifetime. In addition, those studies that accounted for the

feedback of CH_4 on its own lifetime have assumed a factor of 1.4 as the effect of the change in response time for CH_4.

$$\Delta[CH_4] = [CH_4]_{bg} \times \left(-1.4\left(\frac{\Delta\tau}{\tau_{bg}}\right)\right) \quad (5.1)$$

$[CH_4]_{bg}$ and τ_{bg} represent the CH_4 concentration and lifetime in the control simulation. $\Delta[CH_4]$ and $\Delta\tau$ are the changes in CH_4 concentration and lifetime due to the aviation NOx emissions, and 1.4 represents the CH_4 feedback on its own lifetime.

The feedback of CH_4 on its lifetime depends on the magnitude of the initial perturbations of CH_4 and OH. Furthermore, the changes in CH_4 and OH concentration continuously effect their concentrations. Fuglestvedt et al., (1999) illustrated this process as the following sequence of events:

$$\Delta E_{NO_x} \rightarrow \Delta[OH]_0 \rightarrow \Delta[CH_4]_0 \rightarrow \Delta[OH]_1 \rightarrow \Delta[CH_4]_1 \rightarrow \Delta[OH]_1 \rightarrow etc. \quad (5.2)$$

As in Fuglestvedt et al., (1999), based on one-box model calculations the feedback effect due to the initial sequence can be calculated from Equations 5.3.

$$R = \frac{\Delta[CH_4]/[CH_4]_0}{\Delta\tau/\tau_0} \quad (5.3)$$

Here, R corresponds to the initial change in the sequence of the changes in CH_4 lifetime. $[CH_4]_0$ and τ_0 are the CH_4 concentration and lifetime in the NOx-perturbed simulation from the set 1 and $\Delta[CH_4]$ and $\Delta\tau$ are the changes in CH_4 concentration and lifetime due to the small increase in CH_4 mixing ratio at the boundary layer in set 2 (i.e., $\Delta[CH_4]/[CH_4]$ = 0.20 when there is a 20% increase in CH_4 mixing ratio at the boundary layer).

Assuming that the feedback strength does not vary significantly with the strength of the initial perturbation (Karlsdottir and Isaksen, 1998; Fuglestvedt et al., 1999), the feedback factor due to the whole sequential changes can be derived from:

$$f = \left(1 + \sum_{n=1}^{\infty} \left(\frac{1}{R}\right)^n\right) \quad (5.4)$$

In this study we used the latest version of the atmospheric component of the National Center for Atmospheric Research Community Earth System Model (CESM), CAM5 to evaluate the validity of 1.4 feedback factor for the case of aviation perturbation along with the parameterization commonly used to correct for using a flux boundary condition. Methane feedback on its own lifetime has been evaluated for aviation perturbation previously, e.g., feedback factors of 1.3 and 1.52 were calculated in Köhler et al. (2008) and Holmes et al. (2011), respectively, and in this study we re-evaluate this feedback factor using CAM5. However, there has been no evaluation of the validity of the aforementioned parameterization for the case of aviation perturbation, and this study is the first attempt to do so.

The following section describes the data and model used in the study, the section after that describes the model simulations done to test this axiom; the last two sections discuss the results and the concluding argument.

Model Description

CAM5 (Community Atmosphere Model version 5) is the atmospheric component model for the Community Earth System Model (CESM) (http://www.cesm.ucar.edu/). The previous version of the Community Atmosphere Model (CAM) and CAM5 have been documented and discussed in other studies before (e.g. Neale et al., 2011; Gent et al., 2011 and Lamarque et al., 2012).

CAM5 uses the same gas-phase chemical mechanisms as its preceding version (CAM4) including tropospheric and stratospheric chemistry with 133 species and 330 photochemical reactions as described in Lamarque et al. (2012). A complete list of species and reactions can be found in Lamarque et al. (2012).

A major improvement in CAM5 despite its preceding versions that used bulk aerosol module, it uses a new modal aerosol module (MAM) (Lui et al., 2012) with two different versions available: a more complete version with seven lognormal modes (MAM7), and a version with three lognormal modes—Aiken, accumulation, and coarse (MAM3) (Liu and Ghan, 2010). For this study, CAM5 was configured with MAM3. MAM simulates the size distribution of aerosols for both internal and external mixing, the chemical and optical properties of aerosols, as well as various other complicated aerosols processes (Liu and Ghan, 2010). A prognostic, two-moment formulation for cloud droplets and cloud ice is used to represent cloud microphysical processes. For these processes, the mass and number concentrations of cloud droplets and cloud ice follow the Morrison and Gettelman (2008) parameterization. Liquid and ice particle sizes are determined by the gamma function (Gettelman et al., 2008). Furthermore, the time dependent evolution of these particles is affected by grid-scale advection, convective detrainment, and turbulent diffusion. Cloud droplets are activated as a function of aerosol size distribution, aerosol chemistry, temperature and vertical velocity (Neale et al., 2011). For the cloud macrophysics scheme, full consistency between cloud fraction and cloud condensate is employed. Liquid cloud fraction is based on a triangular distribution of total relative humidity. Ice cloud fraction is based on the Gettelman et al. (2010) scheme which allows supersaturation through the modification of the relative humidity over ice. This scheme also includes the ice condensate amount. The aerosols-cloud scheme has the ability to simulate full aerosol-cloud interactions. Some of these interactions include cloud droplet activation by aerosols, different precipitation processes as a result of particle size dependence, and an explicit radiative interaction of cloud particles. Further details on CAM5 can be found on NCAR website (http://www.cesm.ucar.edu/models/cesm1.0/cam/).

Emissions setup

CAM5 was run with a horizontal resolution of 2° latitude x 2.5° longitude with 30 vertical levels from the surface up to ~2 hPa. To reduce the year-to-year climate variability in the model simulation and to be able to detect aviation NOx signal, specified dynamics ("off-line" mode) simulations were performed. As such, there were no interactions between the chemical constituents and dynamics. The model was driven with 2005 meteorology from a

coupled CAM5 simulation. The aviation emissions used are from the AEDT aviation emissions scenarios (Wilkerson et al., 2010; Olsen et al, 2012). Background emissions of non-aviation short-lived species (e.g., NOx, volatile organic compounds (VOCs)) are from the IPCC RCP4.5 scenario (van Vuuren et al., 2011) while longer-lived species, e.g., CO_2, chlorofluorocarbons (CFCs), and nitrous oxide (N_2O), were specified as mixing ratio boundary conditions, also from the IPCC RCP4.5 scenario. To analyze the impact of aviation NOx emissions on CH_4 concentrations, two simulations are performed; one simulation considers all NOx emissions including aviation NOx, while the other simulation excludes aviation NOx (control run). The changes induced by aviation NOx is obtained by taking the difference between these two simulations.

Experiment description and setup

We evaluated the CH_4 feedback factor and the parameterization commonly used to calculate the change in CH_4 concentration based on the changes in its lifetime by performing three sets of simulations: Set 1- a control and a NOx-perturbed run with fixed mixing ratio boundary conditions for CH_4 that had a monthly temporal resolution and a horizontal resolution of 2.8° latitude x 2.8° longitude, Set 2- a NOx-perturbed run with a 20% increase in CH_4 mixing ratio at the boundary layer, and Set 3- a control and a NOx-perturbed run with CH_4 fluxes.

The first set of simulations was done to calculate the changes in CH_4 lifetime in the case of fixed CH_4 mixing ratio at the boundary layer. After running these simulations for 7 years the steady-state condition had been reach. Data from the 7^{th} year was used to calculate the change in CH_4 lifetime due to its reaction with tropospheric OH. The parameterization described in Equation 5.1 (Fuglestvedt et al., 1999) was then used to calculate the change in CH_4 concentration using the changes in its lifetime and the 1.4 feedback factor.

By comparing the parameterized changes in CH_4 concentration calculated from Equation 5.1 to the direct changes in CH_4 concentration calculated from set 3, the accuracy of the Equation 5.1, which assumes the changes in CH_4 concentration is proportional to the changes in its lifetime, was evaluated for the effects of emissions from aviation.

The second set of simulations was done to calculate the CH_4 feedback on its lifetime. For this set, a NOx-perturbed run with a 20% increase in the CH_4 mixing ratio at the boundary layer was performed. By using Equations 5.3 and 5.4 and the CH_4 lifetime in this run and the CH_4 lifetime in the NOx-perturbed run from set 1, the CH_4 feedback factor can be obtained.

The third set of simulations was done to directly calculate the changes in CH_4 concentration. A control run and a NOx-perturbed run with CH_4 fluxes at the surface were done to directly calculate the actual changes in CH_4 response time and concentration. The global mean CH_4 fluxes were obtained using the global steady-state loss in CH_4 from the NOx-perturbed run in set 1 (since burden = loss at steady state). The regional distribution of the CH_4 concentration from the IPCC RCP 4.5 was scaled to match the global mean CH_4 flux calculated from the set 1. Through this process, a reasonable CH_4 input flux, which produced the same background atmosphere as in the set 1, was obtained for set 3. Two simulations were then run until steady-state conditions were achieved (45 years for the NOx-perturbed run and 30 years for the background run).

Results and Discussion

Based on our three set of simulations, the accuracy of the 1.4 feedback factor and parameterization correlation has been evaluated. Based on the first set of simulations, the change in CH_4 lifetime excluding the CH_4 feedback on its lifetime was calculated. The calculated CH_4 lifetime for the control run and the NOx-pertubed simulations using the global burden and the global loss of CH_4 were 10.74 and 10.58 years, respectively. This led to a reduction in CH_4 lifetime of about 1.3% (1.60%/[TgN/yr^{-1}]). This falls within the -1.4±0.40 (%/[TgN/yr-1]) to -1.6±0.37 (%/[TgN/yr-1]) range reported by Hodnebrog et al. (2011) using different emissions and an ensemble of six different atmospheric chemistry models. The use of these calculated CH_4 lifetimes in Equation 5.1 led to the global mean aviation NOx-induced CH_4 change of 31.4 ppb.

Based on the second set of simulations the CH_4 feedback on its lifetime was calculated. The calculated feedback factor was 1.39 which is very close the 1.4 feedback factor. Previously, Köhler et al. (2008) using NOx perturbation from aviation calculated a model-dependent

feedback factor of 1.3. Thus, our results confirm that there is a good agreement on the CH_4 feedback on its own lifetime within the models.

Based on the third set of simulations the change in CH_4 concentration was calculated directly. Figure 5.1 shows the time-series of the global CH_4 concentration in both the control and NOx-perturbed cases from the third set of simulations. As discussed above, the runs in this set included CH_4 fluxes to produce the actual change in CH_4 concentration. As shown in Figure 5.1, the NOx-perturbed run required 45 years to reach steady state while the background run required 30 years.

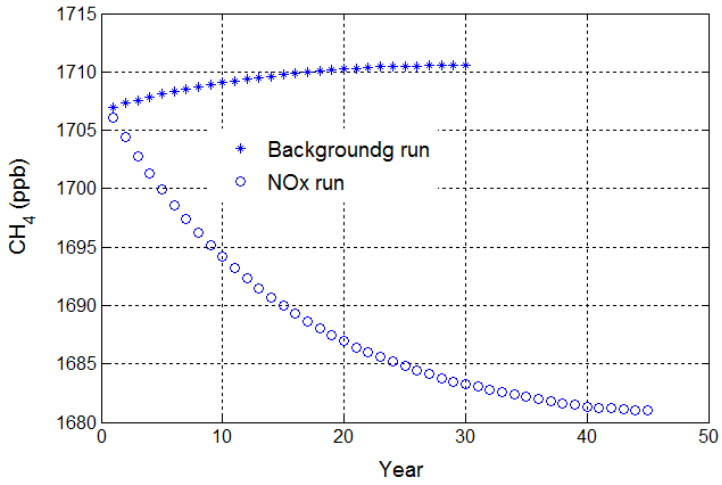


Figure 5.1. CH_4 concentration in the control and NOx-perturbed simulations for the case of having CH_4 fluxes at the surface.

Since the surface CH_4 fluxes used in simulations in set 3 were calculated based on the steady-state loss of CH_4 in set 1, it is expected that the background CH_4 concentration calculated in set 3 would be the same as the background CH_4 concentration in the set 1. A comparison of the global mean background concentration of CH_4 calculated in the two sets indicated that the CH_4 concentration in the background atmosphere between the two sets of runs was the same (to within 0.13%).

The aviation NOx-induced global mean changes in CH_4 concentration calculated from the simulations in set 3 was 28.9 ppb which is about 8.6% lower than the change calculated from set 1 using Equation 5.1.

Table 5.1 shows the results from comparing the three sets of simulations and presents the model calculated feedback factor, the actual model calculated change in CH_4 concentration, the parameterized change in CH_4 concentration, and the percentage difference in the calculated CH_4 feedback factor relative to the 1.4 feedback factor and the percentage difference in the model calculated change in CH_4 concentration relative to the concentration yield from the parameterization. Four approaches were used to calculate the atmospheric concentration of CH_4 and its lifetime. The most representative approach was the global mean, which was calculated by using the global burden and the global loss of CH_4. The other three approaches differed by: (1) using the tropospheric CH_4 burden and loss, with the tropopause marked by the pressure level of the tropopause, (2) using the tropospheric CH_4 burden and loss, with the tropopause marked by the altitude where the ozone concentration dropped below 150 ppb, and (3) using the global CH_4 burden and tropospheric CH_4 loss (same definition of the tropopause, as in (2)). Using these four different approaches, a range for the values of interest is presented in the third column of table 5.1.

Table 5.1. Results from comparisons of the three sets of simulations, a control and a NOx-perturbed simulation with fixed mixing ratio boundary conditions for CH_4, a NOx-perturbed simulation with a 20% increase in CH_4 mixing ratio at the boundary layer, and a control and a NOx-perturbed simulation with CH_4 fluxes.

	Global Mean	Range using other methods
CH_4 lifetime (yr) in the control simulation in set 1	10.7	9.70 to 11.4
CH_4 lifetime (yr) is the NOx-perturbed simulation in set 1	10.58	9.52 to 11.21
Aviation-induced ΔCH_4 (ppb) using Eq. 5.1	31.4	32.45 to 35.28
Aviation-induced ΔCH_4 (ppb) from the set 3	28.9	28.94 to 29.40
CAM5 calculated Feedback Factor	1.39	1.35 to 1.43
Percent error in feedback factor	-0.4%	-3.5% to 2.2%
Percent error in using Eq. 5.1	8. 6%	12.1% to 20.0%

Rows 1 and 2 show the methane lifetime from the control simulation and NOx-perturbed simulation, respectively. Row 3 shows the aviation-induced changes in CH_4 that were calculated from simulations in set 1 using the parameterization described in Equation 5.1 . Row 4 shows the actual change in aviation-induced CH_4 calculated from the simulations in set 3 using CH_4 fluxes at the surface. In row 5, the feedback factor that was calculated using the simulation in set 2 and Equation 5.4 is shown. Row 6 shows the error due to the using the 1.4 feedback factor and row 7 shows the error due to the using Equation 5.1 (assuming the change in CH_4 concentration is proportional to the changes in its lifetime).

The most representative and thereby accurate method was the global mean approach (global burden and loss of CH_4). The feedback factor using this approach was 1.395, very close to the IPCC accepted value of 1.40. For the other methods, the feedback factor ranges from 1.353 – 1.432. The percent difference from the calculated feedback factor and the feedback factor of 1.4 was -0.36% using the global mean approach and between -3.74% and 2.23 % using the other approaches. The percent difference between the actual CH_4 concentration calculated from set 3 and the CH_4 concentration calculated from set 1 using Equation 5.1 is 8.56%. For the other

approaches, the percent difference ranges from 12.14% to 20.01%. Thus, the estimation technique is good to within ~10% when using the total global CH_4 lifetime and decreases the computational requirements by nearly a factor of 8.

Conclusion

We evaluated the accuracy of the correlation widely used in estimating the changes in CH_4 concentration based on the changes in its lifetime and the accuracy of the 1.4 feedback factor of CH_4 on its own lifetime. Results show a 1.31% decrease in CH_4 lifetime due to aviation NOx emissions from the year 2006 in the simulations with fixed CH_4 mixing ratio as the boundary condition. The CAM5 calculated CH_4 feedback factor on its lifetime compared well with the 1.4 feedback factor. It was concluded that the use of the estimation formula for the simulations with fixed CH_4 at the lower boundary condition overestimates the change in CH_4 by 8.6% compared to the change calculated directly from the model using CH_4 surface emissions. Thus, for this simulation the estimation technique is good to within ~10% and decreases the computational requirements by nearly a factor of 8.

BIBLIOGRAPGY

Boucher, O., P. Friedlingstein, B. Collins, K. P. Shine (2009), The indirect global warming potential and global temperature change potential due to methane oxidation, *Environmental Research Letters*, 4 (4): 044007.

Denman, K. L., et al. (2007), Couplings between changes in the climate system and biogeochemistry, in Climate Change 2007: The Physical Science Basis. Contribution of Working Group I to the Fourth Assessment Report of the Intergovernmental Panel on Climate Change, edited by S. Solomon et al., Cambridge Univ. Press, Cambridge, U. K.

Fuglestvedt, J. S., T. K. Berntsen, I. S. Isaksen, H. Mao, X. Z. Liang, & W. C. Wang (1999), Climatic forcing of nitrogen oxides through changes in tropospheric ozone and methane; global 3D model studies. *Atmospheric Environment*, *33*(6), 961-977.

Hodnebrog, Ø., T. K. Berntsen, O. Dessens, M. Gauss, V. Grewe, I. S. A. Isaksen, B. Koffi, G.Myhre, D. Olivié, M. J. Prather, J. A. Pyle, F. Stordal, S. Szopa, Q. Tang, P. Velthoven, J. E. Williams, and K. Ødemark (2011), Future impact of non-land based traffic emissions on atmospheric ozone and OH – an optimistic scenario and a possible mitigation strategy, Atmospheric Chemistry and Physics, 11, 11293–11317. doi:10.5194/acpd-11-11293-2011, www.atmos-chem-phys.net/11/11293/2011/, 2011.

Holmes, C. D., Q. Tang and M. J. Prather (2011), Uncertainties in climate assessment for the case of aviation NO, Proceedings of the National Academy of Sciences, U.S.A., 108, 10 997–11 002, doi:10.1073/pnas.1101458108.

Hoor, P. et al. (2009), The Impact of Traffic Emissions on Atmospheric Ozone and OH: results from QUANTIFY, *Atmospheric Chemistry and Physics*, 9,3113-3136.

IPCC, 2001. Aviation and the global atmosphere. In: E Penner, J., Lister, D.H., Griggs, D.J., Dokken, D.J., McFarland, M. (Eds.), Intergovernmental Panel on Climate Change. Cambridge University Press, Cambridge, UK.

Karlsdottir, S., & , I. S. A. Isaksen (2000), Changing methane lifetime: Possible cause for reduced growth. *Geophysical Research Letters*, *27*(1), 93-96.

Khodayari, A., et al. (2013, in preparation), Aviation NOx-induced effects in community Earth system model (CESM): CAM4 and CAM5.

Kohler, M.O., G. Radel, O. Dessens, K. P. Shine, H. L.Rogers, O. Wild, J. A. Pyle (2008), Impact of perturbations to nitrogen oxide emissions from global aviation, *Journal of Geophysical Research*, 113, D11305. doi:10.1029/2007JD009140.

Prather, M., et al. (2001), Atmospheric chemistry and greenhouse gases, in Climate Change 2001: The Scientific Basis, Contribution of Working Group I to the Third Assessment Report of the Intergovernmental Panel on Climate Change, edited by J. T. Houghton et al., pp. 239–287, Cambridge Univ. Press, Cambridge, U. K.

UNEP, 2001. Annual Evaluation Report. United Nations Environmental Programme.

CHAPTER 6: METRICS FOR AVIATION EFFECTS ON CLIMATE BASED ON ACCRI CONTRIBUTIONS

Introduction

A key goal of the FAA-Aviation Climate Change Research Initiative (ACCRI) has been the refinement of analytical tools or metrics that simplify the complex understanding of the science as an aid to the decision-making. This section provides an overview of the contributions that this study and other ACCRI-based studies have made to the development and application of metrics for aviation effects on climate. These results are directly included in a special report published by the FAA and are also being included in a paper summarizing the findings from the ACCRI program that has been submitted to the Bulletin of the American Meteorological Society.

Metrics are tools used for quantifying and comparing climate impacts of emissions from human activity. Typically they aggregate and simplify complex information to a common scale to simplify comparison of impacts. Metrics such as Radiative Forcing (RF) and Global Warming Potentials (GWPs) have proven to be useful tools in climate policy related studies. These and other metrics have been reevaluated relative to results from the complex chemistry-climate models. Simple models, such as the APMT model developed at MIT, that attempt to reproduce the effects on climate from the highly complex processes and interactions in the Earth's climate system, have proven to be especially useful in assessments and policy analyses considering aviation effects on climate. Significant evaluation and improvements of these simple models have been discussed in Chapter 2.

Radiative Forcing (RF) has been commonly used to compare different climate change effects (e.g., for all IPCC climate assessments since the first one in 1990), including analyses of the effects of aviation on climate (e.g., IPCC, 1999, Sausen et al., 2005; Lee et al., 2009). RF is defined as the net imbalance of incoming and outgoing radiation at the top of the tropopause. The RF concept assumes that the globally averaged annual mean surface temperature at equilibrium is linearly dependent on the globally averaged RF and the climate sensitivity. Until the new findings of ACCRI, the summary analyses for RF in Lee et al. (2009) has been held as the recent standard for understanding of aviation effects on climate. While there remain issues

about its appropriateness as a meaningful metric (Wuebbles et al., 2010), the updated RFs obtained from the synthesis of ACCRI studies are presented and compared with Lee et al. (2009).

ACCRI evaluation of aviation induced RFs

The ACCRI results presented here are obtained from a collaborative effort of 9 different research groups that used 10 different complex climate-chemistry models to evaluate different aviation induced effects. The aviation NOx-induced effects evaluated in this research and discussed in Chapter 3 and 4 are included in the synthesis of ACCRI evaluations of aviation NOx-induced effects. It is just noted that the CAM5 evaluation used in this synthesis was obtained using an earlier development version of CAM5 (cesm1_1_alpha17b_modal) that is different than the recent development version (cesm1_2_beta08_chem) used in Chapter 3. Table 6.1 shows the evaluations of 2006 aviation induced RF components provided by different ACCRI research groups for the same effects as were computed by Lee et al. (2009). The first column describes the different research groups/models contributed to ACCRI evaluations. The second column refers to the short-term ozone effect, third column to CH_4 effect, fourth column to water vapor effect, fifth column to the direct effect of sulfate aerosols, sixth column to the direct effect of black carbon aerosols, seventh column to the effect of linear contrail and the last column to contrail-cirrus effect. The second and third rows correspond to the evaluations obtained in this work using the NCAR CAM4 and CAM5 models (PI: Donald Wuebbles). The fourth row corresponds to the evaluation obtained using NASA ModelE2 at Yale University (PI: Nadine Unger). The fifth row corresponds to the observation-based evaluation obtained at German Aerospace Center (DLR) (PI: Ulrich Schumann). The sixth row corresponds to the observation-based evaluation obtained at NASA Langley (PI: Patrick Minnis). The seventh row corresponds to the evaluation obtained using CAM5 model at NCAR (PI: Andrew Gettelman). The eighth row corresponds to the evaluation obtained using observation and CAM5 model at Texas A&M University (TAMU) (PI: PingYang). The ninth row corresponds to the evaluation obtained using IGSM model at MIT (PI: Ronald Prinn). The tenth row corresponds to the evaluation obtained using NASA GEOS5-CCM model at NASA (PI: Henry Selkrik).

Figure 6.1 shows the ACCRI evaluation of 2006 aviation induced RFs for the same effects as were computed by Lee et al. (2009) and their maximum-minimum range compared to Lee et al. (2009) evaluations and their 90% confidence interval. Figure 6.1 also shows the forcing components normalized by the CO_2 forcing.

Table 6.1. ACCRI evaluation of 2006 aviation induced RFs for the same effects as were computed by Lee et al. (2009).

RF(mW m^{-2})	O_3-S	CH_4	H_2O	SO_4-D	BC-D	Linear contrail	Contrail cirrus
This work, CAM5[1]	24.9	-11.6					
This work, CAM4	36.5	-12.3					
Yale U.	6 ±2	-8±2	1.3 ± 0.04	-7±2	0.6±0.6		
DLR							50 (40-80)
NASA Langley						5.7(3.1 - 17.5)	
NCAR				-3	1	2.9±3.2	12.4 ±8.0
TAMU						11.33±5	
MIT	26	-9.7		-4.4			
NASA Goddard	30.5	-12.3	2				

*O_3-S refers to the short-term changes in O_3. D refers to direct RF.

[1]This evaluation was obtained using an earlier development version of CAM5 (cesm1_1_alpha17b_modal) that is different than the recent development version (cesm1_2_beta08_chem) used in Chapter 3.

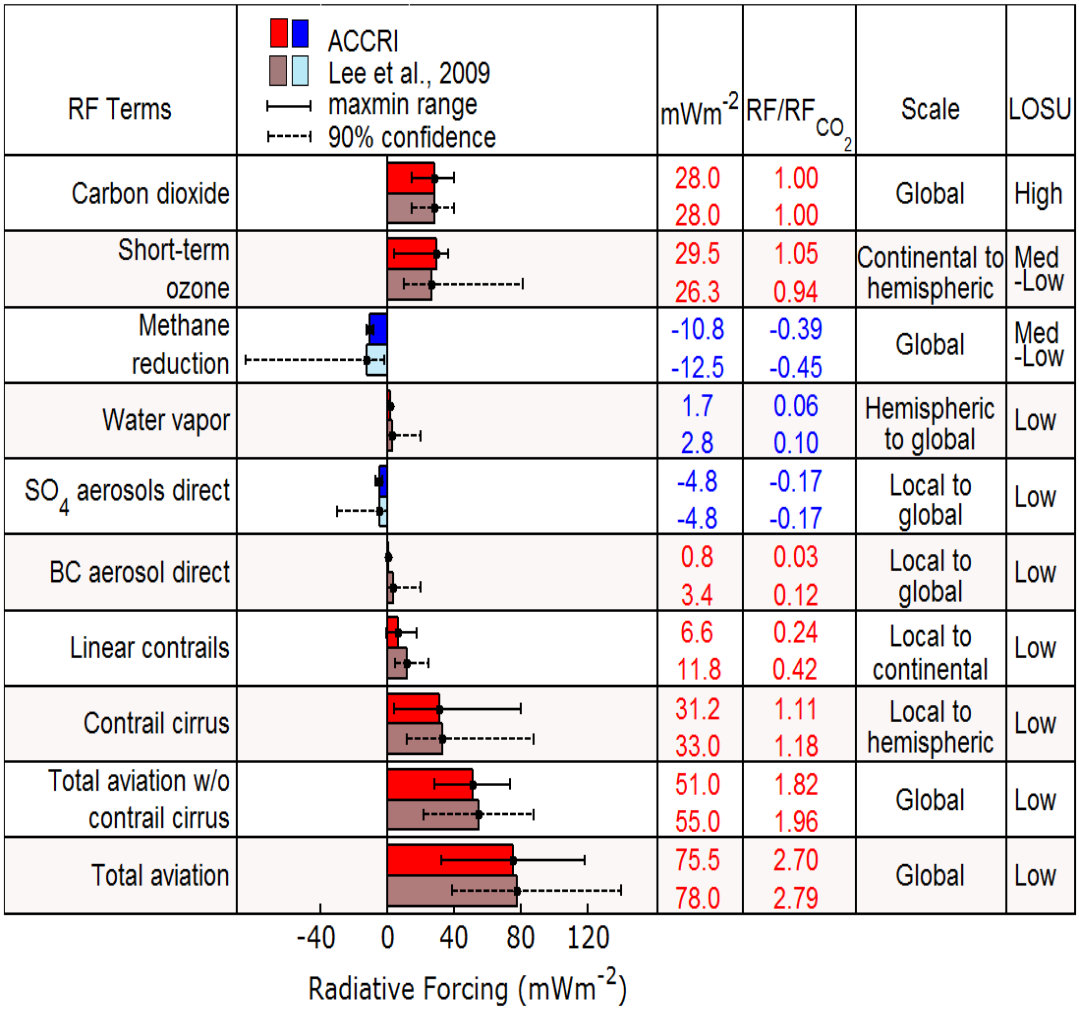


Figure 6.1. Radiative forcing (RF) for different components. Values normalized by CO_2 are also shown. The total RF was calculated but summing all individual RFs except linear contrail RF since linear contrail RF is already included in contrail cirrus RF. The uncertainty whiskers for ACCRI total RFs were obtained by assuming that the uncertainties in the individual RFs ([RFmax-RFmin)/2]) are uncorrelated and random. As discussed below, ACCRI also includes RFs not included in Lee et al.

For CO_2, the RF value used in Lee et al. (2009) was adopted. For all other ACCRI RFs, the averages of the estimates provided by all ACCRI research teams are considered the best estimates (shown as color coded bars in Figure 6.1). The outliers were not included in calculating the average effects. In this case the estimate of short-term O_3 RF (6.4±2 mWm^{-2}) provided by

Yale was not included in calculating the average of O_3 RFs. However, this estimate was included in calculating the minimum and maximum range.

As shown in Figure 6.1, while the overall forcing best estimates from ACCRI and Lee et al. (2009) overlap, the results based on recent observation and modeling analyses from ACCRI generally show smaller range of estimates than those from Lee et al. (2009) for most of the effects. The new ACCRI evaluations have better-constrained estimates of short-term O_3, CH_4, H_2O and aerosol direct forcing. Understanding of the role of NOx and spreading contrails have improved, yet uncertainties remain large in these terms due to significant differences in the results from the ACCRI chemistry-climate modeling studies. Figure 6.1 shows that, while ACCRI evaluations of the relative-to-CO_2 normalized RFs are generally close to those derived by Lee et al. (2009) evaluations, they are about 40% smaller in the case of H_2O and linear contrails. The ACCRI and Lee et al. (2009) evaluations show that the short-term O_3 and contrail cirrus contributions to warming are equivalent to the CO_2 contribution.

ACCRI investigators identified five additional effects that were not included in Lee et al. (2009). These effects and their associated RFs are shown in Table 6.2. The first column describes the different research groups/models contributed to ACCRI evaluations. The second column refers to the long-term ozone effect, third column to the stratospheric water effect, fourth column to the direct and indirect effect of sulfate aerosols, fifth column to the effect of nitrate aerosols and the last column to the direct and indirect effects of black carbon aerosols. The second and third rows correspond to the evaluations obtained in this work using NCAR CAM4 and CAM5 models (PI: Donald Wuebbles). The fourth row corresponds to the evaluation obtained using NASA ModelE2 at Yale University (PI: Nadine Unger). The fifth row corresponds to the evaluation obtained using CAM5 model at NCAR (PI: Andrew Gettelman). The sixth row corresponds to the evaluation obtained using IGSM model at MIT (PI: Ronald Prinn). The seventh row corresponds to the evaluation obtained using NASA GEOS5-CCM model at NASA (PI: Henry Selkrik). The eighth row corresponds to the evaluation obtained using NCAR CAM/IMPACT and CoCiP models at University of Michigan (MICH) (PI: Joyce Penner).

Table 6.2. ACCRI evaluation of five additional 2006 aviation induced effects that were not included in Lee et al. (2009).

RF(mW m^{-2})	O_3-L	SWV	SO_4-D&I	Nitrate	BC-D&I
This work, CAM5[1]	-4.21	-2.43			
This work, CAM4	-4.5	-2.59			
Yale				-4±1	
NCAR			-46 (-23 to -160)		-96, 8
MIT	-3.5*	-2.0*			
NASA Goddard	-4.4*	-2.6*			
U. MICH					0, -210,-780

[1]This evaluation was obtained using an earlier development version of CAM5 (cesm1_1_alpha17b_modal) that is different than the recent development version (cesm1_2_beta08_chem) used in Chapter 3.

*Values were not directly provided by the corresponding research groups, but were scaled based on the CH_4 forcing. O_3-L refers to the long-term changes in O3. D&I refers to direct plus indirect RF.

These effects and their associated RFs (mW m^{-2}) are: long-term ozone (-4.2 and -4.5) and stratospheric water vapor (SWV; -2.4 and -2.6) which are induced by NOx emissions, nitrate aerosol effect (-4), BC direct plus indirect effect (0 (-96 to 8) and 0 (-210 to -780)) and SO_4 direct plus indirect effect (-46 (-23 to -160)). The numbers after these effects represent a mean and a range (min, max). It is noted that Lee et al. (2009) estimates of BC and SO_4 RFs only include the direct effect while the new ACCRI evaluation of these effects includes both direct and indirect effects. For nitrate and SO_4 direct plus indirect effects, there is only a single evaluation while for the BC direct plus indirect effect, there were two independent evaluations. It is noted that the evaluations for the BC direct plus indirect effects provided by Gettelman et al. and Penner et al. are noticeably different (0 (-96 to 8) and 0 (-210 to -780) mW m^{-2}) since their assumptions for nucleation efficiencies and particle size are vastly different. The new highly uncertain evaluations of BC and SO_4 direct plus indirect forcing, if found to be robust, will significantly decrease the total aviation forcing and increase its associated uncertainty.

Overall, the comparison of new ACCRI evaluations to the corresponding Lee et al. (2009) evaluations indicates that ACCRI provides a better-constrained evaluations due to the improved

understanding of aviation induced effects. Moreover, ACCRI provides new evaluations for some of the effects that were not considered before; this could have a potential profound effect on the magnitude of the net aviation induced RF. This indicates a need for further investigations on these new effects. Also, given the wide range of model evaluation for some of these effects, a more thoroughly analyses of these models relative to observations should be considered as the most important possible path to reduce the uncertainties in such effects.

Outlook of non-CO_2 effects in SCMs

As was discussed in chapter 2, most Simple Climate Models (SCMs) used for aviation studies are composed of three major sub-models: (1) a carbon cycle sub-model which calculates the flow of carbon between different carbon reservoirs and calculates the atmospheric concentration of CO_2, (2) a forcing sub-model which calculates the radiative forcing for different aviation forcing components, and (3) an energy balance sub-model which calculates the temperature change for a given change in Earth system forcing budget. In most SCMs, due to the high level of scientific understanding of the carbon cycle, CO_2 long atmospheric lifetime, and the well-recognized capabilities for its representation in such models, it is feasible to directly calculate the change in the atmospheric concentration of CO_2 using parameterization. However, this is not the case for aviation induced non-CO_2 effects due to the low level of scientific understanding of these effects, the relatively short lifetime of such effects, and their high regional dependence. As such, in most SCMs a simple parameterization is utilized to calculate the radiative forcing associated with the non-CO_2 effects instead of calculating the change in the atmospheric concentration of these effects. In this simple parameterization, it is assumed that the induced effects depend linearly on the aviation emission rate. Therefore, to calculate non-CO_2 induced RFs at a given year, global mean RFs (RF per unit of NOx emissions) calculated from 3-D global climate model simulations are lineally scaled by the total annual emissions for the specific emitted species for that given year. The specific RFs used in such parameterizations are calculated either based on observations or from a steady-state response of a 3-D global climate model simulation to annually repeating emissions. For short-lived species (i.e. short-term O_3, soot, sulfate and nitrate aerosols, water vapor and contrail cirrus) the linearly scaled RF at a given year would be a representative of forcing at that given year. However, as was discussed in

Chapter 3, for long-lived components of aviation-induced RFs (i.e. CH_4, long-term O_3), since the effect would last beyond the perturbed year, a decay of the linearly scaled RF should be considered. As such, a complete history of aviation emissions and the lifetime of the perturbed species are required to be included into these analyses.

The evaluation of an appropriate carbon cycle and energy balance model were already discussed in Chapter 2 and the appropriate treatment for calculating the forcing of aviation induced long-lives species versus short-lives species were discussed in Chapter 4. Based on the synthesis of ACCRI evaluations of aviation induced RFs, the new specific RFs recommended for use in SCMs for calculating aviation induced non-CO_2 RFs are given in Table 6.3. It is noted that since ACCRI evaluations are for the year 2006, to calculate the 2006 NOx-induced specific RFs, ACCRI RFs are divided by aviation 2006 NOx emissions (0.82 TgN/yr^{-1}) and for to calculate the other non-CO_2 specific RFs, ACCRI RFs are divided by aviation 2006 NOx fuel burn (1.88×10^2 $TgFuel/yr^{-1}$). Table 6.3 shows the specific RFs that need to be used for calculating the non-CO_2 effects in SCMs. It is noted that for SO_4 and BC, only the specific forcing of direct RF is provided, as the level of scientific understanding of their indirect component is very low and still further research is required to better constrain such numbers.

On top of using RF as a metric to evaluate aviation induced climate impacts, different studies have developed new approaches for forward-looking temperature responses as a function of time that could also prove to be valuable in policy analyses. The evaluation of an appropriate energy balance model that could be used for temperature response calculations in a simple climate model context was discussed in Chapter 2.

Table 6.3. ACCRI evaluation of specific RFs for aviation induced non-CO_2 effects evaluated for the year 2006.

Specific RFs (mWm^{-2}/ TgN)					Specific RFs $\times 10^3$(mWm^{-2}/ Tgfuel)					
	O_3-S	CH_4	O_3-L	SWV	H_2O	SO_4 -D	Nitrate	BC-D	Linear contrail	Contrail cirrus
Best estimate	35.9	-13.1	-4.8	-2.8	0.9	-2.6	-2.1	0.4	3.5	16.6
max	44.5	-15.0	-5.5	-3.2	1.1	-3.7	-2.7	0.6	9.3	42.6
min	4.9	-9.8	-3.5	-2.0	0.7	-1.6	-1.6	0.0	-0.2	2.3

The way forward

There are several areas of research arising from this work that should be pursued. As has been discussed so far, to project the future aviation non-CO_2 effects in SCMs, the current state of SCMs is to scale a reference specific radiative forcing calculated from a 3-D climate-chemistry model with NOx emissions (for NOx-induced effects) or fuel usage for other effects for future years. This approach neglects the effects that the change in the future background atmosphere could have on the radiative forcing of different aviation induced effects. Therefore, it is of a considerable interest to find a way to incorporate the effect of the future change in the background atmosphere in the calculation of the future radiative forcings induced by non-CO_2 effects. This is especially important for NOx-induced effects since as it has been discussed in Chapter 4, such effects are strongly influenced by the chemistry of the background atmosphere.

The other area of the possible future research is related to the detailed sensitivity study of the aviation NOx-induced effects in 3-D climate-chemistry models. As it has been shown in Chapter 3, NOx-induced effects are strongly dependent on the model treatment of aerosols. As such, there are discrepancies between models and remain uncertainties in quantifying aviation NOx-induced effects. More detailed investigation of the effect of aerosol treatment on the aviation NOx-induced effects is necessary to better understand such effects.

It was shown that there is a wide range of evaluations of aviation NOx-induced effects among ACCRI models. Since there is not a consistent set of model evaluation against observation for all these models, a more thoroughly analyses of these models relative to observations is the most important possible path to reduce these uncertainties.

One of the other major uncertainties with respect to aviation's effect on climate is related to aerosol indirect effects. This is caused by the process of the formation of cloud condensation nuclei (CCN) by aerosols and the subsequent formation of contrails in an already existing cloud field. This could also impact the hydrological cycle and other parts of the global circulation, e.g. by ice particle sedimentation and triggering of precipitation at lower altitudes. As was noted earlier in this chapter, there are currently very few estimates of aviation induced soot and SO4 indirect effects and the uncertainty associated with these effects are significant. As such, further evaluation of these effects in fully coupled 3-D climate-chemistry models and other advanced models should improve our quantitative understanding of the impact of aviation induced aerosols indirect effects on climate.

The use of global RF, GWP or global temperature change potential (GTP) as a metrics to evaluate the impact of aviation emissions on climate has been of a considerable interest in climate policy related studies. While there are many advantages in using such metrics, there is the potential that important information on regional scales gets lost. Therefore, it is important to improve the understanding of how regional emissions affect both the regional and global response, and how global emissions affect the local response. This would especially apply to aviation-induced changes in ozone, methane, aerosol concentrations and cloudiness that are highly heterogeneous. The inclusion of a measure of the spatial heterogeneity in metrics that are for addressing aviation non-CO_2 effects on climate could be useful to policy considerations.

BIBLIOGRAPGY

IPCC, (1999), Aviation and the global atmosphere 1999, In: E Penner, J., Lister, D.H., Griggs, D.J., Dokken, D.J., McFarland, M. (Eds.), Intergovernmental Panel on Climate Change. Cambridge University Press, Cambridge, UK.

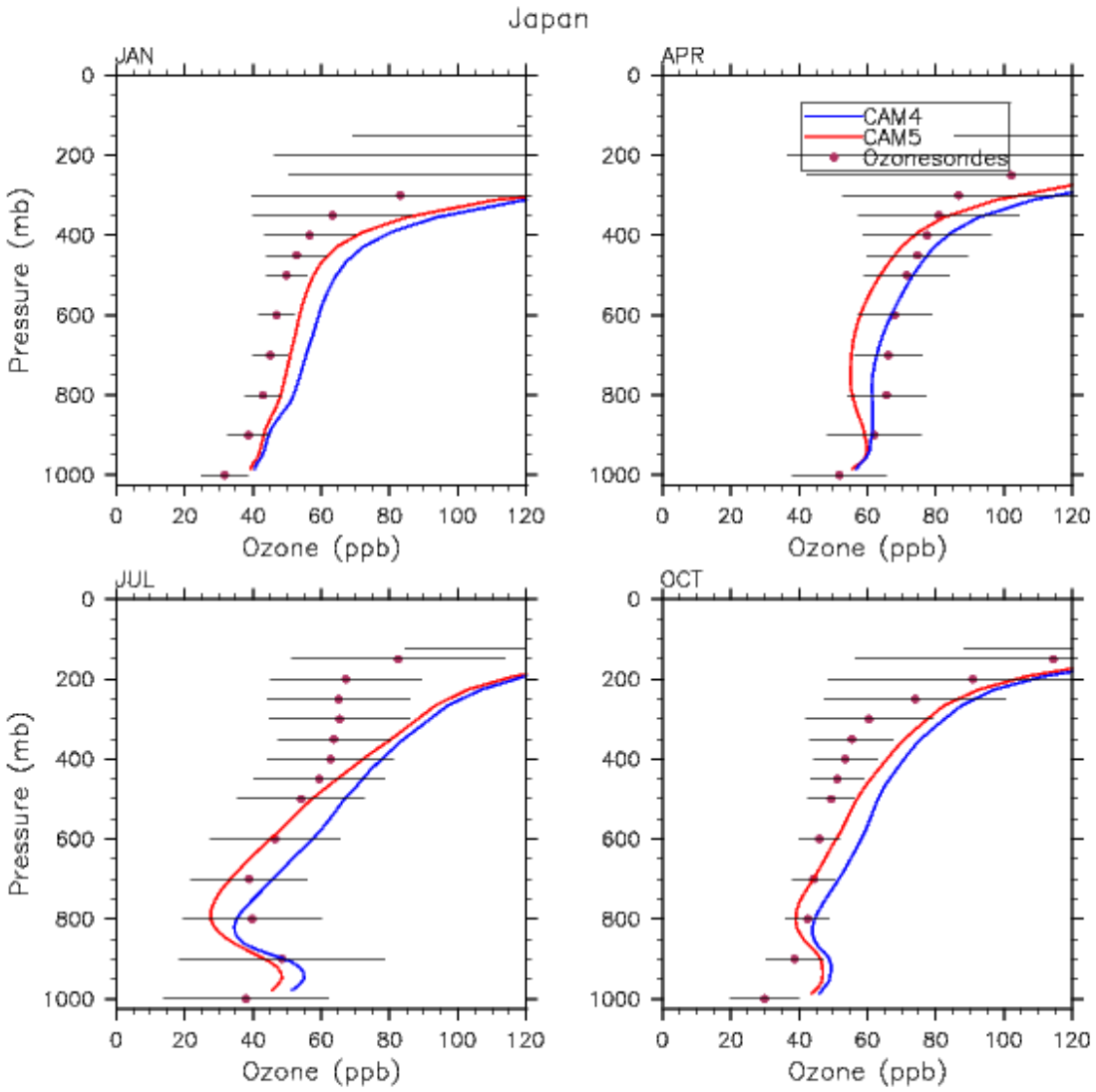
Lee, D. S., D. W. Fahey, P. M. Forster, P. J. Newton, R. C. N. Wit, L.L., Lim, B. Owen, R. Sausen (2009), Aviation and global climate change in the 21st century, *Atmospheric Environment*, doi:10.1016/j.atmosenv.2009.04.024.

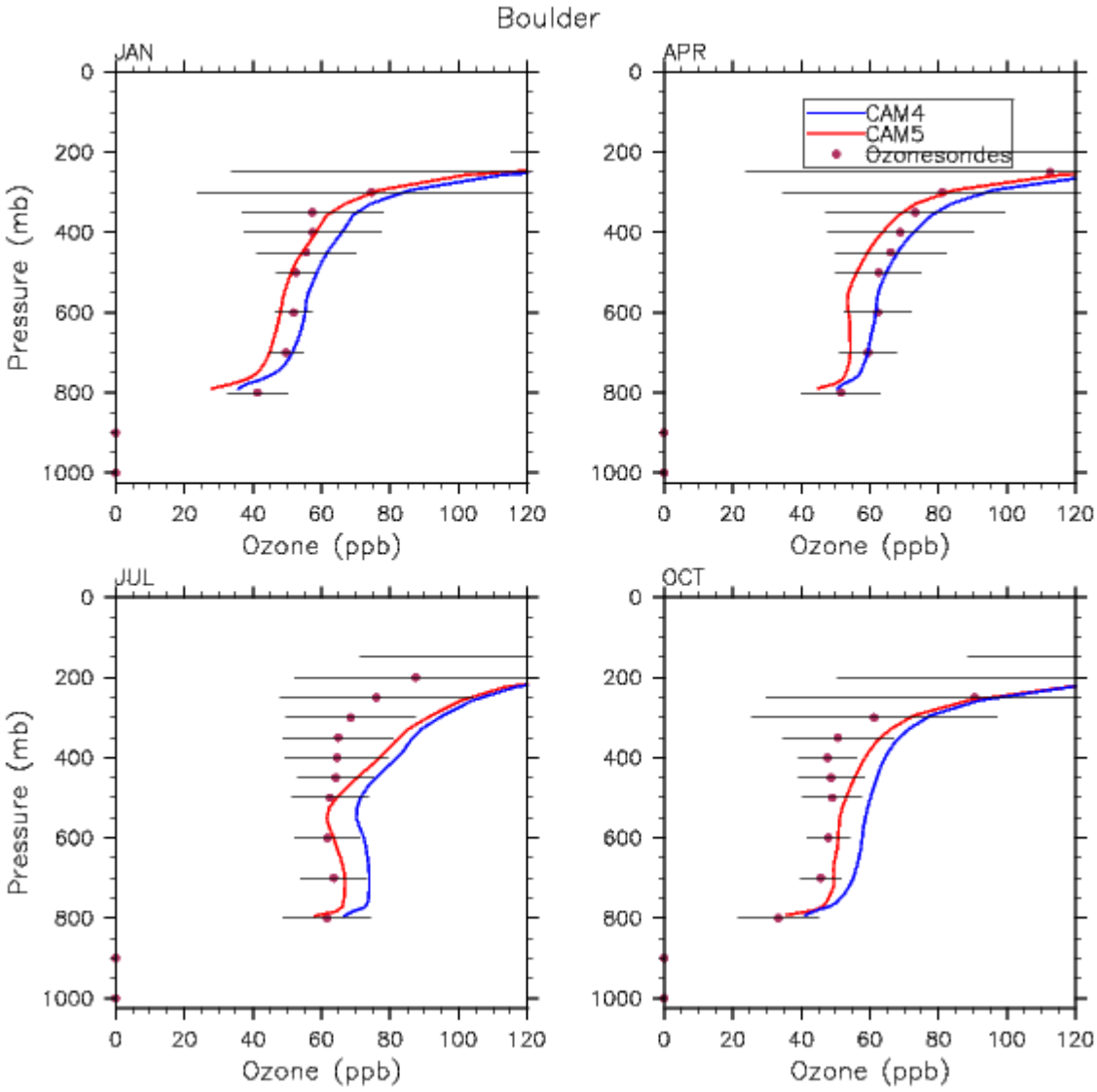
Sausen, R., I. Isaksen, V. Grewe, D. Hauglustaine, D.S. Lee, G. Myhre, M.O. Kohler, G. Pitari U. Schumann, F. Stordal, and C. Zerefos (2005), Aviation radiative forcing in 2000: an update of IPCC (1999), *Meteorologische Zeitschrif,* 114, 555–561.

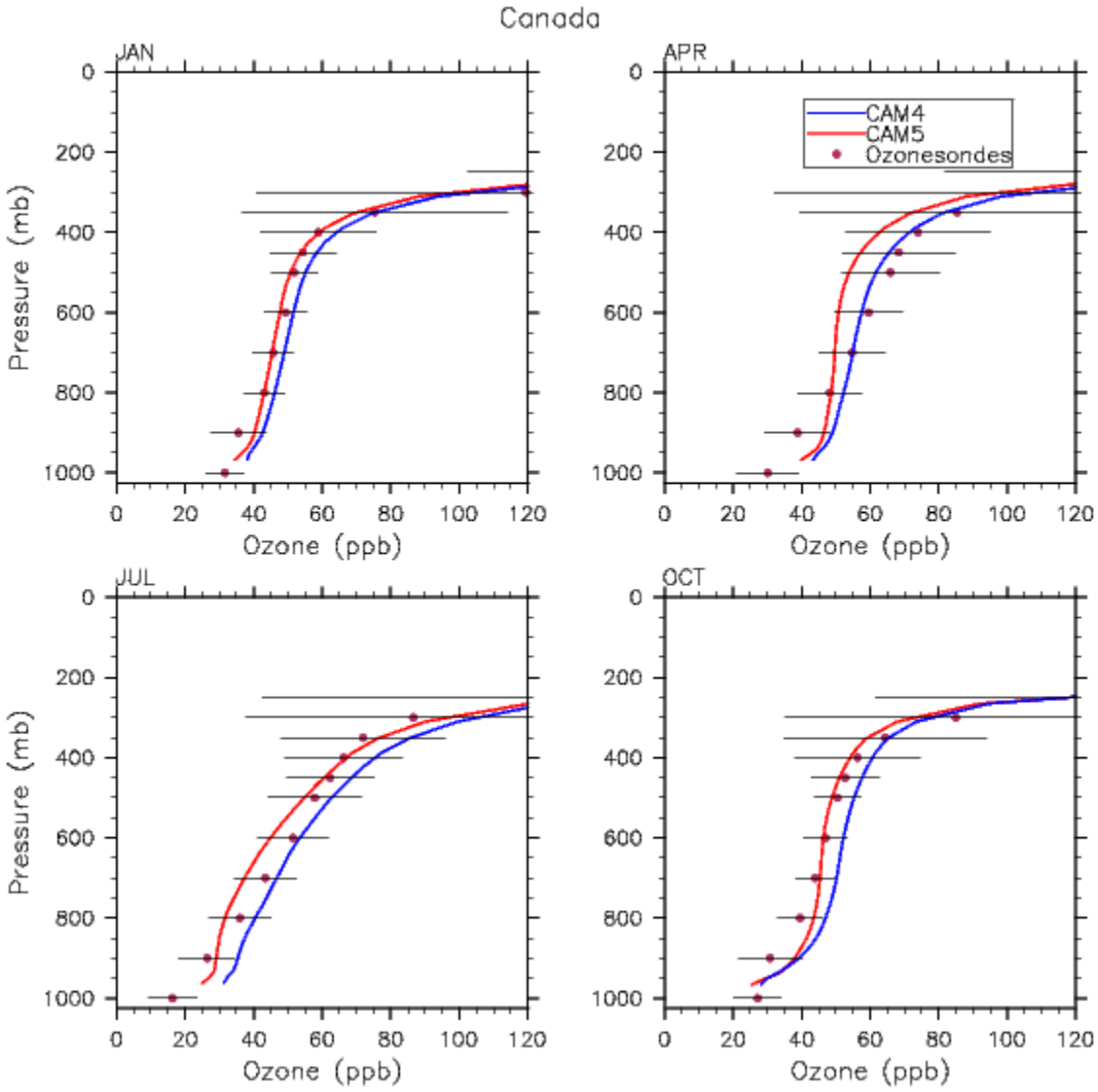
Wuebbles D., P. Forster, H. Rogers, and R. Herman (2010), Issues and uncertainties affecting metrics for aviation impacts on climate, *Bulletin* of the *American* Meteorological *Society*, 91, 491–496.

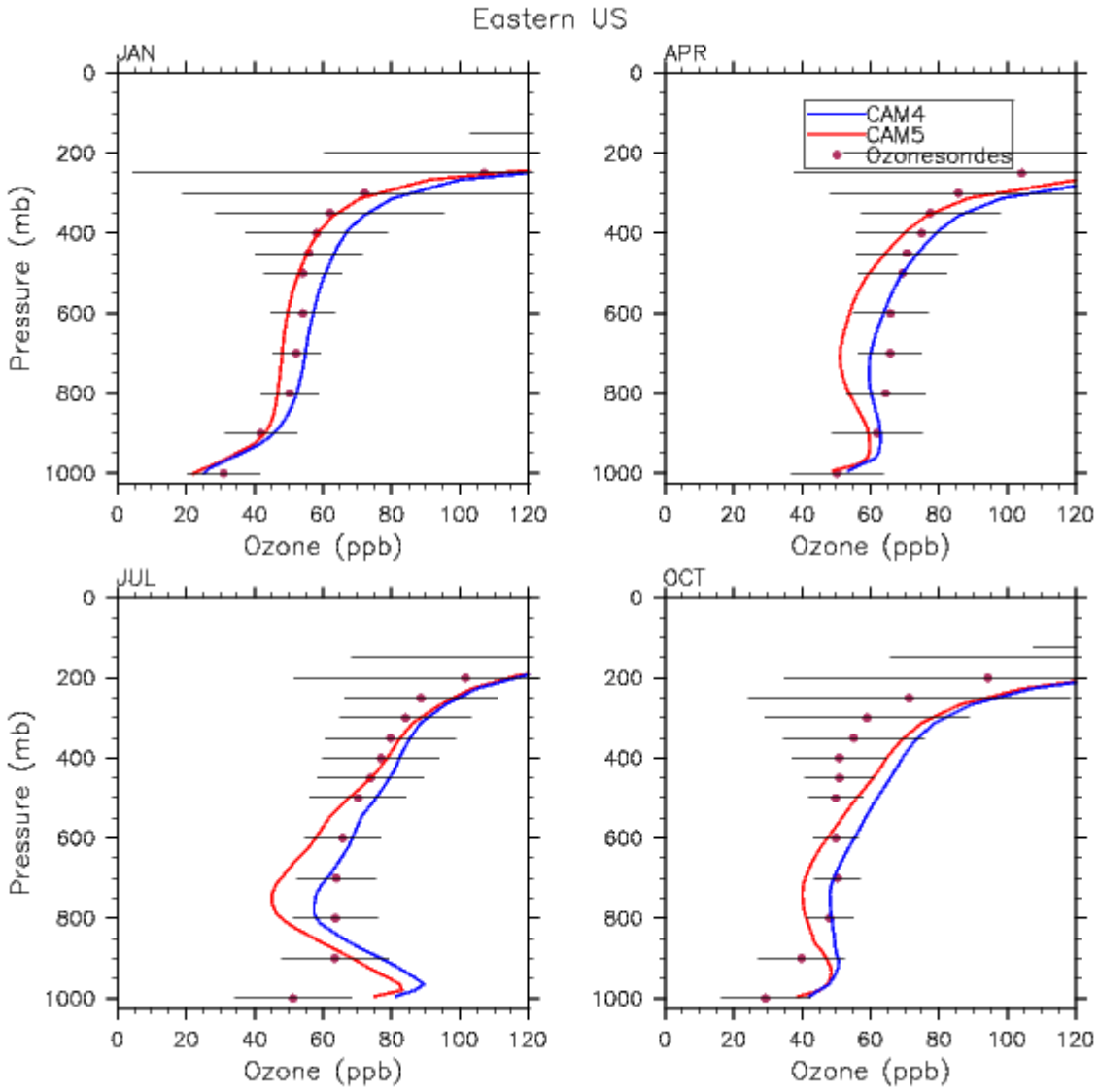
APPENDIX A

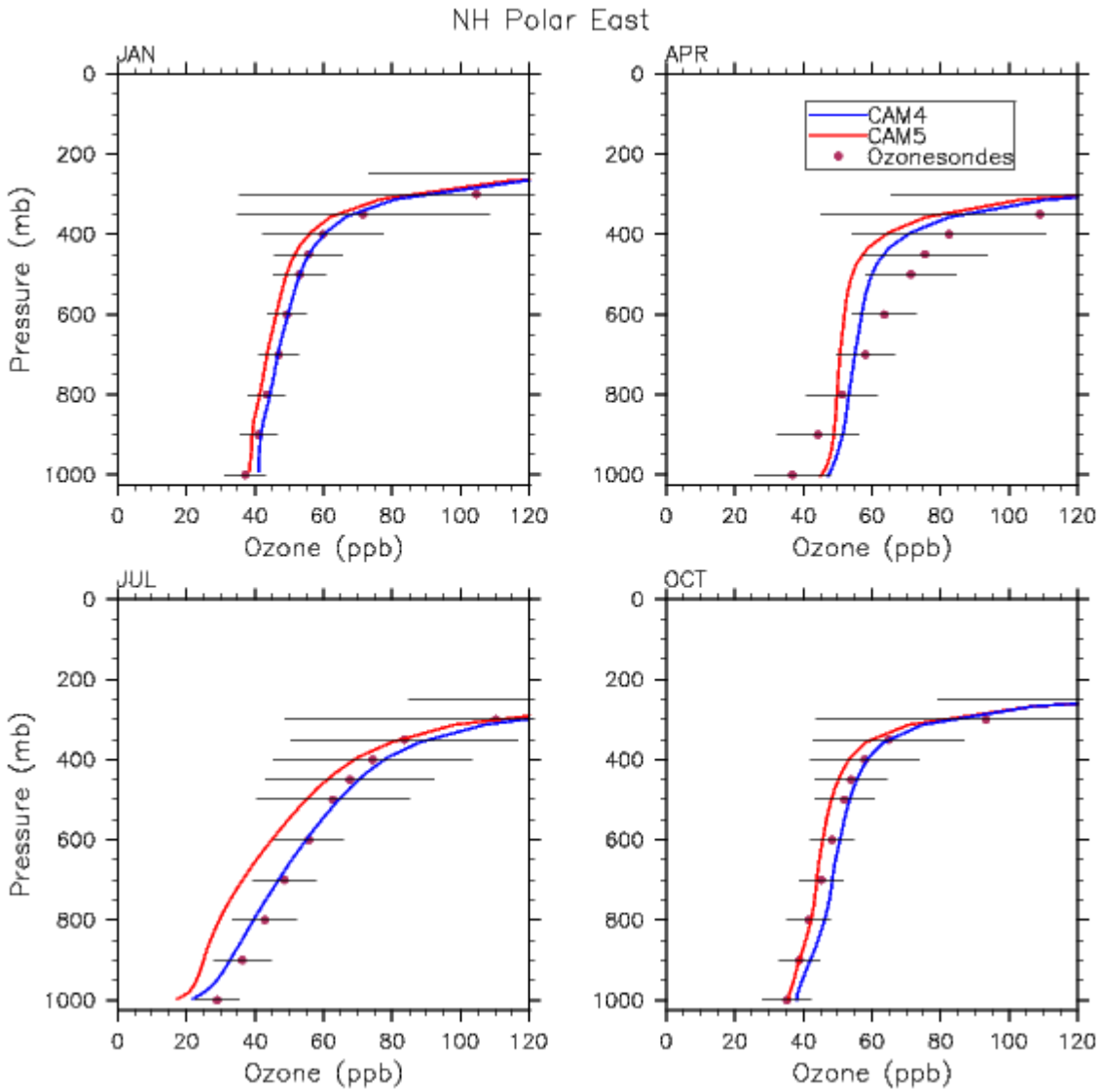
Comparison of CAM5 and CAM4 simulated ozone to ozonesonde for different regions

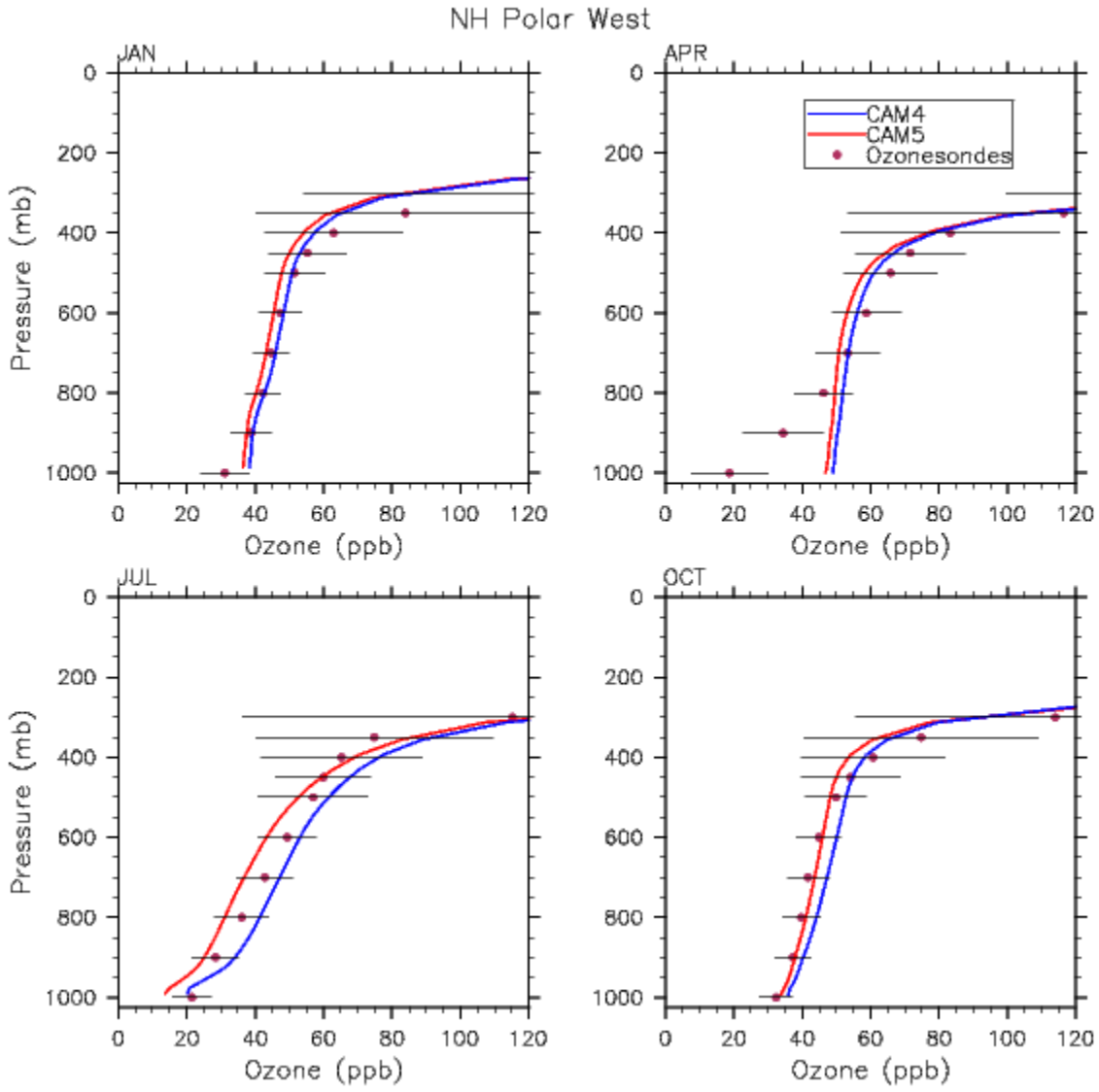


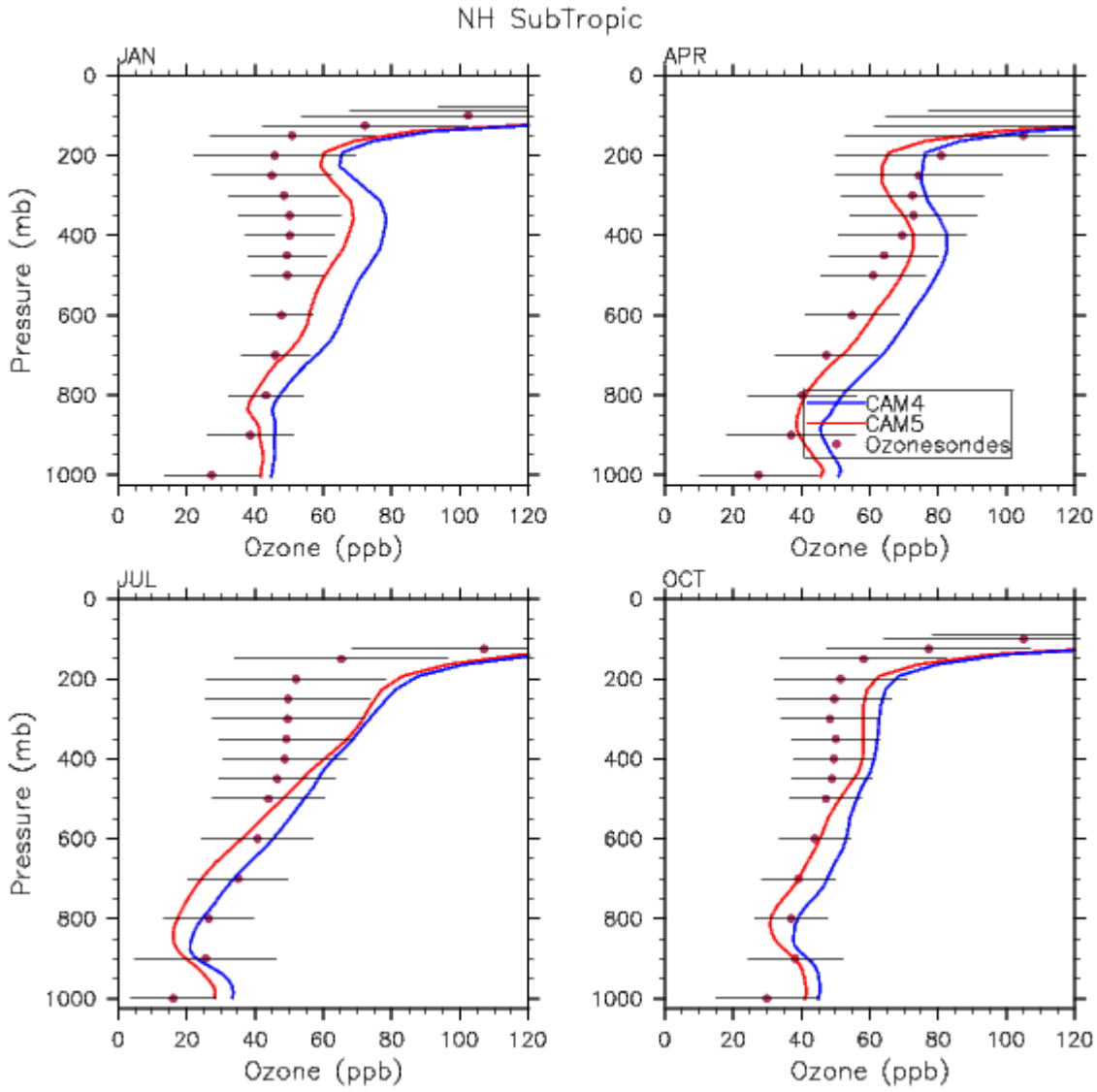

Boulder
JAN
APR
JUL
OCT
CAM4
CAM5
Ozonesondes
Pressure (mb)
Ozone (ppb)
0
200
400
600
800
1000
0
20
40
60
80
100
120

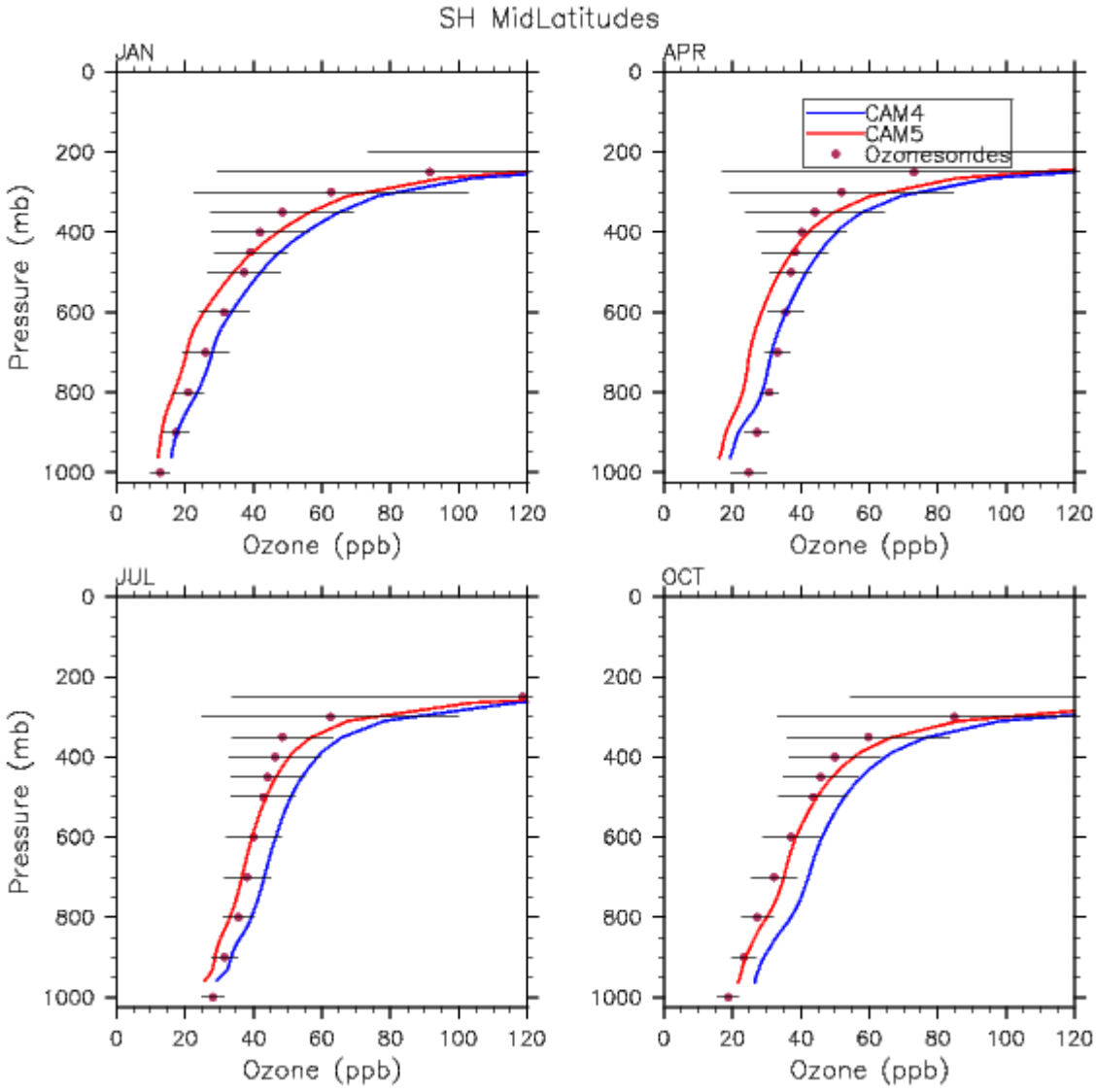

Canada
JAN
APR
JUL
OCT
CAM4
CAM5
Ozonesondes
Pressure (mb)
Ozone (ppb)
0
200
400
600
800
1000
0
20
40
60
80
100
120

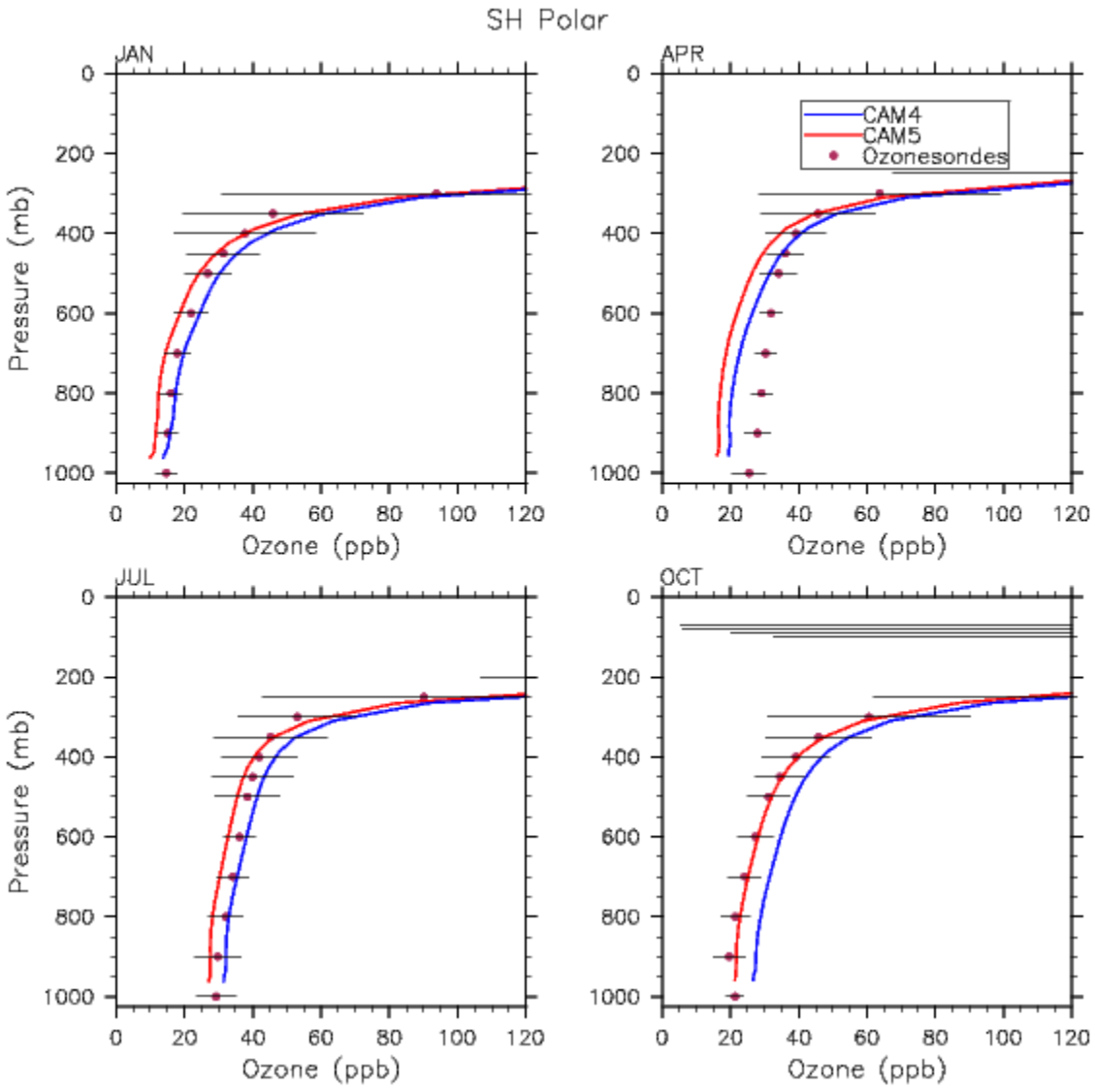

Eastern US
JAN
APR
JUL
OCT
CAM4
CAM5
Ozonesondes
Pressure (mb)
Ozone (ppb)
0
200
400
600
800
1000
0
20
40
60
80
100
120

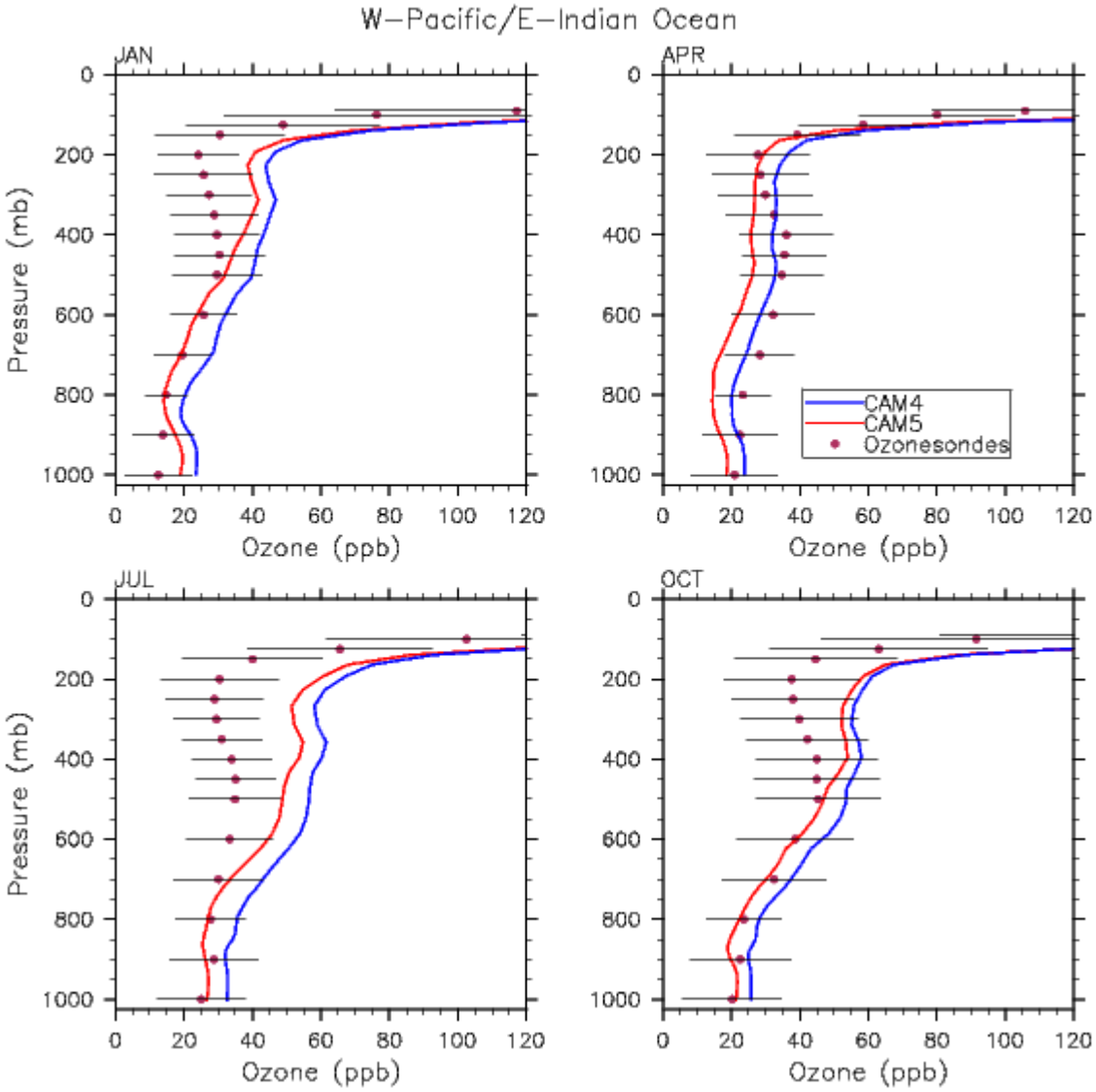

NH Polar East
JAN
APR
JUL
OCT
CAM4
CAM5
Ozonesondes
Pressure (mb)
Ozone (ppb)
0
200
400
600
800
1000
0
20
40
60
80
100
120

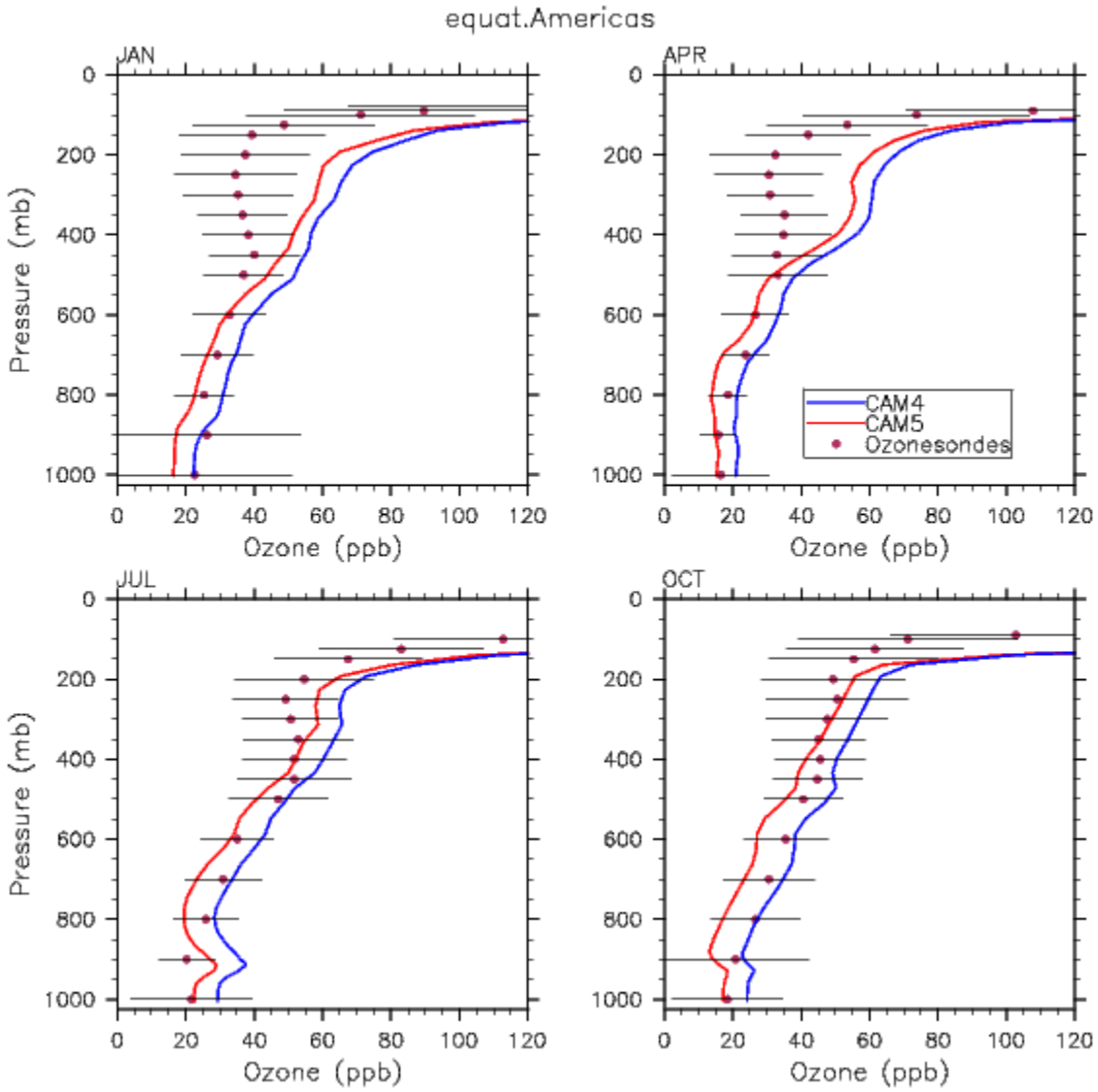

NH Polar West
JAN
APR
JUL
OCT
CAM4
CAM5
Ozonesondes
Pressure (mb)
Ozone (ppb)
0
200
400
600
800
1000
0
20
40
60
80
100
120

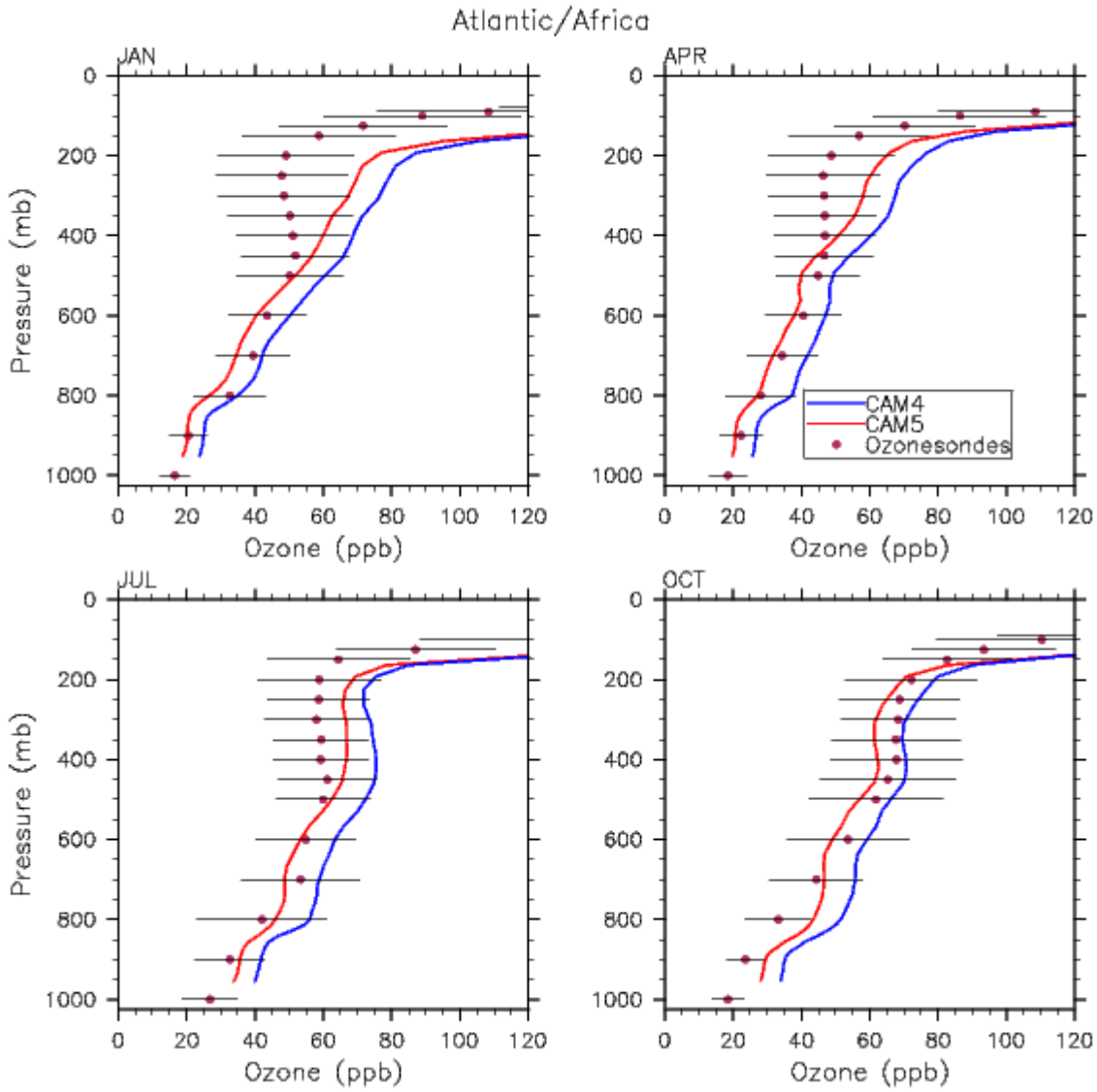

NH SubTropic
JAN
APR
JUL
OCT
Pressure (mb)
Ozone (ppb)
0
200
400
600
800
1000
0
20
40
60
80
100
120
CAM4
CAM5
Ozonesondes

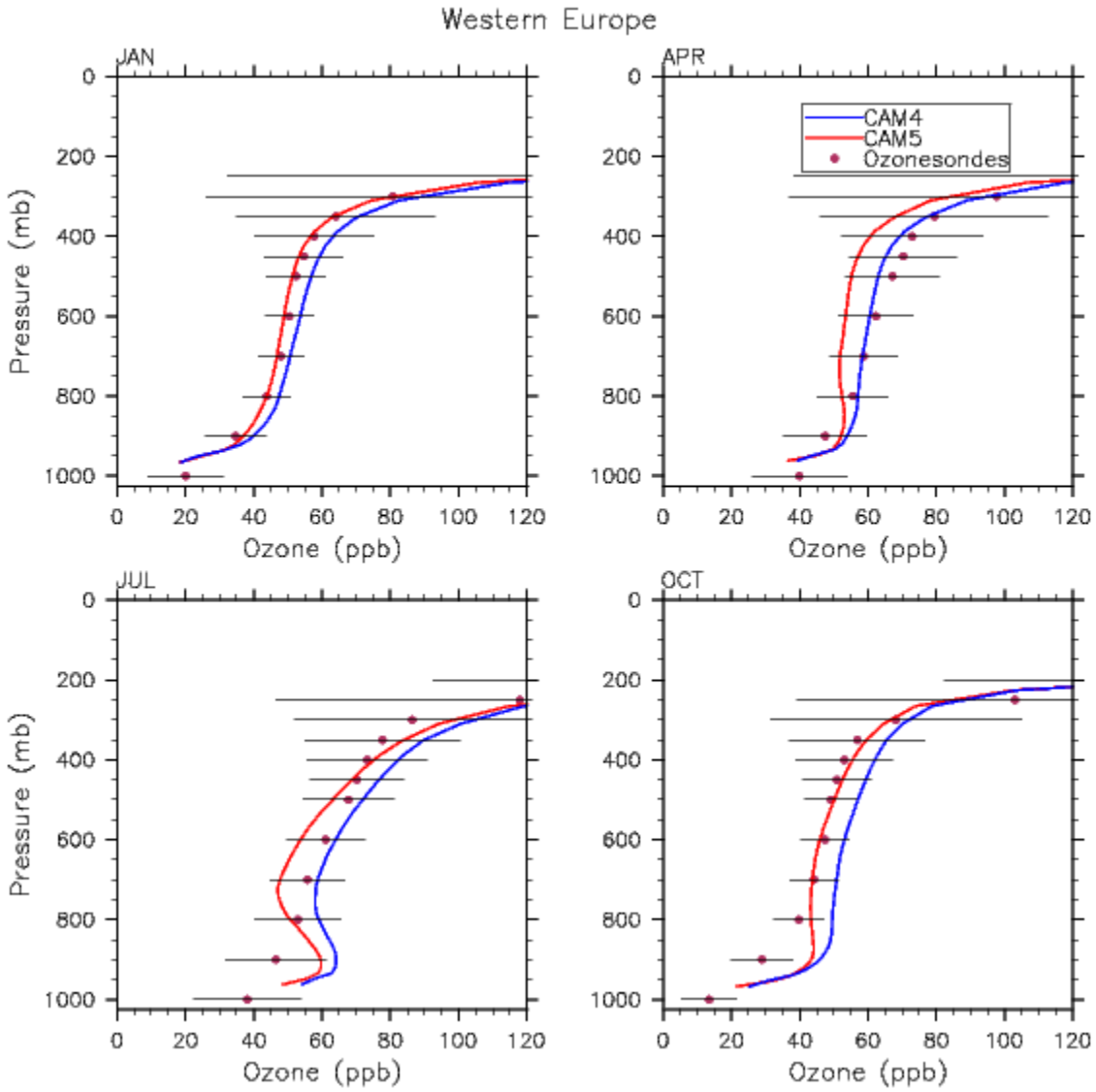

SH MidLatitudes
JAN
APR
JUL
OCT
CAM4
CAM5
Ozonesondes
Pressure (mb)
Ozone (ppb)
0
200
400
600
800
1000
0
20
40
60
80
100
120


SH Polar
JAN
APR
JUL
OCT
CAM4
CAM5
Ozonesondes
Pressure (mb)
Ozone (ppb)
0
200
400
600
800
1000
0
20
40
60
80
100
120


W–Pacific/E–Indian Ocean
JAN
APR
JUL
OCT
Pressure (mb)
Ozone (ppb)
0
200
400
600
800
1000
0
20
40
60
80
100
120
CAM4
CAM5
Ozonesondes


equat.Americas
JAN
APR
JUL
OCT
Pressure (mb)
Ozone (ppb)
0
200
400
600
800
1000
0
20
40
60
80
100
120
CAM4
CAM5
Ozonesondes


Atlantic/Africa
JAN
APR
JUL
OCT
Pressure (mb)
Ozone (ppb)
0
200
400
600
800
1000
0
20
40
60
80
100
120
CAM4
CAM5
Ozonesondes


Western Europe
JAN
APR
JUL
OCT
CAM4
CAM5
Ozonesondes
Pressure (mb)
Ozone (ppb)
0
200
400
600
800
1000
0
20
40
60
80
100
120